Response to Referee #1 (acp-2022-729)

We Thank Reviewer for his/her constructive comments

Responses to the Specific comments

General comments: This work estimated multiple emissions using the EnKF with the state augmentation method during the COVID-19 pandemic. Then, they assessed the unbalanced emission reduction of different species during the restriction. The manuscript is well organized and contains detailed analysis. However, the authors have some issues to be clarified in the manuscript for the final publication in ACP.

Reply: The authors appreciate the reviewer for his/her constructive and up-to-point comments. We have carefully considered the comments and revised the manuscript accordingly. Please refer to our responses for more details given below.

Comment 1: Line 91 & 285 (Weak motivation): The EnKF coupled with the state augmentation used in this study could be a more advanced method than inversed single estimation (Zhang et al., 2020; 2021, Feng et al., 2020, & Hu et al., 2022) in terms of emission estimation for multiple species. However, it could be less cost-effective. Also, as mentioned in the manuscript (line 285), it shows a similar performance with the single estimation of SO_2 (Hu et al., 2022). In other words, the inversed single estimation can be better, considering both performance and computational cost. Therefore, considering these issues, the authors need some more explanation or justify the use of your method to enhance the motivation for this work.

Reply: Thanks for this suggestion. The EnKF coupled with the state augmentation is a commonly used method for the estimations of multi-species' emissions (Miyazaki et al., 2017; Ma et al., 2019; Peng et al., 2018). In this method, the emissions of different species are simultaneously estimated by including them as a part of the state vector together with the chemical concentrations using the ensemble model simulations and observations. The mass balanced method used in Zhang et al. (2020) and Zhang et al. (2021) is to adjust the model emissions based on the modeled local ratio between concentrations and emissions. Although it has lower computational cost than the EnKF method since it does not need to run an ensemble of model simulation, it has difficulties in accounting for the nonlinear relationship between the concentrations and emissions, thus is more commonly used in the inversions of short-lived species (e.g., NO_x) under relatively coarse (>1°) resolution (Streets et al., 2013). The EnKF method instead can consider the nonlinear relationship between the emissions and concentrations (as we illustrated in our

response to comment 2), and can be used for longer-lived species (e.g., SO_2, $PM_{2.5}$ and CO) at finer model resolutions (Streets et al., 2013). The four-dimensional variational assimilation (4DVar) method used in Hu et al. (2022) is an advanced inversion method similar to the EnKF method, and they have different strengths and weakness (Skachko et al., 2014). The 4DVar uses an adjoint model of a chemical transport model (CTM) to estimate the emissions, thus it requires the development and maintenance of an adjoint model, which is technically difficult and cumbersome for the complex CTM. The EnKF method does not require an adjoint model and is easily implemented. Besides, although 4DVar does not need to run an ensemble of simulation, it needs to solve a complex optimization problems for a large chemical model system, therefore, the 4DVar have comparable computational costs with the EnKF method (Skachko et al., 2014). Similar to our method, Feng et al. (2020) used the EnKF method to estimate the emission changes of NO_x during COVID-19 pandemic, but they did not constrain the emissions of other species. Due to the chemical reactions in the atmosphere, the concentrations of different species are interrelated with each other. For example, the ambient $PM_{2.5}$ is not only primarily emitted, a large portion of them is also formed secondarily through reactions with several gaseous precursors, such as NO_2 and SO_2. This means that inversed single estimation may cause biases in the inversed $PM_{2.5}$ emission if the errors in emissions of NO_2 and SO_2 were not corrected synchronously. Assimilations of CO measurement also influences the inversion of NO_2 emission due to its influence on the OH concentration in the atmosphere (Miyazaki and Eskes, 2013). Therefore, doing the multi-species inversion estimation can provide more constraints on the atmospheric chemical system than the inversed single estimation and thus can produce more reasonable inversion results (Miyazaki and Eskes, 2013; Peng et al., 2018). The inversion estimation for SO_2 may be less affected by assimilations of other species due to its less dependence on other species. As a result, our inversion results showed a similar performance with the single estimation of SO_2 in Hu et al. (2022). Besides, the emissions of different species were perturbed simultaneously in our method, thus the ensemble simulation only needs to be performed once. The computational cost only increased slightly in the analysis step. Therefore, the multi-species' inversion method used in our study has its strength over the inversed single estimation method used in previous studies. Following the suggestions of reviewers, we give more explanation for the use of our method in the revised manuscript (please see lines 161–178)

Changes in the manuscript: lines 161–178.

Comment 2: Line 126: The authors need to clarify how to consider the non-linearity between NOx

emission (for estimation) and NO_2 concentration (of observation). Additionally, in-situ NO_2 observation may be based on the commercial chemiluminescent instrument. While the instrument system converts NO_2 to NO through a molybdenum converter, other species, such as peroxyacetyl nitrates (PANs) and HNO3, are also simultaneously converted to NO. The other species account for a large portion of the converted NO molecules. For example, Dunlea et al. (2007) showed the interference in the chemiluminescence detection accounting for up to 50% of ambient NO_2. In other words, the observed NO_2 is almost equivalent to ambient NO_y. Also, PAN is thermally sensitive (and it is also related to the temperature shown in Figure 10). The rapid decrease in NO_x emission is strongly linked to this issue. Therefore, the authors also need to explain how to treat these issues in your calculation.

Reply: Thanks for this important comment. In EnKF method, the relationship between the concentrations and emissions of related species was determined by the background error correlations, which is estimated from the ensemble model simulations. Since the chemistry transport model used in our study is a nonlinear model which considers the physical and chemical processes in the atmosphere, the ensemble simulation is able to represent the nonlinear evolution of the error correlations. This allows the nonlinear relationships between NO_2 concentrations and NO_x emissions to being considered through the use of background error covariance produced by ensemble simulations (Evensen, 2009; Miyazaki et al., 2012). Following the suggestions of reviewer, we have clarified this in the revised manuscript (please see lines 165–167).

As the reviewer mentioned, the NO_2 measurement made by CNEMC is based on the chemiluminescent analyser with a molybdenum converter. We agree with the reviewer that the interference of HNO_3, PAN and alkyl nitrates (AN) can lead to an overestimation of NO_2 (Dunlea et al., 2007; Lamsal et al., 2008) and may lead to spurious decreases of NO_x emissions. Due to the lack of synchronous observations of HNO_3, PAN and AN, it is hard to directly correct such overestimations in the NO_2 measurements. Previous studies (Cooper et al., 2020; He et al., 2022) usually use chemical transport model to simulate NO_x, HNO_3, PAN and AN to produce correction factors (CFs) for the NO_2 measurements using the following relationship proposed by Lamsal et al. (2008):

$$CF = \frac{[NO_2]}{[NO_2]+0.95[PAN]+0.35[HNO_3]+\sum[AN]} \tag{R1}$$

but the calculation of CF could be affected by the simulation errors in the model caused by uncertainties in emission inventory or other error sources, which may contaminate the observations. Therefore, similar to Feng et al. (2020), we did not correct the NO_2 measurement in our inversion of NO_x emissions since there were large uncertainties in the NO_x emissions during the COVID-19 pandemic that possibly led to

erroneous CF. Instead, the EnKF is capable of considering the errors in the observations during the assimilation through the use of observation error covariance matrix. The interference in the chemiluminescence detection to the NO_2 measurement was thus treated as a kind of observation error in our study. According to our estimates, the total observation error of NO_2 measurements was about 6–10 $μg/m^3$. To investigate whether our settings of observation error can fully cover the errors induced by the chemiluminescence monitor interference, we calculated the CF according to Eq. (R1) based on the simulated NO_2, HNO_3, PAN and AN using the inversed emission inventory to alleviate the effects of emission uncertainty on the CF calculations. Figure R1 shows the calculated CFs for NO_2 measurements over different regions of China during COVID-19 pandemic, which generally ranged from 0.75 to 0.99. The CF values over NCP, NE, NW and Central were generally stable throughout the COVID-19 pandemic, all larger than 0.9, suggesting that chemiluminescence monitor interference only has slight effects on the NO_2 measurement. Over the SE and SW regions, there was a drop of CF values during the lockdown period, followed by an increase after the lockdown. This indicates that the decline of NO_2 concentrations during lockdown period may be larger in these two regions.
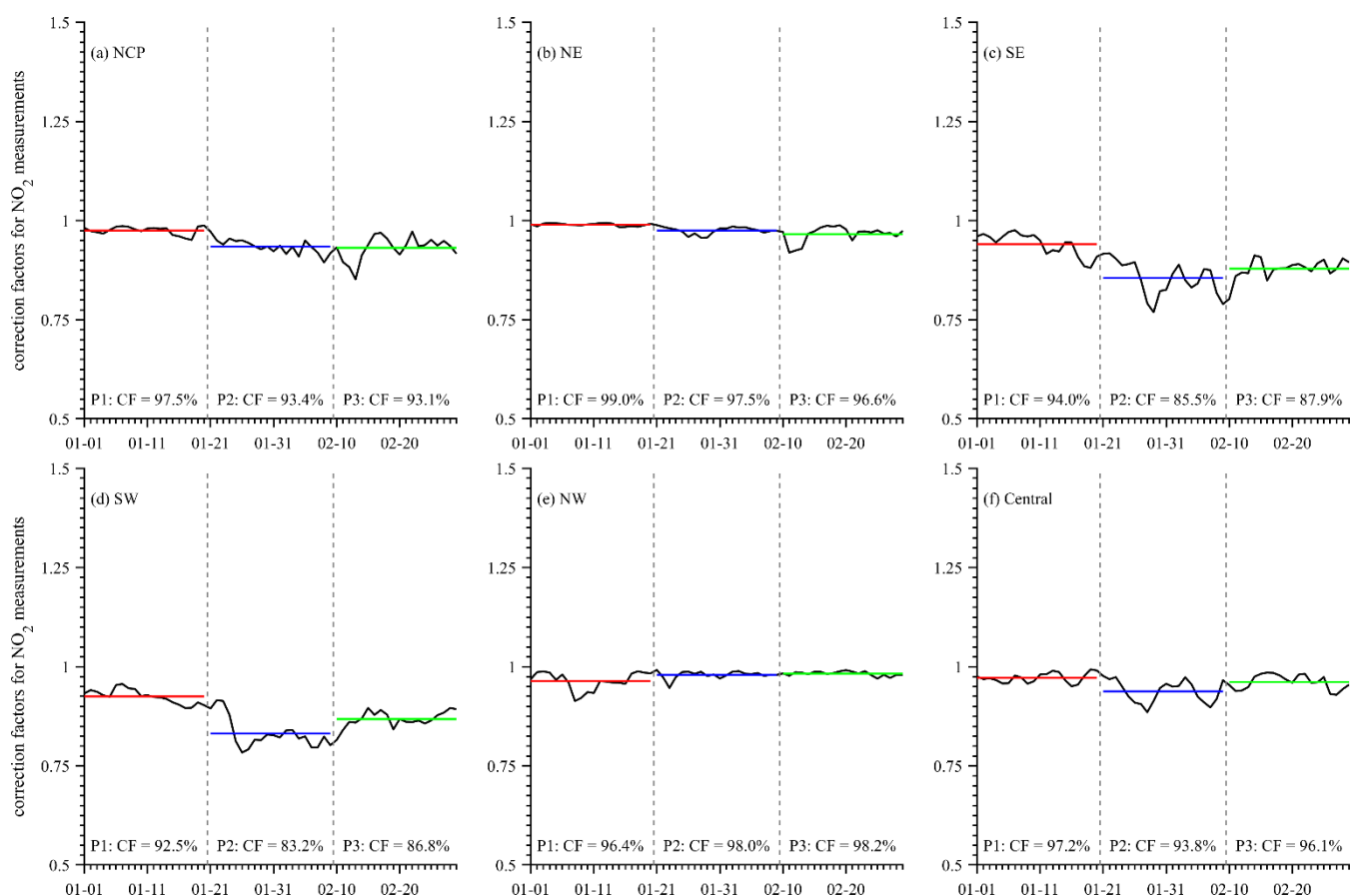

Figure R1: Time series of calculated CFs for NO_2 measurements over (a) NCP, (b) NE, (c) SE, (d) SW, (e) NW and (f) Central region during COVID-19 pandemic. The averaged CF values during different stages of COVID-19 pandemic are also labeled.

As shown in Figure R2, the overestimations were generally lower than 3 $μg/m^3$ over different

regions of China throughout the COVID-19 pandemic, which is smaller than the observation errors we assigned in the assimilation, suggesting that the observation error caused by the chemiluminescence monitor interference were contained in the assimilation. In order to quantify the influences of chemiluminescence monitor interference on the inversed NO_x emission, an additional inversion experiment was conducted based on the corrected NO_2 measurement using the calculated CF. The results suggest the chemiluminescence monitor interference in the NO_2 observations had weak impacts on the inversed NO_x emissions as seen in Fig. R3 and Fig. R4, which display the comparisons of the inversed NO_x emission with and without correction in respect of the magnitude and change ratio during different stage of COVID-19 pandemic. The differences in the magnitude of inversed NO_x emissions caused by correction were about 2–7% over the NCP, NE, NW and Central, and were about 10–13% over the SE and SW. Differences in the emission reductions of NO_x were also small, which was about 0.3 to 4.1 percentage points. Consistent with the reviewer, the result suggests that the chemiluminescence monitor interference is a potential factor that influence the inversion of NOx emission, which is a limitation of current work. However, it might not significantly influence our inversion results and the main conclusions. Considering this, we added a discussion about the effects of chemiluminescence monitor interference to inform the potential reader in the revised manuscript (please see lines 143–158) and supplement (please see lines 15–39 and Figure S16–S19).

Changes in the manuscript: lines 165–167 and lines 143-158.

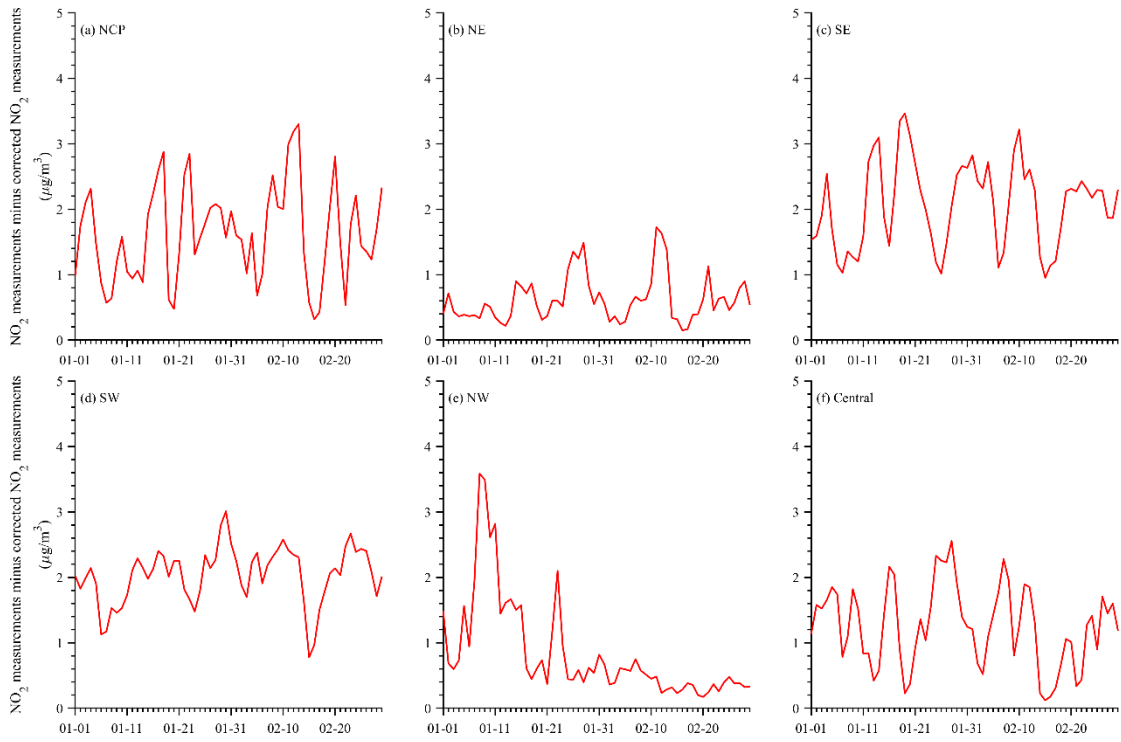**Changes in the supplement: lines 15–39 and Figure S16–S19.**

Figure R2: the difference of NO₂ measurement before and after the corrections of chemiluminescence monitor interference over (a) NCP, (b) NE, (c) SE, (d) SW, (e) NW and (f) Central during the COVID-19 period.
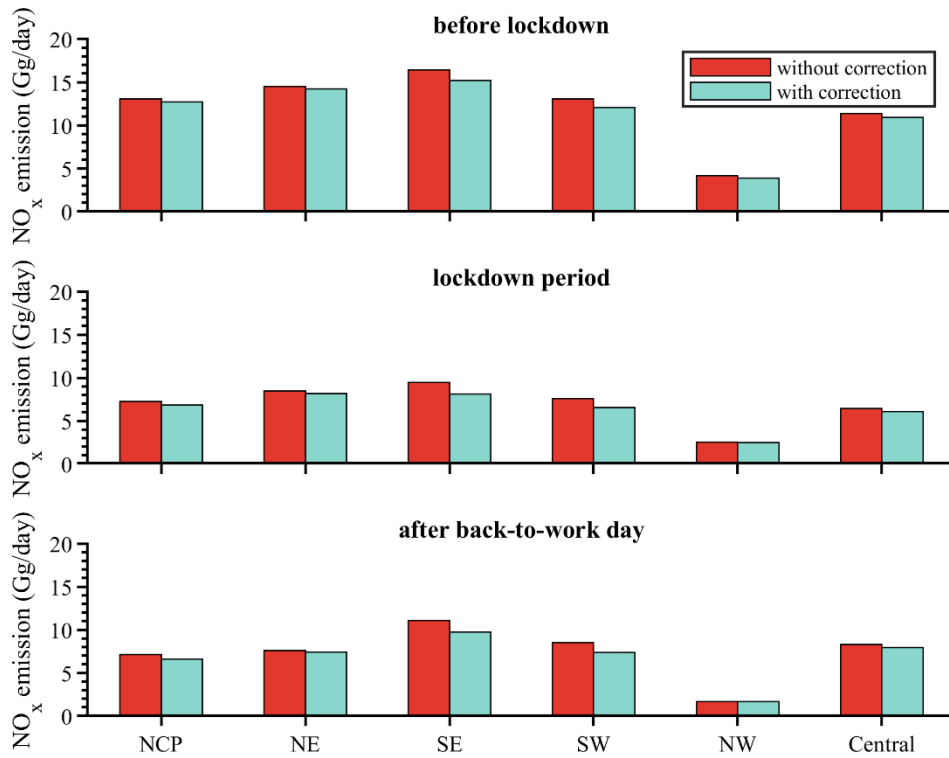

Figure R3 Comparisons of inversed NO$_x$ emissions with (blue) and without (red) correction of NO₂ measurement over different regions of China during different period of COVID-19 pandemic.
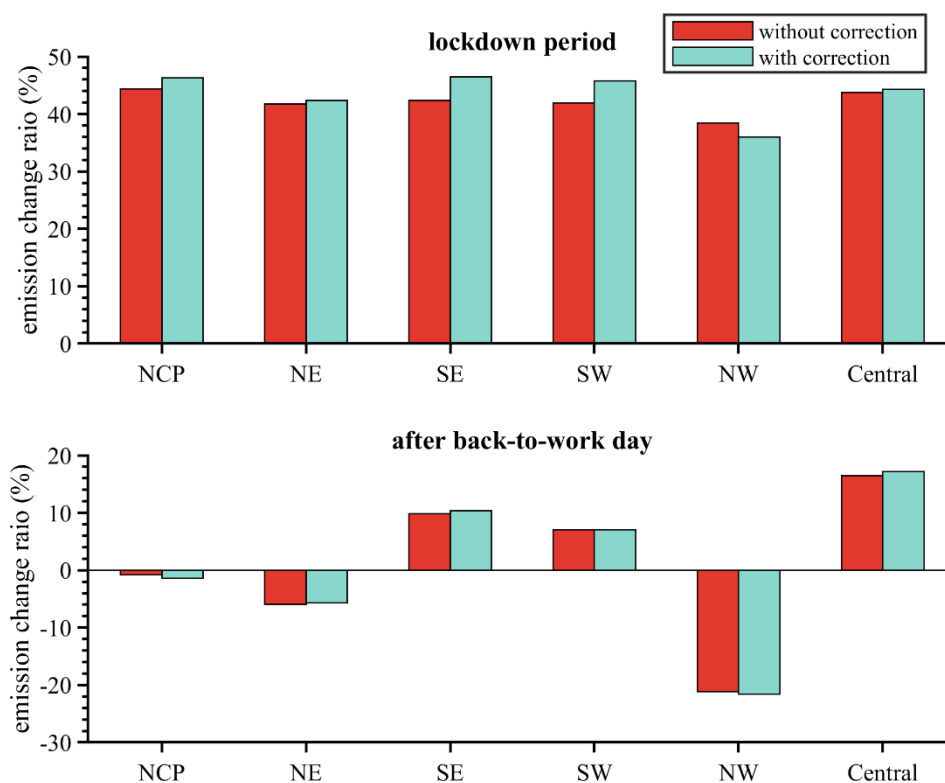
Figure R4 Comparisons of the calculated emission change of NO$_x$ emissions based on the inversion results with (blue) and without (red) correction of NO$_2$ measurement over different regions of China.

Comment 3: Line 90: Levelt et al. (2022) is not related to the emission inversion technique. The authors had better discard this paper in the manuscript.

Reply: We feel sorry for this inappropriate citation. We have removed this paper in the revised manuscript.

Changes in the manuscript: line 90.

Comment 4: Line 105: Anthropogenic and other emission inventories used in the simulations during the COVID-19 pandemic are based on 2010 or relatively long ago. These emission rates could be significantly higher than those during the COVID-19 pandemic. The higher emission rates are significantly related to the concentration of atmospheric species like O$_3$. Therefore, the authors need to justify the uses of such emission inventories in the simulations

Reply: Thanks for this important comment. We agree with the reviewer that a prior emission inventory used in our study is significantly higher than those during the COVID-19 pandemic due to the restrict emission control policy over the past decades. However, due to the lack of updated activity data and emission factors, the latest bottom-up anthropogenic emission inventory in China that were available is for the base year 2018, which could be also higher than those during COVID-19 pandemic. Considering this, we have developed the iteration emission inversion technique to address this issue. According to the inversion results, the iteration emission inversion significantly reduced the large biases in the a priori

emission inventory and is able to reproduce the emission levels during the COVID-19 pandemic. Therefore, we did not update the a priori emission inventory to more recent emission inventory during the assimilation.

To test the influences of the choice of a priori emission inventory on the inversion estimation, a new inversion run was conducted based on the a priori emission inventory for base year 2018. This new emission inventory is comprised of the anthropogenic emissions obtained from HTAPv3 (Crippa et al., 2023), the biogenic, soil and oceanic emissions obtained from the CAMS global emission inventory (https://ads.atmosphere.copernicus.eu/cdsapp#!/dataset/cams-global-emission-inventories?tab=overview, last access: March 15, 2023) and biomass burning emissions obtained from the Global Fire Assimilation System (GFAS)(Kaiser et al., 2012). The detailed steps of the new inversion estimation were same as those elucidated in Sect.2. Figure R5–7 show the comparisons of inversion results based on the a priori emissions for base 2010 with those based on the a priori emissions for 2018. The results suggest that the inversion results based on the 2010 and 2018 inventory were broadly close to each other, while the inversion results based on 2018 inventory were relatively higher than those based on 2010 inventory, reflecting the uncertainty in our inversion results caused by the choice of the a priori emission inventory. Figure R8 and R9 show the temporal variations of the multi-species' emissions during COVID-19 pandemic at the national and regional scales derived from the inversion results based on 2018 inventory, which consistently showed that the NO_x emissions decreased much larger than other species. In all, the sensitivity experiment demonstrates that the choice of a priori emission inventory may not obviously influence the main conclusion of our study, but can lead to uncertainty in the magnitude of the inversion results which is a limitation of current work. Therefore, a discussion about the influence of a priori emission inventory has been added to the revised manuscript (please see lines 492–505) and supplement (please see Figure S20–S24) to inform the potential readers.

Changes in the manuscript: lines 492–505.
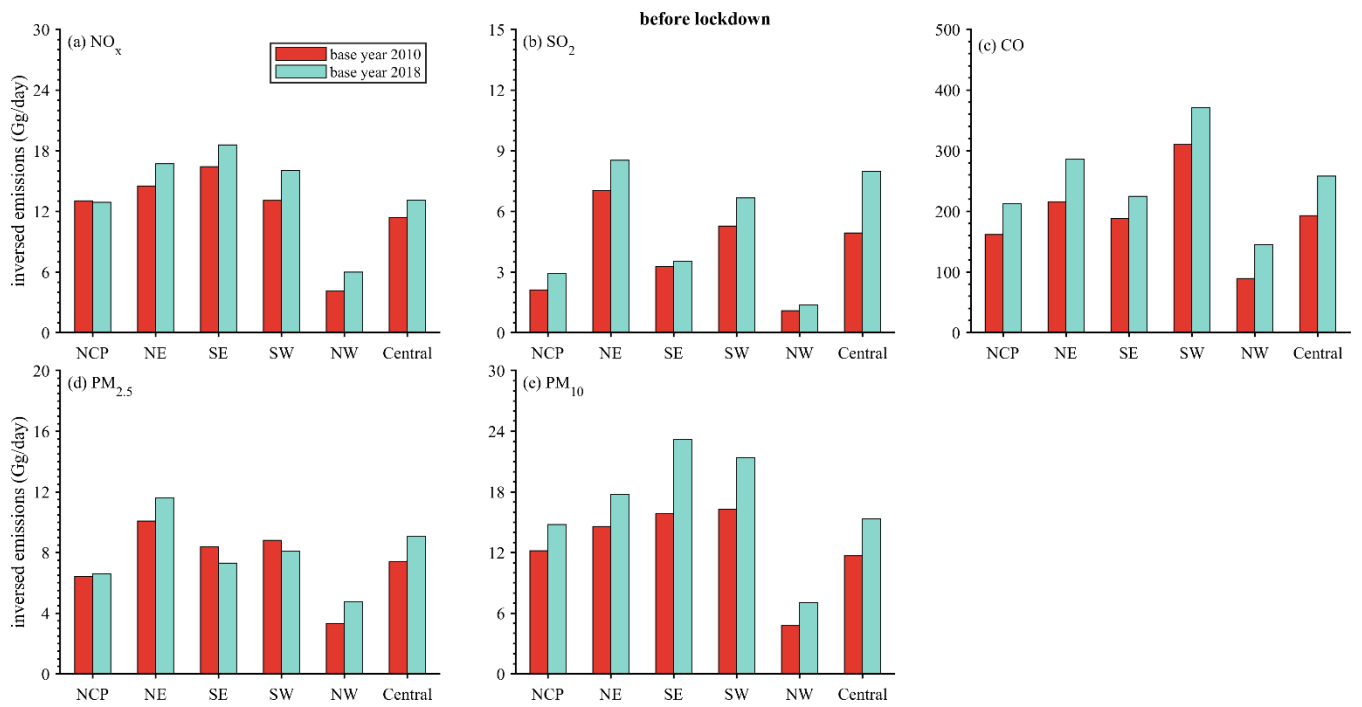
Changes in the supplement: Figure S20–S24.

Figure R5: Comparisons of the inversion estimated total emissions of (a) NO$_x$, (b) SO$_2$, (c) CO, (d) PM$_{2.5}$ and (e) PM$_{10}$ before lockdown using the a priori emission inventory for base year 2010 (read) with those using the a priori emission inventory for base 2018 (blue).

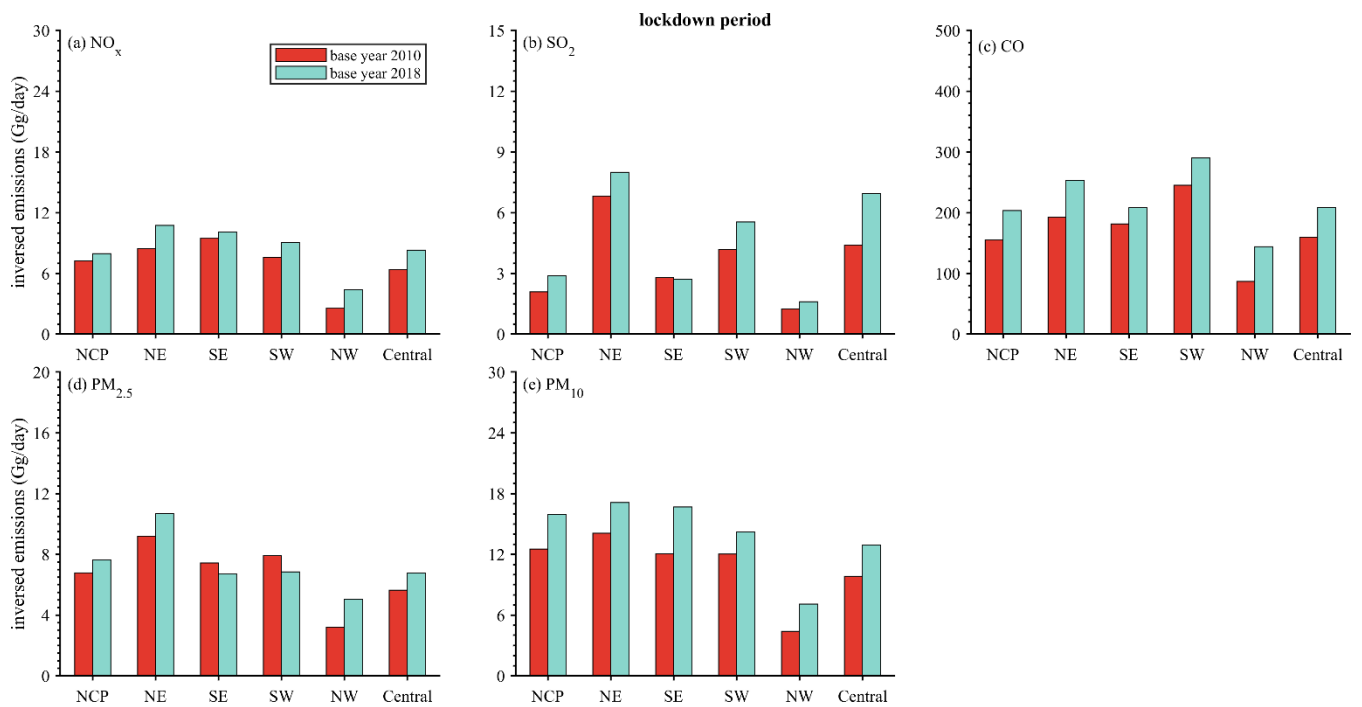
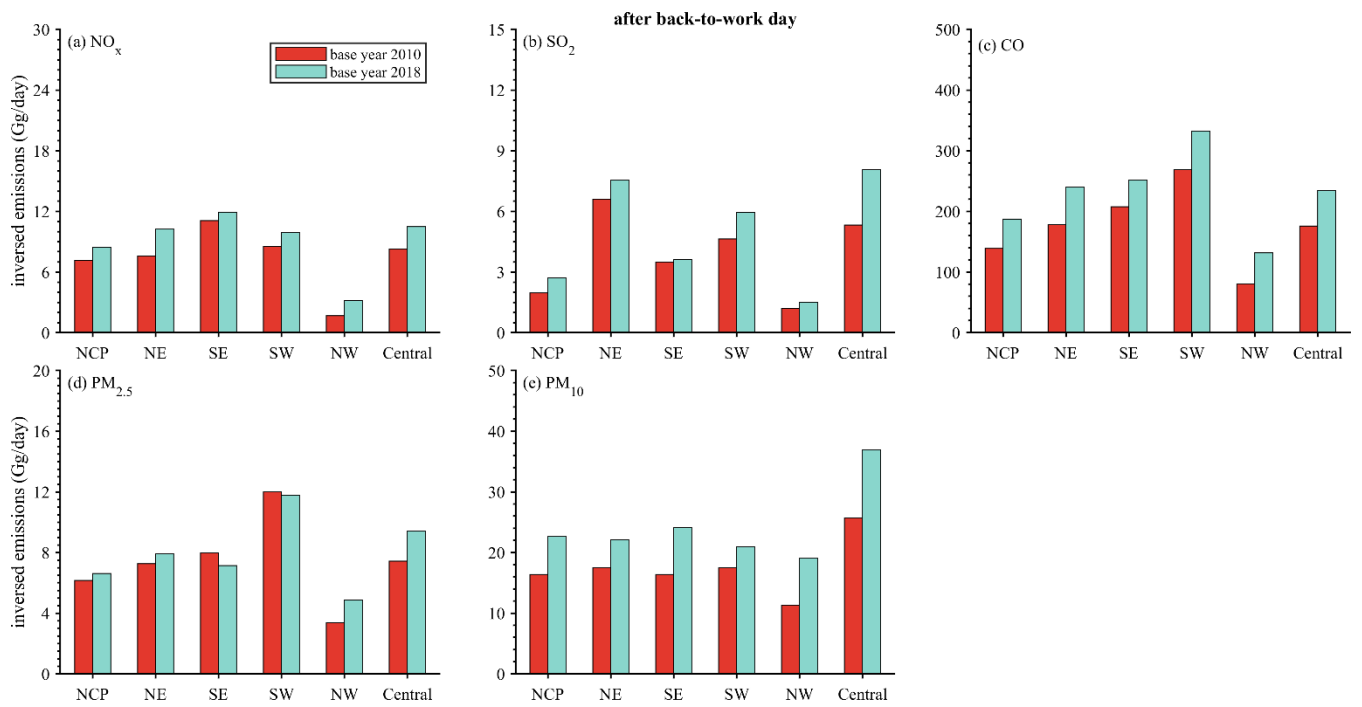**Figure R6: Same as Fig.R5 but for the p2 period (lockdown period).**

Figure R7: Same as Fig. R5 but for the P3 period (after back-to-work day).
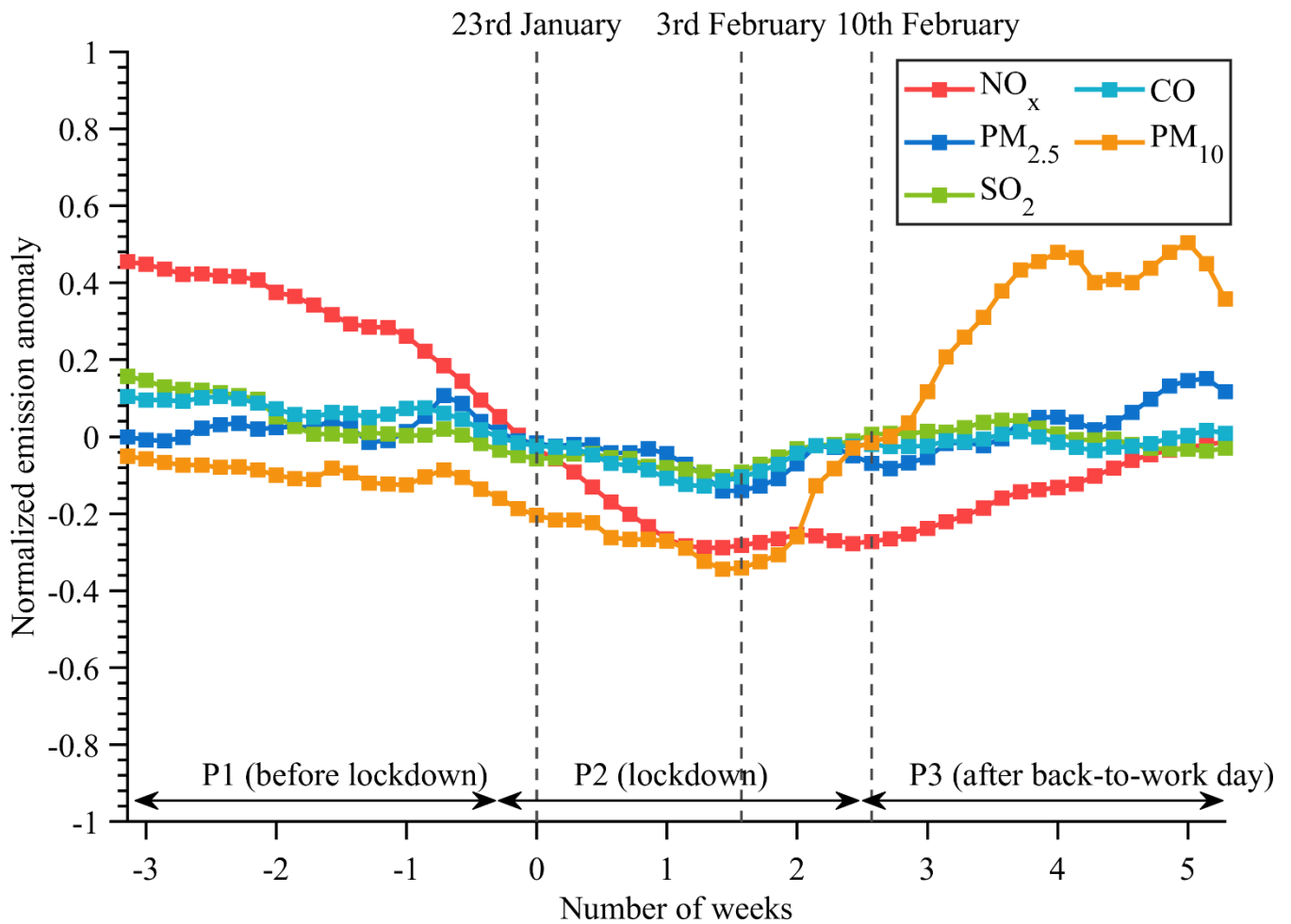

Figure R8: Time series of normalized emission anomalies estimated by inversion results for different species in China from 1st January to 29th February 2020 using the a priori emission inventory for 2018.
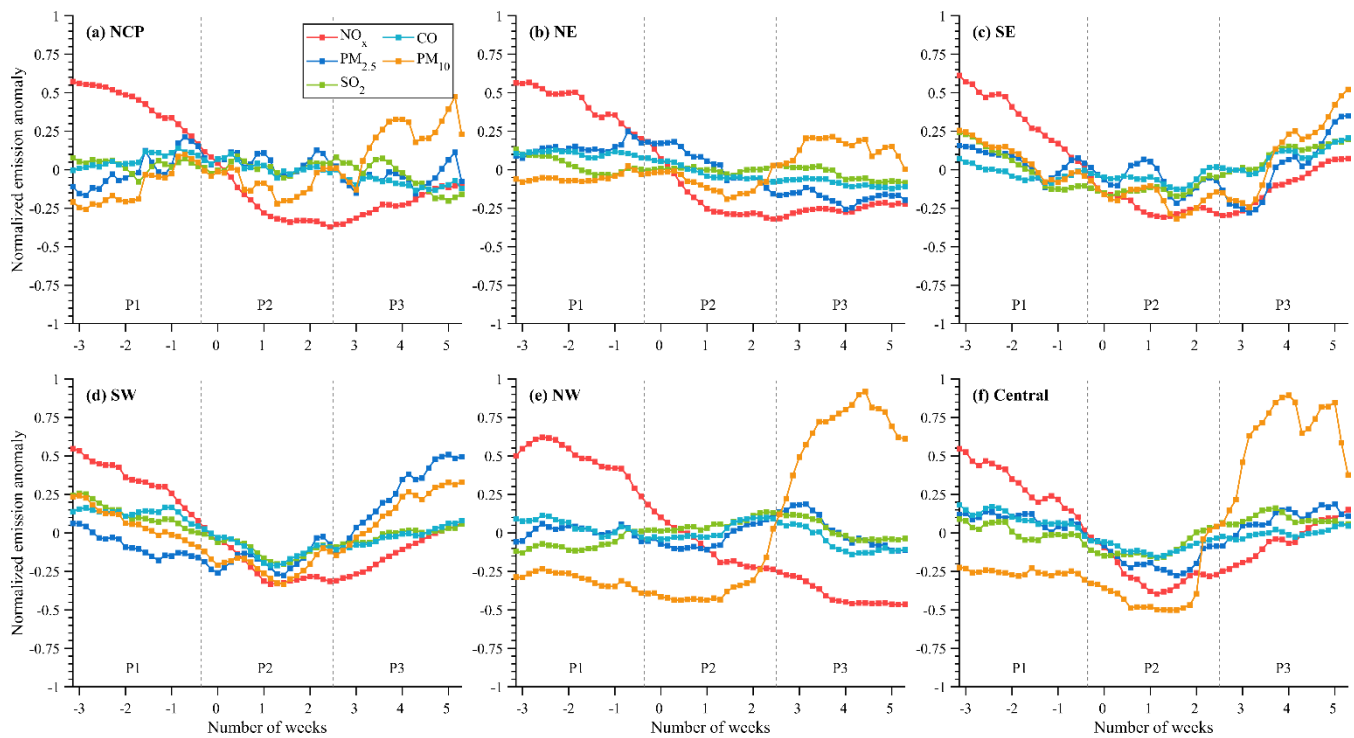
Figure R9: Time series of normalized emission anomalies estimated by inversion results for different species over (a) NCP region, (b) NE region, (c) SE region, (d) SW region, (e) NW region and (f) Central region from 1st January to 29th February 2020 using the a priori emissions for 2018.

Comment 5: Line 138: The explanation of EI and MI (from both MET and EMIS change scenarios) is rather complicated. The authors need to clarify it. Tabulating or illustrating the scenarios or cases makes it easier for the readers to understand them.

Reply: Thanks for this suggestion. We have added two tables in the revised manuscript to illustrate the different scenarios and the meaning of different items in the calculation of EI and MI (please see Table 2 and Table 3 in the revised manuscript):

Table R1 configuration of simulation scenarios

Scenarios	Meteorology input	Emission input	Purpose
BASE scenario	varied meteorological condition from pre lockdown to lockdown period	varied emission from pre-lockdown to lockdown period	To estimate the total changes of air pollutant concentrations induced by emission and meteorological change
MET change scenario	varied meteorological condition from pre-lockdown to lockdown period	constant emissions during pre-lockdown and lockdown period	To estimate the impacts of meteorological changes on the air pollutants
EMIS change scenario	constant meteorological during pre-lockdown and lockdown period	varied emission from pre-lockdown to lockdown period	To estimate the impacts of emission changes on the air pollutants

Table R2 descriptions of different items used in the calculation of meteorological-induced and emission-induced changes of air pollutant concentrations

notation	Description
MI	meteorological-induced changes of air pollutant concentrations
EI	emission-induced changes of air pollutant concentrations
$MI_{MET\ change\ scenario}$	meteorological-induced changes of air pollutant concentrations calculated by the MET change scenario
$EI_{MET\ change\ scenario}$	emission-induced changes of air pollutant concentrations calculated by total changes minus $MI_{MET\ change\ scenario}$
$EI_{EMIS\ change\ scenario}$	emission-induced changes of air pollutant concentrations calculated by the EMIS change scenario
$MI_{EMIS\ change\ scenario}$	meteorological-induced changes of air pollutant concentrations calculated by total changes minus $EI_{EMIS\ change\ scenario}$
$conc_{p1,BASE\ scenario}$	averaged concentrations of air pollutants during P1 period under the BASE scenario
$conc_{p2,BASE\ scenario}$	averaged concentrations of air pollutants during P2 period under the BASE scenario
$conc_{p1,MET\ change\ scenario}$	averaged concentrations of air pollutants during P1 period (pre-lockdown) under the MET change scenario
$conc_{p2,MET\ change\ scenario}$	averaged concentrations of air pollutants during P2 period (lockdown) under the MET change scenario
$conc_{p1,EMIS\ change\ scenario}$	averaged concentrations of air pollutants during P1 period under the EMIS change scenario
$conc_{p2,EMIS\ change\ scenario}$	averaged concentrations of air pollutants during P2 period under the EMIS change scenario
$contri_{met}$	relative contributions (%) of the meteorological variations to the changes in air pollutant concentrations
$contri_{emis}$	relative contributions (%) of the emission changes to the changes in air pollutant concentrations

Changes in the manuscript: table 2 and table 3.

Comment 6: Line 218: The authors need to define P1, P2, and P3 on Line 218, not on Line 247. Also, the authors need to add some lines for P1, P2, and P3 on the x-axis of Figure 4.

Reply: Thank you so much for your careful check. We have changed the position where the P1, P2 and P3 were defined in the revised manuscript (please see lines 104–106) and some lines for P1, P2 and P3

12

were also added on the x-axis of Figure 4 and Figure 5.

Changes in the manuscript: lines 104–106, Figure 4 and Figure 5.

Comment 7: Line 268: The performance in the O_3 simulation is relatively poor. As mentioned in the manuscript, the lower performance is related to VOC emission. Since the VOC emission used in the simulations is made for 2010, there are some time gaps. Therefore, the authors need to compare the VOC emission rates with the recent or 2019 database and then make an additional explanation of (expected) ozone concentrations.

Reply: Thanks for this comment. Following the suggestions of reviewer, we have compared the NMVOC emissions for base year 2010 with the NOVOC emissions for base year 2018. To prevent the inconsistency between different inventory, the anthropogenic part of NMVOC emissions were obtained from the HTAP_v3 inventory(Crippa et al., 2023), which is an updated version of the anthropogenic emission inventory (HTAP_v2.2) we used in our study. The biogenic part was obtained from the CAMS biogenic emissions calculated using the Model of Emissions of Gases and Aerosols from Nature (MEGAN) driven by ERA-Interim meteorological fields (Granier, C. et al., 2019). The NMVOC emissions from wildfires and biomass burning was obtained from the Global Fire Assimilation System (GFAS)(Kaiser et al., 2012). Figure R5 shows the comparisons of NMVOC emissions for base year 2010 with those for base year 2018 over different regions of China. It shows that the NMVOC emissions for base year 2010 were generally lower than those for 2018 except over the SW regions. Considering the increasing trend of NMVOC emissions in China (Li et al., 2019), the underestimates of NMVOC emissions for base year 2020 due to the use of old emission inventory may be larger. This is in line with the negative biases in the simulated O_3 concentrations over these regions. Following the suggestion of reviewer, we have clarified it in the revised manuscript (please see lines 294–297).
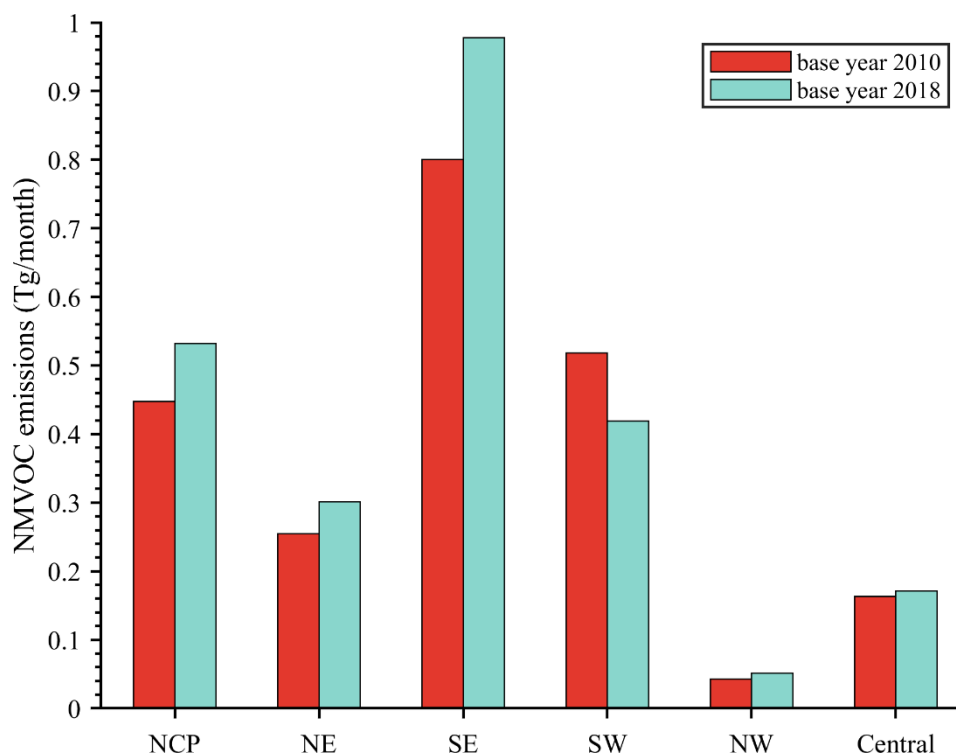
Changes in the manuscript: lines 294–297.

Figure R5 comparisons of the NMVOC emissions for base year 2010 with those for 2018 over different regions of China.

Comment 8: Line 289 & 303 – 304: The authors need to explain what causes increases in PM_{10} during the P3 in Figure 4, Figure 5e, and 5f. The authors explained these are related to the sandstorm. However, the concentration of PM_{10} during the P3 period was rather low in the NW and Central regions.

Reply: Thanks for this suggestion. The $PM_{2.5}/PM_{10}$ ratio was used to investigate the causes of the increases in PM_{10} emission in the revised manuscript, which is an indicator of the potential sources of particular matter. A lower $PM_{2.5}/PM_{10}$ ratio usually indicates significant contributions from natural sources such as dust (Wang et al., 2015; Fan et al., 2021). As we can see from Fig.R6, the $PM_{2.5}/PM_{10}$ ratio was stable during the P1 and P2 period, but it decreased substantially during the P3 period, from 0.81 to 0.48 over the NW region and from 0.77 to 0.53 over the Central region, which suggests larger contributions of dust emissions to the PM10 concentrations during the P3 period. Moreover, the NW and Central region are typical source areas of dust in China, therefore the increasing of PM_{10} emissions over NW and Central regions may be mainly related to the enhanced dust emissions. following the suggestion of reviewer, we added more explanations to the increased PM_{10} emissions over the NW and Central region in the revised manuscript (please see lines 342–348).
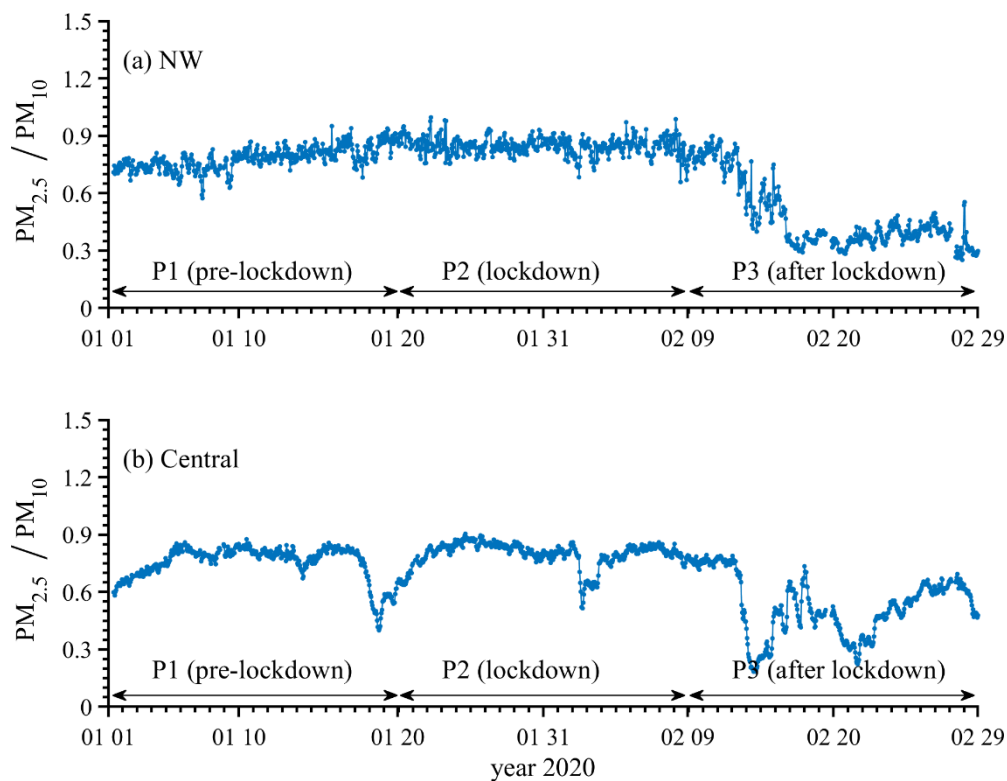
Changes in the manuscript: lines 342–348.

Figure R6 timeseries of $PM_{2.5}/PM_{10}$ ratio during COVID-19 pandemic over (a) NW and (b) Central region

Comment 9: Line 295: The explanation is not sufficient for the $PM_{2.5}$ emission increase in the NCP region. The observation done by Dai et al. (2020) was carried out at a single site in Tianjin.

Reply: Thanks for this important comment. We conducted a more detailed analysis on the possible causes of the $PM_{2.5}$ emission increases in the NCP region through literature review and analysis of the $PM_{2.5}$ compositions. Previous researches suggested that the increases of $PM_{2.5}$ emissions over the NCP region may be due to the increased emissions from industry and fireworks (Dai et al., 2020; Li et al., 2021; Ma et al., 2022; Zuo et al., 2022). Based on the measurement of stable Cu and Si isotopic signature and distinctive metal ratios in Beijing and Hebei, Zuo et al. (2022) analyzed the variations in the $PM_{2.5}$ sources in Beijing and Hebei during the COVID-19 pandemic, which provides evidences that the primary $PM_{2.5}$ emissions did not decrease in Beijing and Hebei, and that the PM-associated industrial emissions may instead increase during the lockdown period. The increased industrial heat sources detected by Li et al. (2022) based on VIIRS active fire data also supported the increased industrial emissions over the NCP region during lockdown period. Figure R7 shows the variations of the concentrations of potassium (K^+) and magnesium (Mg^{2+}) ion, two important fingerprints of the firework emissions, over the NCP region during COVID-19 pandemic. Measurement of K^+ and Mg^{2+} over the NCP region were obtained from China National Environmental Monitoring Center (CNEMC) with site distribution shown in Fig. 11. Substantial increases of K^+ and Mg^{2+} concentrations could be observed during the Spring Festival over

the NCP region, which indicates larger contributions of firework emissions to the $PM_{2.5}$ concentrations during the lockdown period. this is consistent with the field measurements in Beijing and Tianjin conducted by Ma et al. (2022) and Dai et al. (2020). These results suggested that the increased industrial $PM_{2.5}$ emissions, together with firework emissions may contribute to the increased $PM_{2.5}$ emissions over NCP region, which compensated the emission reductions from the traffic emissions. Based on this analysis, we have added more detailed discussions about the possible reason for the increases of $PM_{2.5}$ emissions over the NCP region in the revised manuscript (please see lines 322–333) and supplement (please see Figure S15).

Changes in the manuscript: lines 322–333.

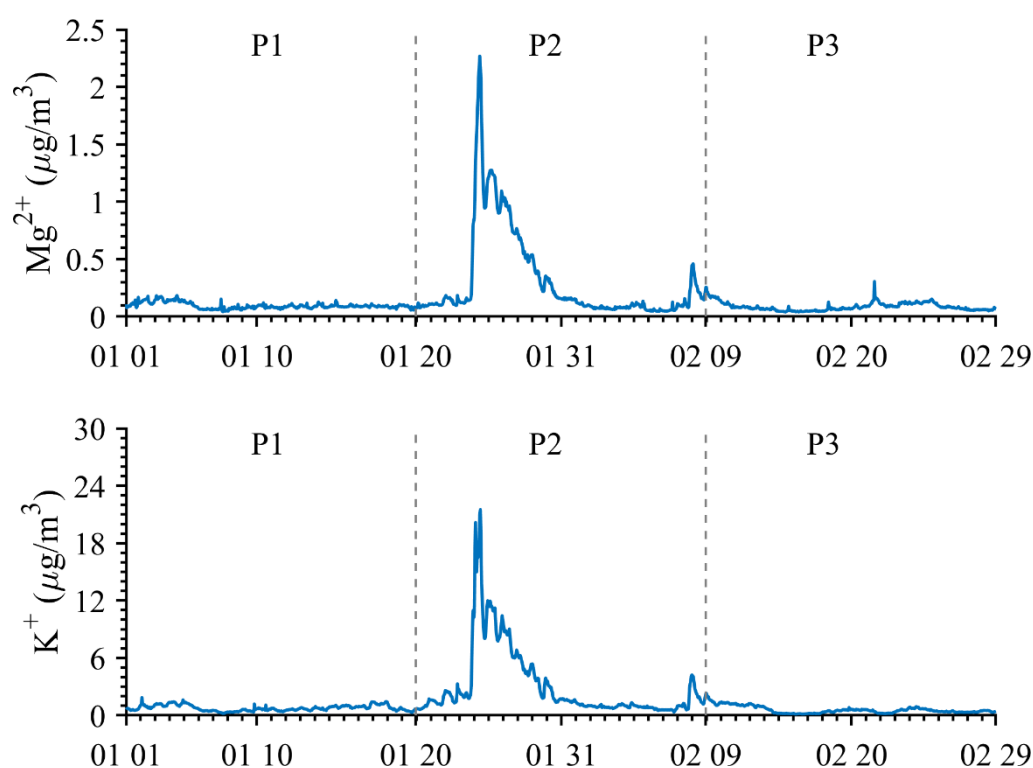**Changes in the supplement: Figure S15.**

Figure R7: Timeseries of averaged concentrations of potassium and magnesium ion during COVID-19 pandemic over the NCP region.

Comment 10: Line 340: The authors also need to mention that the O_3 is under-simulated in all regions (refer to Figure S6).

Reply: Thanks for this comment. The underestimations of the O_3 have been pointed out in the revised manuscript (please see lines 389).

Changes in the manuscript: line 389.

Minor comments:

Comment 11: Line 32: measurement -- > measure or measures

Reply: Done.

Changes in the manuscript: line 31.

Comment 12: Line 33: remove 'both'.

Reply: Done.

Changes in the manuscript: line 32.

Comment 13: Line 261. It is probably Table S1, not Table S4

Reply: Done.

Changes in the manuscript: line 284.

Comment 13: Lines 277 and 280: The authors need to confirm the numbers in these lines (and Table 2).

Reply: Thanks a lot for your careful check. We have corrected the wrong number in lines 277 and 280. Please see lines 305 and 308 in the revised manuscript.

Changes in the manuscript: lines 305 and 308.

References

Cooper, M. J., Martin, R. V., McLinden, C. A., and Brook, J. R.: Inferring ground-level nitrogen dioxide concentrations at fine spatial resolution applied to the TROPOMI satellite instrument, Environ. Res. Lett., 15, 12, https://doi.org/10.1088/1748-9326/aba3a5, 2020.

Crippa, M., Guizzardi, D., Butler, T., Keating, T., Wu, R., Kaminski, J., Kuenen, J., Kurokawa, J., Chatani, S., Morikawa, T., Pouliot, G., Racine, J., Moran, M. D., Klimont, Z., Manseau, P. M., Mashayekhi, R., Henderson, B. H., Smith, S. J., Suchyta, H., Muntean, M., Solazzo, E., Banja, M., Schaaf, E., Pagani, F., Woo, J. H., Kim, J., Monforti-Ferrario, F., Pisoni, E., Zhang, J., Niemi, D., Sassi, M., Ansari, T., and Foley, K.: HTAP_v3 emission mosaic: a global effort to tackle air quality issues by quantifying global anthropogenic air pollutant sources, Earth Syst. Sci. Data Discuss., 2023, 1-34, https://doi.org/10.5194/essd-2022-442, 2023.

Dai, Q., Liu, B., Bi, X., Wu, J., Liang, D., Zhang, Y., Feng, Y., and Hopke, P. K.: Dispersion Normalized PMF Provides Insights into the Significant Changes in Source Contributions to PM2.5 after the COVID-19 Outbreak, Environ. Sci. Technol., 54, 9917-9927, https://doi.org/10.1021/acs.est.0c02776, 2020.

Dunlea, E. J., Herndon, S. C., Nelson, D. D., Volkamer, R. M., San Martini, F., Sheehy, P. M., Zahniser, M. S., Shorter, J. H., Wormhoudt, J. C., Lamb, B. K., Allwine, E. J., Gaffney, J. S., Marley, N. A., Grutter, M., Marquez, C., Blanco, S., Cardenas, B., Retama, A., Villegas, C. R. R., Kolb, C. E., Molina, L. T., and Molina, M. J.: Evaluation of nitrogen dioxide chemiluminescence monitors in a polluted urban environment, Atmos. Chem. Phys., 7, 2691-2704, https://doi.org/10.5194/acp-7-2691-2007, 2007.

Evensen, G.: The Ensemble Kalman Filter for Combined State and Parameter Estimation MONTE CARLO TECHNIQUES FOR DATA ASSIMILATION IN LARGE SYSTEMS, IEEE Control Syst. Mag., 29, 83-104, https://doi.org/10.1109/mcs.2009.932223, 2009.

Fan, H., Zhao, C., Yang, Y., and Yang, X.: Spatio-Temporal Variations of the PM$_{2.5}$/PM$_{10}$ Ratios and Its Application to Air Pollution Type Classification in China, Front. Environ. Sci., 9, https://doi.org/10.3389/fenvs.2021.692440, 2021.

Feng, S., Jiang, F., Wang, H., Wang, H., Ju, W., Shen, Y., Zheng, Y., Wu, Z., and Ding, A.: NOx Emission Changes Over China During the COVID-19 Epidemic Inferred From Surface NO2 Observations, Geophys. Res. Lett., 47, e2020GL090080, https://doi.org/10.1029/2020gl090080, 2020.

He, T. L., Jones, D. B. A., Miyazaki, K., Bowman, K. W., Jiang, Z., Chen, X., Li, R., Zhang, Y., and Li, K.: Inverse modelling of Chinese NOx emissions using deep learning: integrating in situ observations with a satellite-based chemical reanalysis, Atmos. Chem. Phys., 22, 14059-14074, https://doi.org/10.5194/acp-22-14059-2022, 2022.

Hu, Y., Zang, Z., Ma, X., Li, Y., Liang, Y., You, W., Pan, X., and Li, Z.: Four-dimensional variational assimilation for SO2 emission and its application around the COVID-19 lockdown in the spring 2020 over China, Atmos. Chem. Phys., 22, 13183-13200, https://doi.org/10.5194/acp-22-13183-2022, 2022.

Kaiser, J. W., Heil, A., Andreae, M. O., Benedetti, A., Chubarova, N., Jones, L., Morcrette, J. J., Razinger, M., Schultz, M. G., Suttie, M., and van der Werf, G. R.: Biomass burning emissions estimated with a global fire assimilation system based on observed fire radiative power, Biogeosciences, 9, 527-554, https://doi.org/10.5194/bg-9-527-2012, 2012.

Lamsal, L. N., Martin, R. V., van Donkelaar, A., Steinbacher, M., Celarier, E. A., Bucsela, E., Dunlea, E. J., and Pinto, J. P.: Ground-level nitrogen dioxide concentrations inferred from the satellite-borne Ozone Monitoring Instrument, J. Geophys. Res.-Atmos., 113, https://doi.org/10.1029/2007JD009235, 2008.

Li, B., Fan, J., Han, L., Sun, G., Zhang, D., and Zhang, P.: An Industrial Heat Source Extraction Method: BP Neural Network Using Temperature Feature Template (in Chinese with English abstract), Journal of Geo-Information Science, 24, 533-545, 2022.

Li, M., Zhang, Q., Zheng, B., Tong, D., Lei, Y., Liu, F., Hong, C. P., Kang, S. C., Yan, L., Zhang, Y. X., Bo, Y., Su, H., Cheng, Y. F., and He, K. B.: Persistent growth of anthropogenic non-methane volatile organic compound (NMVOC) emissions in China during 1990-2017: drivers, speciation and ozone formation potential, Atmos. Chem. Phys., 19, 8897-8913, https://doi.org/10.5194/acp-19-8897-2019, 2019.

Li, R., Tao, M. H., Zhang, M. G., Chen, L. F., Wang, L. L., Wang, Y., He, X. J., Wei, L. F., Mei, X., and Wang, J.: Application Potential of Satellite Thermal Anomaly Products in Updating Industrial Emission Inventory of China, Geophys. Res. Lett., 48, 7, https://doi.org/10.1029/2021gl092997, 2021.

Ma, C. Q., Wang, T. J., Mizzi, A. P., Anderson, J. L., Zhuang, B. L., Xie, M., and Wu, R. S.: Multiconstituent Data Assimilation With WRF-Chem/DART: Potential for Adjusting Anthropogenic Emissions and Improving Air Quality Forecasts Over Eastern China, J. Geophys. Res.-Atmos., 124, 7393-7412, https://doi.org/10.1029/2019jd030421, 2019.

Ma, T., Duan, F. K., Ma, Y. L., Zhang, Q. Q., Xu, Y. Z., Li, W. G., Zhu, L. D., and He, K. B.: Unbalanced emission reductions and adverse meteorological conditions facilitate the formation of secondary pollutants during the COVID-19 lockdown in Beijing, Sci. Total Environ., 838, 8, https://doi.org/10.1016/j.scitotenv.2022.155970, 2022.

Miyazaki, K. and Eskes, H.: Constraints on surface NOx emissions by assimilating satellite observations of multiple species, Geophys. Res. Lett., 40, 4745-4750, https://doi.org/10.1002/grl.50894, 2013.

Miyazaki, K., Eskes, H. J., and Sudo, K.: Global NOx emission estimates derived from an assimilation of OMI tropospheric NO2 columns, Atmos. Chem. Phys., 12, 2263-2288, https://doi.org/10.5194/acp-12-2263-2012, 2012.

Miyazaki, K., Eskes, H., Sudo, K., Boersma, K. F., Bowman, K., and Kanaya, Y.: Decadal changes in global surface NOx emissions from multi-constituent satellite data assimilation, Atmos. Chem. Phys., 17, 807-837, https://doi.org/10.5194/acp-17-807-2017, 2017.

Peng, Z., Lei, L. L., Liu, Z. Q., Su, J. N., Ding, A. J., Ban, J. M., Chen, D., Kou, X. X., and Chu, K. K.: The impact of multi-species surface chemical observation assimilation on air quality forecasts in China, Atmos. Chem. Phys., 18, 18, https://doi.org/10.5194/acp-18-17387-2018, 2018.

Skachko, S., Errera, Q., Ménard, R., Christophe, Y., and Chabrillat, S.: Comparison of the ensemble Kalman filter and 4D-Var assimilation methods using a stratospheric tracer transport model, Geosci. Model Dev., 7, 1451-1465, https://doi.org/10.5194/gmd-7-1451-2014, 2014.

Streets, D. G., Canty, T., Carmichael, G. R., de Foy, B., Dickerson, R. R., Duncan, B. N., Edwards, D. P., Haynes, J. A., Henze, D. K., Houyoux, M. R., Jacob, D. J., Krotkov, N. A., Lamsal, L. N., Liu, Y., Lu, Z., Martin, R. V., Pfister, G. G., Pinder, R. W., Salawitch, R. J., and Wecht, K. J.: Emissions estimation from satellite retrievals: A review of current capability, Atmos. Environ., 77, 1011-1042, https://doi.org/10.1016/j.atmosenv.2013.05.051, 2013.

Wang, Y. Q., Zhang, X. Y., Sun, J. Y., Zhang, X. C., Che, H. Z., and Li, Y.: Spatial and temporal variations of the concentrations of PM_{10}, $PM_{2.5}$ and PM_1 in China, Atmos. Chem. Phys., 15, 13585-13598, https://doi.org/10.5194/acp-15-13585-2015, 2015.

Zhang, Q., Pan, Y., He, Y., Walters, W. W., Ni, Q., Liu, X., Xu, G., Shao, J., and Jiang, C.: Substantial nitrogen oxides emission reduction from China due to COVID-19 and its impact on surface ozone and aerosol pollution, Sci. Total Environ., 753, 142238, https://doi.org/10.1016/j.scitotenv.2020.142238, 2021.

Zhang, R. X., Zhang, Y. Z., Lin, H. P., Feng, X., Fu, T. M., and Wang, Y. H.: NOx Emission Reduction and Recovery during COVID-19 in East China, Atmosphere, 11, 15, https://doi.org/10.3390/atmos11040433, 2020.

Zuo, P. J., Zong, Z., Zheng, B., Bi, J. Z., Zhang, Q. H., Li, W., Zhang, J. W., Yang, X. Z., Chen, Z. G., Yang, H., Lu, D. W., Zhang, Q. H., Liu, Q., and Jiang, G. B.: New Insights into Unexpected Severe PM2.5 Pollution during the SARS and COVID-19 Pandemic Periods in Beijing, Environ. Sci. Technol., 56, 155-164, https://doi.org/10.1021/acs.est.1c05383, 2022.

Response to Referee #2 (acp-2022-729)

We Thank Reviewer for his/her constructive comments

Responses to the Specific comments

General comments: This manuscript evaluates the changes in air quality during the COVID-19 lockdown by dividing them into meteorological and emissions parts. The authors specifically assessed the impact of emission reduction during the lockdown using a multi-air pollutant inversion system and observational data, which is a unique approach compared to previous studies. The findings from this study will be valuable in evaluating the effectiveness of emission reduction policies by policymakers in polluted regions, including China. However, to be published in ACP, the authors must address the following issues:

Reply: The authors appreciate the reviewer for his/her constructive suggestions. In the revised manuscript we have considered each comment for improvement, revision, and correction. Please refer to our responses for more details given below.

Comment 1: Line 39: During the COVID-19 period, a haze event also occurred. However, the use of the term "COVID-19 haze" may convey the notion that the pandemic was the cause of the haze phenomenon. Thus, the authors should choose terms more carefully.

Reply: Thanks for pointing out this issue. The "COVID-19 haze" has been replaced by "unexpected $PM_{2.5}$ pollution during the COVID-19 lockdown" in the revised manuscript.

Comment 2: Lines 128-129: Despite removing unrealistic observations through the Wu et al. (2018) method, some extreme values persist in the time-series plots (e.g., Figures 3(b), S1(b), and S2(b)). Hence, the authors should thoroughly verify that the raw data has been properly filtered.

Reply: Thanks for this important comment. We have checked the quality of observation data we used in the assimilation. According to Fig. 3(b), S1(b) and S2(b), the possible extreme values for $PM_{2.5}$, PM_{10} and SO_2 mainly occurred over the NE region around 25th January. Figure R1(a) shows the spatial distributions of daily averaged $PM_{2.5}$ concentrations over the NE region. Obvious high $PM_{2.5}$ concentrations could be found at multiple monitoring sites over Liaoning province, where the $PM_{2.5}$ concentrations increased sharply (over 400 $\mu g/m^3$) at the night of 24th January and early morning of 25th January (Fig. R1(b)). Same phenomena also occurred in the city Baotou at Inner Mongolia (Fig.R1(c)). Considering that the 24th January was the 2020 Chinese New Year Eve and there are traditions of setting

fireworks at the night of that day, the peak PM$_{2.5}$ concentrations at the night of 24th January may be related to the firework emissions. Meanwhile, there were multiple sites that showed same signals of high PM$_{2.5}$ concentrations. Thus, we think the high PM$_{2.5}$ concentrations during 24th January is reasonable, and did not treat them as outliers. Similar conclusions can be drawn for PM$_{10}$ and SO$_2$, as seen in Fig. R2 and R3.
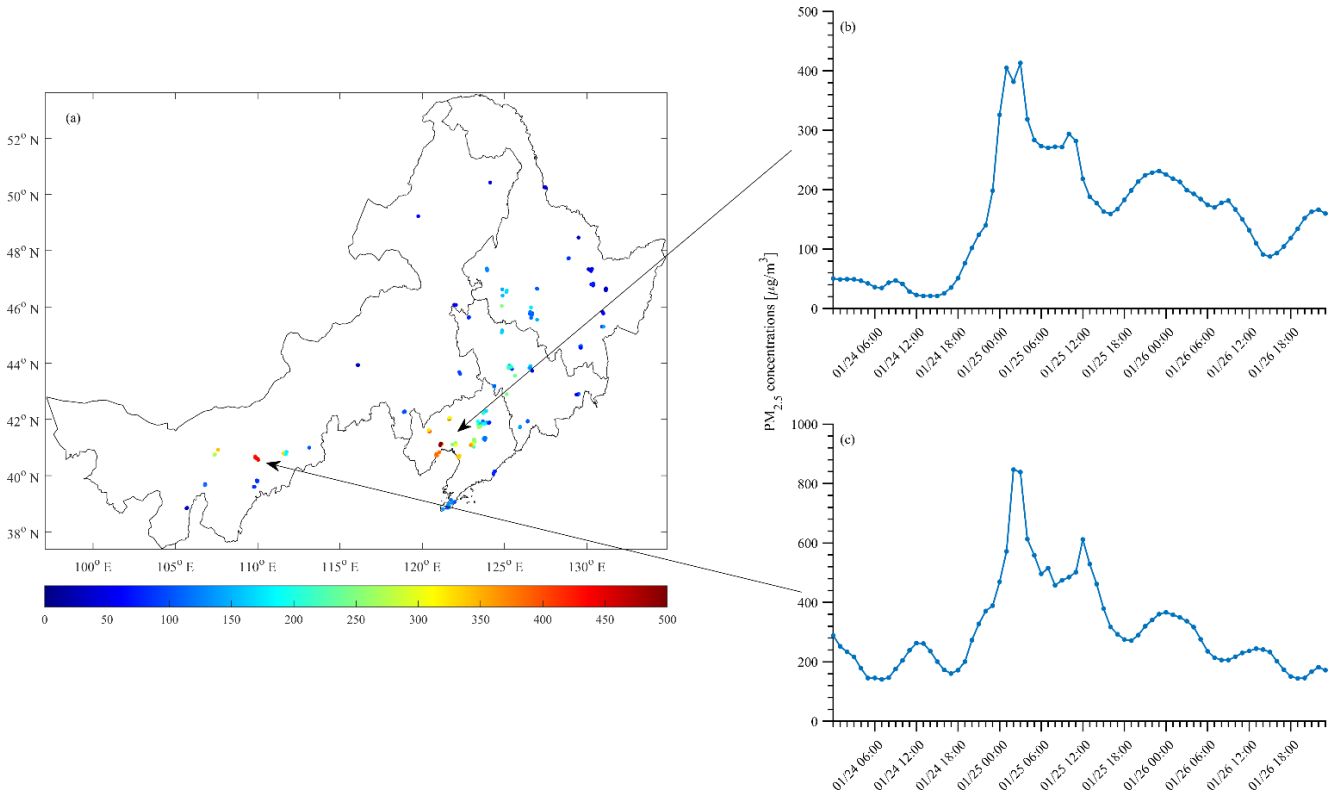

Figure R1: (a) spatial distribution of daily averaged PM$_{2.5}$ concentrations over the NE region at 25th January 2020, and the time series of averaged PM2.5 concentrations at (b) Liaoning province and (c) the city of Baotou at Inner Mongolia from 24th to 26th January 2020.
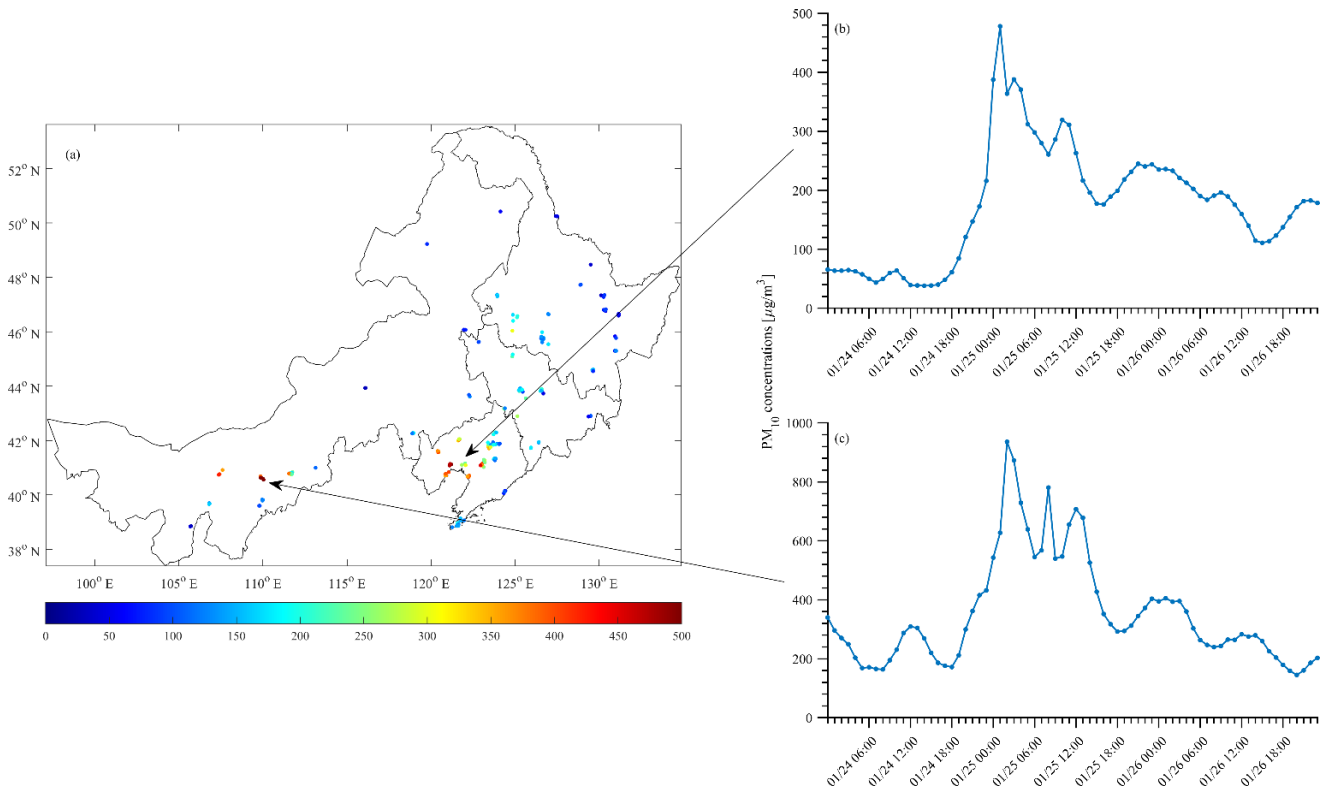
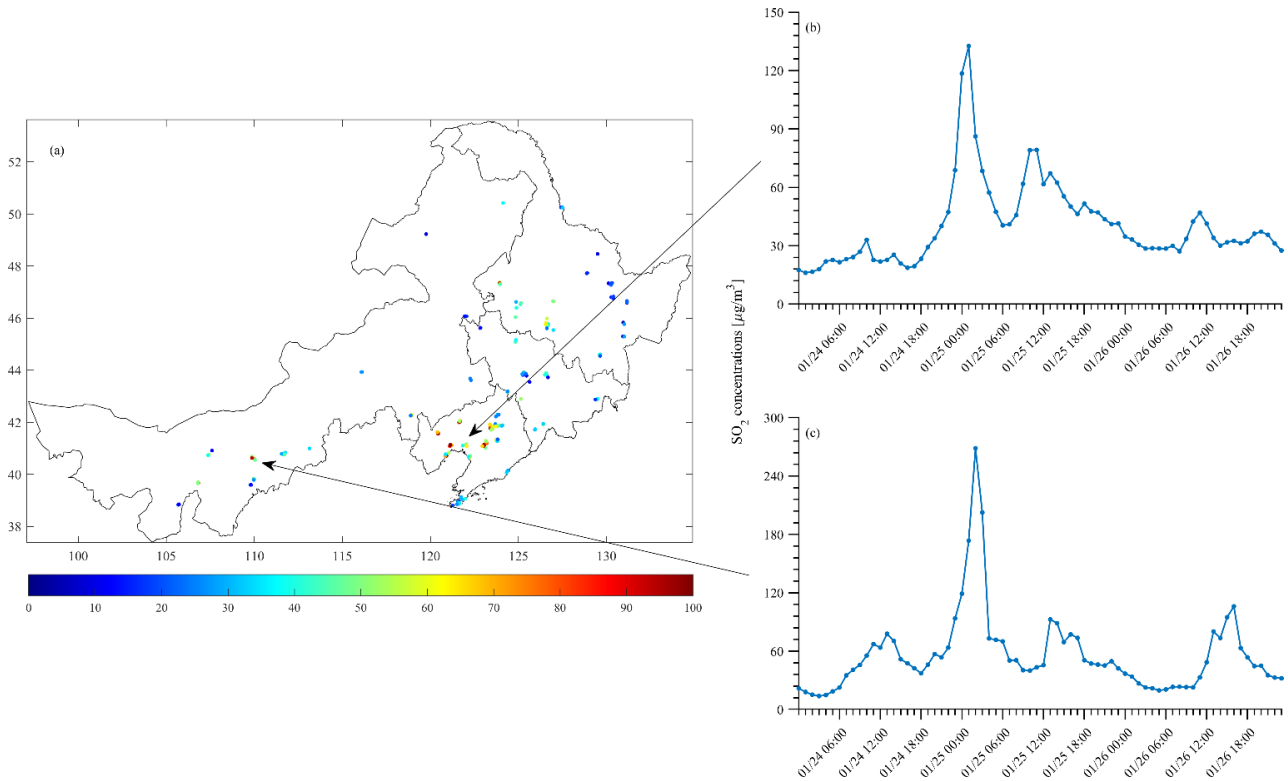**Figure R2: Same as Fig. R1 but for PM₁₀ concentrations**

Figure R3: Same as Fig. R1 but for SO₂ concentrations

Comment 3: Lines 208-242: (Section 2.4) The authors assess both the MI and EI approaches for decreasing nonlinear effects. If the extent of nonlinearity (or sensitivity) demonstrated by the two methods is documented in the paper, it can provide a helpful reference for future research.

Reply: Thanks for the suggestion. We analyzed the differences between the MI and EI method in the revised manuscript (please see lines 393–398) and supplement (please see Figure S13 and S14). According to Figure R4 and R5, the calculated MI and EI changes of PM₂.₅ and O₃ concentrations were consistent with each other over the Beijing and the NCP region, and indicates similar conclusions. The differences of calculated MI and EI were within 2 $\mu g/m^3$ for PM₂.₅ concentrations, which were small in this application. In terms of O₃ concentrations, the differences were larger, which were around 5 $\mu g/m^3$ over the Beijing and NCP region. In addition, the sign of calculated MI using EMIS change scenario and MET change scenario were opposite although both suggested weak contributions of meteorological variation to the changes of O₃ concentrations, suggesting that the calculated MI and EI changes of O₃ concentrations could be more sensitive to the used scenarios. This may be due to the stronger nonlinearity of O₃ concentrations to the meteorology and emissions.

Changes in the manuscript: lines 393–398.

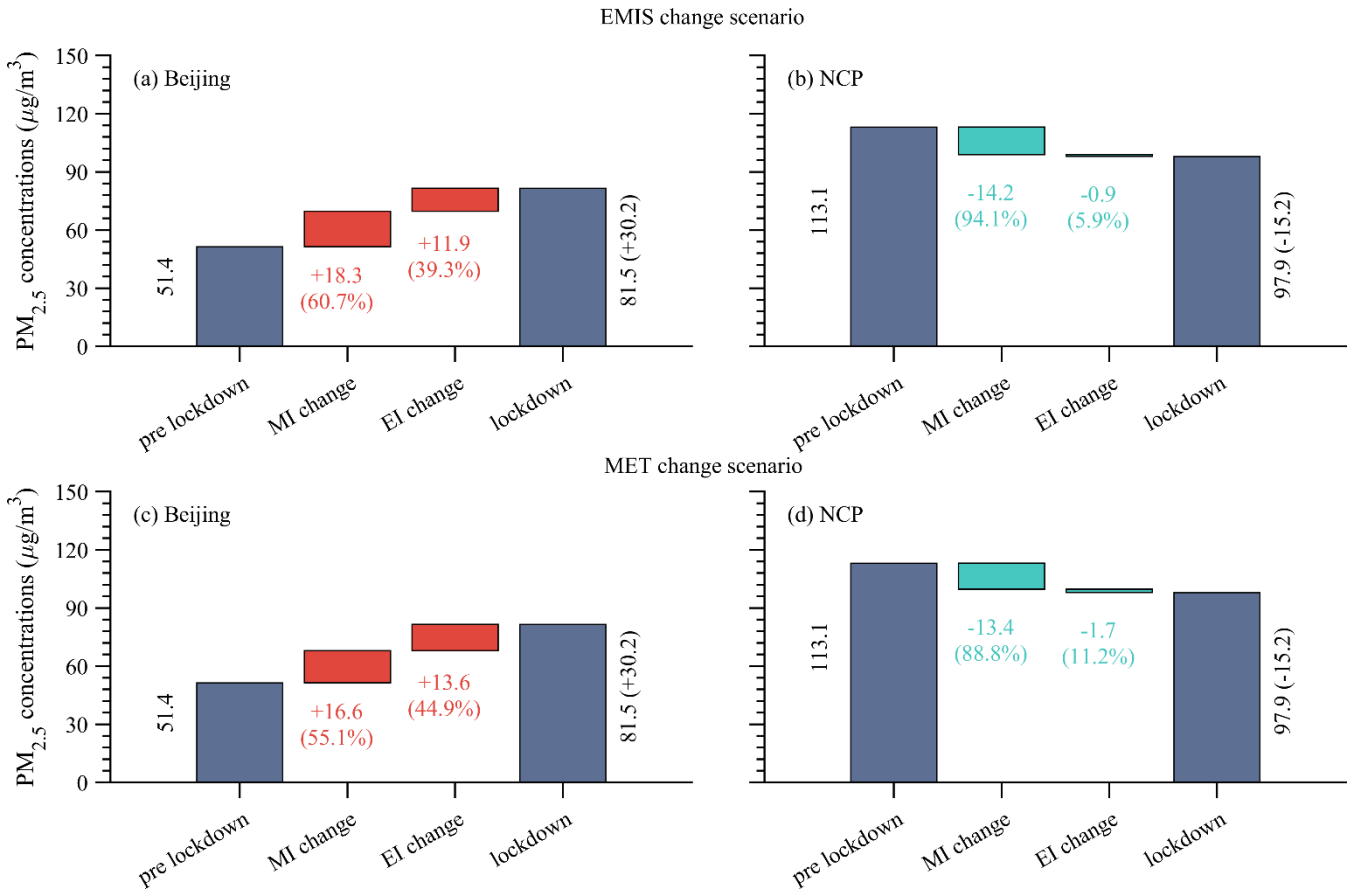**Changes in the supplement: Figure S13 and Figure S14.**

Figure R4: The calculated MI and EI changes of PM$_{2.5}$ concentrations over the (a, c) Beijing and (b, d) the NCP region using the EMIS change scenario (upper panel) and MET change scenario (lower panel).
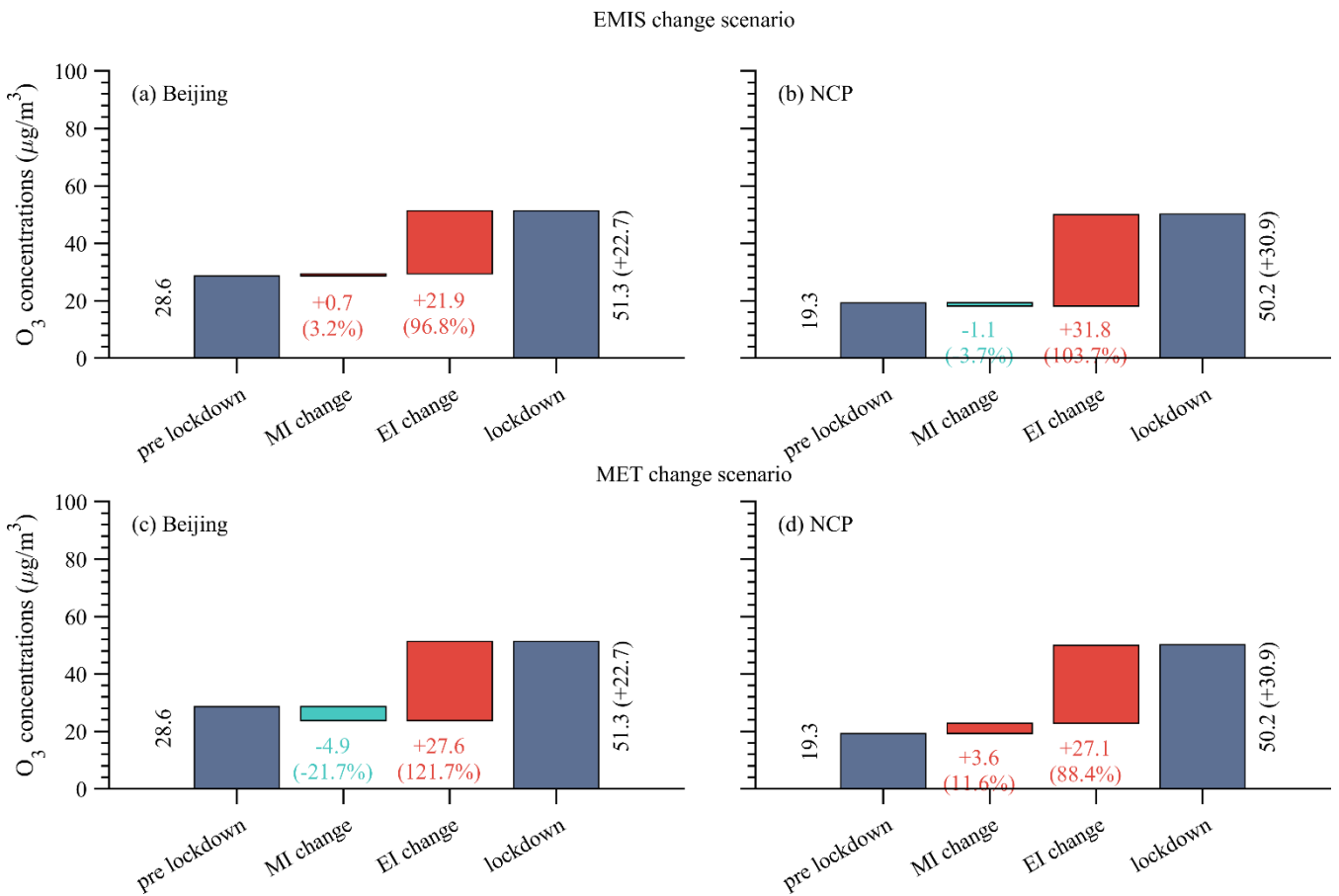

Figure R5: Same as Fig. R4 but for O$_3$ concentrations.

Comment 4: Lines 302-304: The authors posit that the rise in PM_{10} emissions in the NW and central regions during P3 is due to sandstorms but do not provide clear evidence. Furthermore, the simulation using a priori in the central region does not show a significant deviation from observation. Thus, the authors must provide further evidence for the sandstorm hypothesis.

Reply: Thanks for raising this issue. As we illustrated in Sect. 2.3 (lines 215–217 and table 1), the PM_{10} emissions were calculated by the sum of the emissions of $PM_{2.5}$ and PMC (coarse mode unspeciated aerosol) which were respectively constrained by the concentrations of $PM_{2.5}$ and $PM_{10-2.5}$. As we can see from Fig. R6, there were significantly larger deviations in the simulated PM_{10} – $PM_{2.5}$ concentrations from the observations over the Central region during the P3 period, which led to the rise in PM_{10} emissions over there. However, as the reviewer mentioned, the a priori PM_{10} simulation does not show a significant deviation from observations (Figure S2(f)), this may due to that the underestimations of $PM_{10-2.5}$ were partly compensated by the overestimated $PM_{2.5}$ concentrations over the Central region (Fig. S1(f)).

Meanwhile, we used the $PM_{2.5}/PM_{10}$ ratio to investigate the potential causes of the increases in PM_{10} emission over the NW and Central regions in the revised manuscript, which is an indicator of the potential sources of particular matter. A lower $PM_{2.5}/PM_{10}$ ratio usually indicates significant contributions from natural sources such as dust (Wang et al., 2015; Fan et al., 2021). As we can see from Fig.R7, the $PM_{2.5}/PM_{10}$ ratio was stable during the P1 and P2 period, but it decreased substantially during the P3 period, from 0.81 to 0.48 over the NW region and from 0.77 to 0.53 over the Central region, which suggests larger contributions of dust emissions to the PM10 concentrations during the P3 period. Moreover, the NW and Central region are typical source areas of dust in China, therefore the increasing of PM_{10} emissions over NW and Central regions may be mainly related to the enhanced dust emissions. following the suggestion of reviewer, we added more explanations to the increased PM_{10} emissions over the NW and Central region in the revised manuscript (please see lines 342–348).
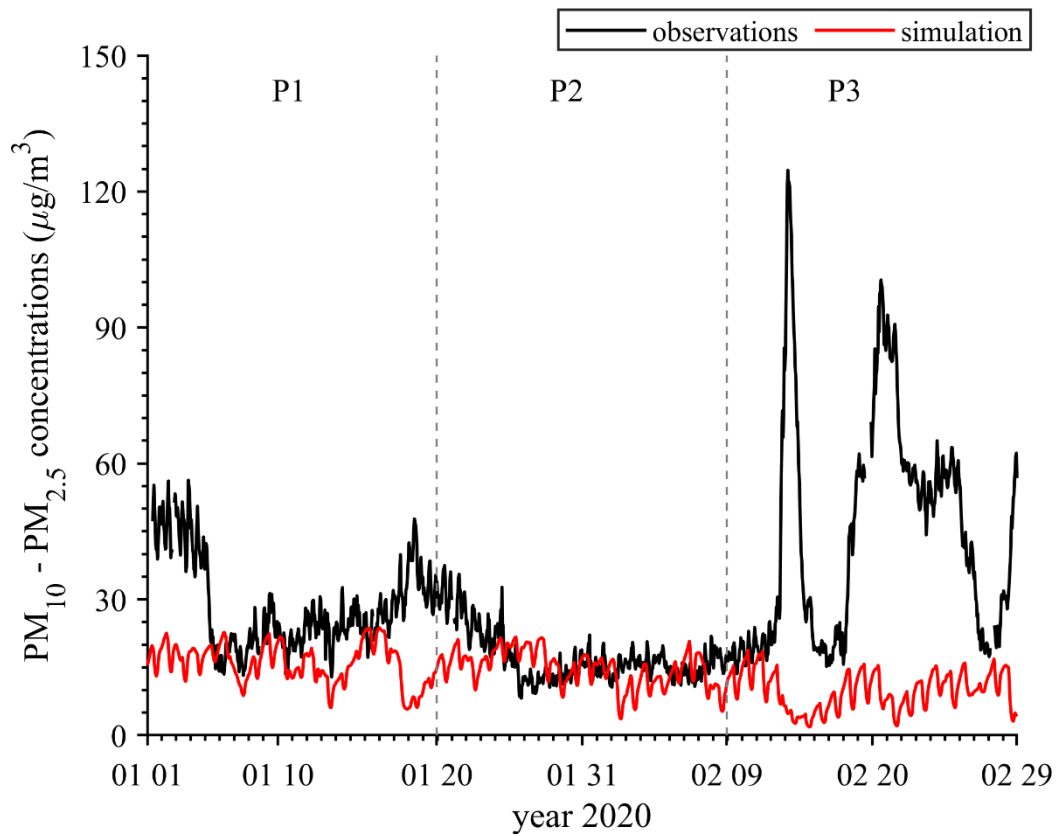
Changes in the manuscript: lines 342–348.

Figure R6: Timeseries of observed and simulated PM$_{10}$ – PM$_{2.5}$ concentrations over Central region during COVID-19 pandemic.
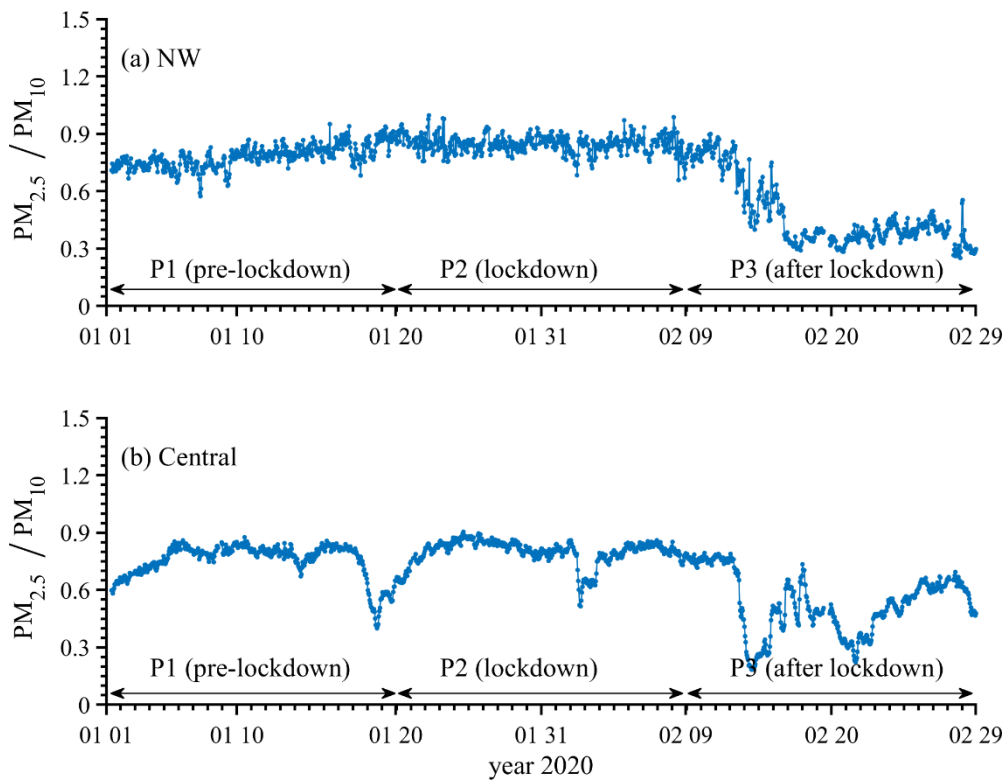

Figure R7: Timeseries of PM$_{2.5}$/PM$_{10}$ ratio during COVID-19 pandemic over (a) NW and (b) Central region

Comment 5: Line 306: east China -> southeast China

Reply: Done

Changes in the manuscript: line 350.

6

Comment 6: Lines 311-312: There is a change in the values of SO_2 and PM_{10}.

Reply: Thanks for pointing out this mistake. The captions of Fig. 4d and Fig. 4f were wrongly labeled. We have corrected this in the revised manuscript.

Changes in the manuscript: Figure 4.

Comment 7: Lines 313-315: The authors suggest that CO emissions decline significantly, as CO's transportation share (18%) is higher than SO_2(5%) and $PM_{2.5}$ (6%) (as shown in Figure 4). However, the percentage decrease in emissions is insignificant (-10.6% vs. -9.7% and -7.9%, as shown in Table 2). Furthermore, while the transportation share of PM_{10} emissions is only 2%, the emission decrease is -12.1%, which is greater than that of CO. Hence, other factors beyond transportation may have influenced the reduction in anthropogenic emissions during P2. Therefore, the authors should clarify their results.

Reply: Thanks for raising this important issue. We agree with the review that the percentage decrease in emissions of CO, SO_2 and $PM_{2.5}$ is not significant compared with the differences in their transportation share. This may be on the one hand due to the uncertainty in the estimated relative contributions of different sectors to the total emissions of CO, SO_2 and $PM_{2.5}$, on the other hand were possibly due to the uncertainty in the emission inversions, especially considering that the decreasing trend of CO, SO_2 and $PM_{2.5}$ were not significant. Also, other factors beyond transportation may have influenced the reductions of anthropogenic emissions during P2 period. For example, the larger reductions of PM_{10} emissions may be related in part to the reduced dust emissions due to shutting down of construction sites during the lockdown period (Li et al., 2020). Following the suggestion of reviewer, we have clarified it in the revised manuscript (please see lines 359–366).

Changes in the manuscript: lines 359–366.

Comment 8: Lines 317-318: The values given are incorrect (e.g., SO_2 is 77.6%, not 86%).

Reply: Thanks very much for your careful check. The given value is correct. It was that the caption of Fig. 4d and Fig. 4f was labeled wrongly, and we have corrected this mistake in the revised manuscript.

Changes in the manuscript: Figure 4.

Comment 9: Lines 329-389: (section 3.3) The results presented by the authors, such as the significant contribution of meteorological fields to $PM_{2.5}$ during the pandemic and the titration effect on O_3, have been reported in previous studies. Hence, the authors should distinguish the difference between their results and previous studies using numerical values.

Reply: Thanks for this suggestion. However, it is difficult to directly compare our results with previous studies due the altered definition of meteorological contribution, different reference period that used to quantify the meteorological contributions and different targeted region. For example, in Song et al. (2021), the reference period used to determine the meteorological contribution is the corresponding period of COVID-19 pandemic in 2019. Le et al. (2020) used the multiyear climatology as the reference period. in Wang et al. (2020) and Sulaymon et al. (2021), the MI changes of $PM_{2.5}$ concentrations were defined as the difference between the modeled concentrations in high-pollution days and those in low-pollution days under hypothetical emission reduction scenario. Zhao et al. (2020) used a similar reference period to ours to determine the MI changes but they used the outdated emission inventory.

Table R1 summarized the studies that differentiated the contributions of meteorology and emission to the $PM_{2.5}$ concentrations over Beijing and the Beijing-Tianjin-Hebei (BTH) region. Note that some studies only provided the relative changes in the modeled $PM_{2.5}$ concentrations. It shows that due to the unknown emission changes during COVID-19 pandemic, the EI changes estimated by Zhao et al. (2020) were possibly largely overestimated compared to our studies (55% versus 24.7%). Both Sulaymon et al. (2021) and Wang et al. (2020) suggested negative EI changes during COVID-19 period in Beijing. This because they presumed that the emissions were largely reduced during COVID-19 lockdown which may deviate from the real changes of emissions according to our inversion results. Meanwhile, although they used same method and reference period, their results differed largely (-2.7 versus -13.4 $\mu g/m^3$) due to the different emission reduction scenario they assumed to represent the emissions during COVID-19 pandemic. Le et al. (2020) only considered the emission reductions of NO_x in their sensitivity simulations without considerations of other species, therefore their calculated EI changes may be underestimated compared to our results (almost 0% versus 24.7%). However, the calculated MI changes were consistent between our study and Le et al. (2020). In terms of O_3, the calculated EI changes by our study were also higher than that calculated by Zhao et al. (2020) in Beijing (85.7% versus 70%). These results suggested that the EI and MI changes calculated by our study could be more reasonable, as the emissions of different species were well constrained which could better represent the temporal variation and spatial heterogeneity of emission changes during COVID-19. Following the suggestions of reviewer, we have added the comparison of our results with previous studies in the revised manuscript (please see lines 442–464)

Table R1. calculated MI and EI changes in PM$_{2.5}$ concentrations during COVID-19 pandemic by previous studies

	MI changes	EI changes	Region	Reference period	Method	Reference
1	26.79 μg/m^3	-21.84 μg/m^3	Beijing	January 23-March 10, 2019 versus January 23-March 10, 2020	observation-based wind-decomposition method	Song et al. (2021)
2	Around 20 μg/m^3	-2.7 μg/m^3	Beijing	January 01 to February 29, 2020	CTM with hypothetical emission reduction scenario	Sulaymon et al. (2021)
3	Around 45 μg/m^3	-13.4 μg/m^3	Beijing	January 01 to February 29, 2020	CTM with hypothetical emission reduction scenario	Wang et al. (2020)
4	31.3%	Around 0%	Beijing-Tianjin-Hebei	January 01 to February 13, 2020	CTM sensitivity simulations using different emission rates and multiyear climatology	Le et al. (2020)
5	Around 5%	Around 55%	Beijing	January 16-22, 2020 versus January 26 to February 1, 2020	CTM with fixed emission inventory for 2017	Zhao et al. (2020)
6	17.5 μg/m^3 (34.0%)	12.7 μg/m^3 (24.7%)	Beijing	January 1-20, 2020 versus January 21 to February 9, 2020	CTM with inversion emission inventory	This study

Changes in the manuscript: lines 442–464 and Table 6.

Comment 9: Lines 340-341: The relative overestimation of ozone is not clear. Please provide a specific value. Also, Figure 7 is not related to this.

Reply: Thanks for this comment. The simulated increases in O$_3$ concentrations from pre-lockdown to lockdown period were 30.9 μg/m^3 over the NCP region, which is slightly higher than the observed increases in O$_3$ concentrations (28.3 μg/m^3). Following the suggestions of reviewer, we have clarified in the revised manuscript (please see lines 389–390), and we feel sorry for the wrong quotation of "Fig. 7" there which has been corrected in the revised manuscript (please see lines 390).

Changes in the manuscript: line 390.

Comment 10: Lines 359-361: The author's assertion that the rise in PM$_{2.5}$ levels in the Beijing region is mainly due to fireworks during the Spring Festival is not supported by sufficient evidence, as there is no evidence that the increase in fireworks emissions is unique to Beijing.

Reply: Thanks for this important comment. Following the suggestions of reviewer, we have added more explanation of the possible causes of the PM$_{2.5}$ emission increases in the Beijing during the lockdown

period through literature review and analysis of the PM$_{2.5}$ compositions. Zuo et al. (2022) analyzed the variations in the PM$_{2.5}$ sources based on the measurement of stable Cu and Si isotopic signature and metal concentrations of PM$_{2.5}$ in Beijing, which indicated that the primary PM$_{2.5}$ emissions did not decrease in Beijing during COVID-19 lockdown, and that the PM-associated industrial emissions may increase in Beijing and its upwind region during the lockdown period. Meanwhile, substantial high levels of potassium (K) and barium (Mg) were observed over Beijing during Spring Festival as seen from Fig. R8, which is an important fingerprint of the firework emissions. This suggest that the emissions from fireworks during Spring Festival were also a potential contributor to the increased of PM$_{2.5}$ emissions in Beijing, which is consistent with the measurement by Ma et al. (2022) and Dai et al. (2020). Therefore, the increased PM$_{2.5}$ emissions during lockdown period in Beijing may be attributed to the increased industrial PM$_{2.5}$ emissions and the firework emissions, which compensated the emission reductions from the traffic emissions. Following the suggestions of reviewer, we have clarified this in the revised manuscript (please see lines 416–418).

Changes in the manuscript: lines 416–418.
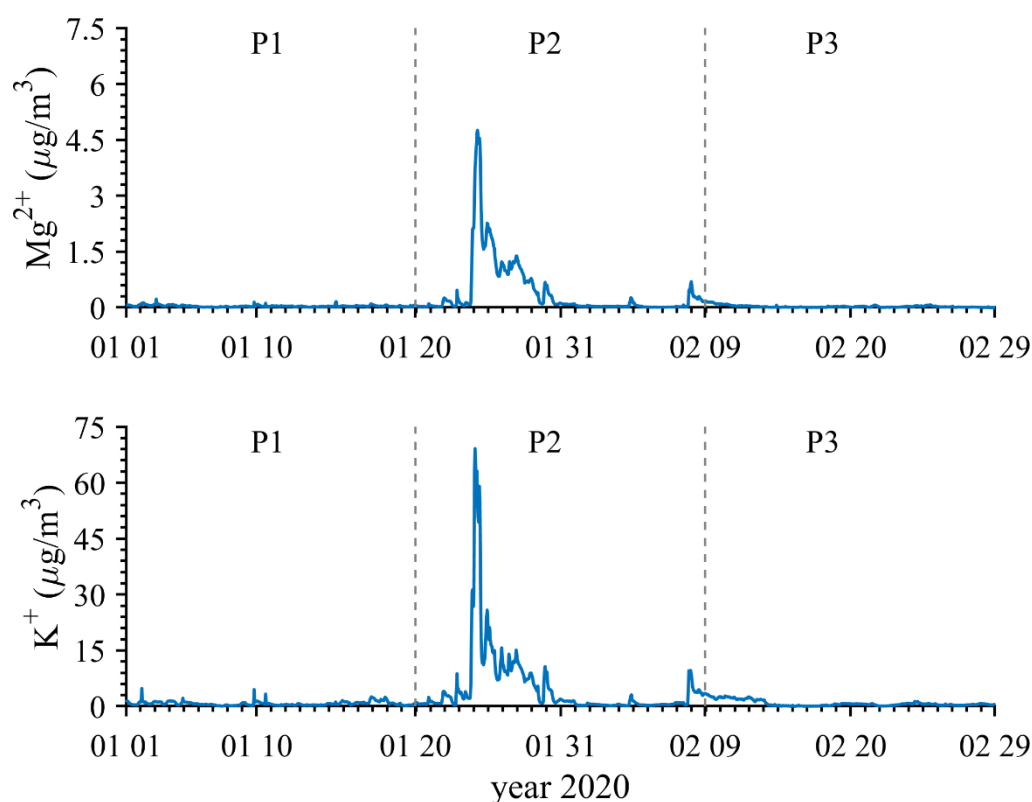
Changes in the supplement: Figure S15.

Figure R8: Timeseries of averaged concentrations of potassium and magnesium ion during COVID-19 pandemic over the Beijing.

Comment 11: Line 441: Some subscripts are misspelled.

Reply: We have corrected it in the revised manuscript.

Changes in the manuscript: line 577.

Comment 12: Lines 460-461: Is the unit for ozone also µg m^{-3}?

Reply: Yes, the unit for ozone is also µg/m^3.

Comment 13: Line S36: Figure S4 -> Figure S7

Reply: We have corrected it in the revised manuscript.

Changes in the supplement: lines S75.

References

Dai, Q., Liu, B., Bi, X., Wu, J., Liang, D., Zhang, Y., Feng, Y., and Hopke, P. K.: Dispersion Normalized PMF Provides Insights into the Significant Changes in Source Contributions to PM2.5 after the COVID-19 Outbreak, Environ. Sci. Technol., 54, 9917-9927, https://doi.org/10.1021/acs.est.0c02776, 2020.

Fan, H., Zhao, C., Yang, Y., and Yang, X.: Spatio-Temporal Variations of the PM2.5/PM10 Ratios and Its Application to Air Pollution Type Classification in China, Front. Environ. Sci., 9, https://doi.org/10.3389/fenvs.2021.692440, 2021.

Le, T. H., Wang, Y., Liu, L., Yang, J. N., Yung, Y. L., Li, G. H., and Seinfeld, J. H.: Unexpected air pollution with marked emission reductions during the COVID-19 outbreak in China, Science, 369, 702-+, https://doi.org/10.1126/science.abb7431, 2020.

Li, L., Li, Q., Huang, L., Wang, Q., Zhu, A., Xu, J., Liu, Z., Li, H., Shi, L., Li, R., Azari, M., Wang, Y., Zhang, X., Liu, Z., Zhu, Y., Zhang, K., Xue, S., Ooi, M. C. G., Zhang, D., and Chan, A.: Air quality changes during the COVID-19 lockdown over the Yangtze River Delta Region: An insight into the impact of human activity pattern changes on air pollution variation, Sci. Total Environ., 732, 139282, https://doi.org/10.1016/j.scitotenv.2020.139282, 2020.

Ma, T., Duan, F. K., Ma, Y. L., Zhang, Q. Q., Xu, Y. Z., Li, W. G., Zhu, L. D., and He, K. B.: Unbalanced emission reductions and adverse meteorological conditions facilitate the formation of secondary pollutants during the COVID-19 lockdown in Beijing, Sci. Total Environ., 838, 8, https://doi.org/10.1016/j.scitotenv.2022.155970, 2022.

Song, Y. S., Lin, C. Q., Li, Y., Lau, A. K. H., Fung, J. C. H., Lu, X. C., Guo, C., Ma, J., and Lao, X. Q.: An improved decomposition method to differentiate meteorological and anthropogenic effects on air pollution: A national study in China during the COVID-19 lockdown period, Atmos. Environ., 250, 9, https://doi.org/10.1016/j.atmosenv.2021.118270, 2021.

Sulaymon, I. D., Zhang, Y., Hopke, P. K., Hu, J., Zhang, Y., Li, L., Mei, X., Gong, K., Shi, Z., Zhao, B., and Zhao, F.: Persistent high PM2.5 pollution driven by unfavorable meteorological conditions during the COVID-19 lockdown period in the Beijing-Tianjin-Hebei region, China, Environ. Res., 198, 111186, https://doi.org/10.1016/j.envres.2021.111186, 2021.

Wang, P., Chen, K., Zhu, S., Wang, P., and Zhang, H.: Severe air pollution events not avoided by reduced anthropogenic activities during COVID-19 outbreak, Resources, Conservation and Recycling, 158, 104814, https://doi.org/10.1016/j.resconrec.2020.104814, 2020.

Wang, Y. Q., Zhang, X. Y., Sun, J. Y., Zhang, X. C., Che, H. Z., and Li, Y.: Spatial and temporal variations of the concentrations of PM_{10}, $PM_{2.5}$ and PM_1 in China, Atmos. Chem. Phys., 15, 13585-13598, https://doi.org/10.5194/acp-15-13585-2015, 2015.

Zhao, Y. B., Zhang, K., Xu, X. T., Shen, H. Z., Zhu, X., Zhang, Y. X., Hu, Y. T., and Shen, G. F.: Substantial Changes in Nitrogen Dioxide and Ozone after Excluding Meteorological Impacts during the COVID-19 Outbreak in Mainland China, Environ. Sci. Technol. Lett., 7, 402-408, https://doi.org/10.1021/acs.estlett.0c00304, 2020.

Zuo, P. J., Zong, Z., Zheng, B., Bi, J. Z., Zhang, Q. H., Li, W., Zhang, J. W., Yang, X. Z., Chen, Z. G., Yang, H., Lu, D. W., Zhang, Q. H., Liu, Q., and Jiang, G. B.: New Insights into Unexpected Severe PM2.5 Pollution during the SARS and COVID-19 Pandemic Periods in Beijing, Environ. Sci. Technol., 56, 155-164, https://doi.org/10.1021/acs.est.1c05383, 2022.

Unbalanced emission reductions of different species and sectors in China during COVID-19 lockdown derived by multi-species surface observation assimilation

Lei Kong[1,3], Xiao Tang[*,1,3], Jiang Zhu[2,3], Zifa Wang[1,3,4], Yele Sun[1,3], Pingqing Fu[5], Meng Gao[6], Huangjian Wu[1,3], Miaomiao Lu[7], Qian Wu[1,3], Shuyuan Huang[8], Wenxuan Sui[1], Jie Li[1,3], Xiaole Pan[1,3], Lin Wu[1,3], Hajime Akimoto[9], Gregory R. Carmichael[10]

[1]State Key Laboratory of Atmospheric Boundary Layer Physics and Atmospheric Chemistry (LAPC), Institute of Atmospheric Physics, Chinese Academy of Sciences, Beijing 100029, China

[2]CAS-TWAS Center of Excellence for Climate and Environment Sciences (ICCES), Institute of Atmospheric Physics, Chinese Academy of Sciences, Beijing 100029, China

[3]University of Chinese Academy of Sciences, Beijing 100049, China

[4]Center for Excellence in Regional Atmospheric Environment, Institute of Urban Environment, Chinese Academy of Sciences, Xiamen 361021, China

[5]Institute of Surface-Earth System Science, Tianjin University, Tianjin 300072, China

[6]Department of Geography, State Key Laboratory of Environmental and Biological Analysis, Hong Kong Baptist University, Hong Kong SAR, China

[7]State Environmental Protection Key Laboratory of Urban Ambient Air Particulate Matter Pollution Prevention and Control, College of Environmental Science and Engineering, Nankai University, Tianjin 300350, China

[8]Chengdu University of Information Technology, Chengdu 610225, China

[9]National Institute for Environmental Studies, Onogawa, Tsukuba 305-8506, Japan

[10]Center for Global and Regional Environmental Research, University of Iowa, Iowa City, IA 52242, USA

Correspondence to: Xiao Tang (tangxiao@mail.iap.ac.cn)

Abstract. The unprecedented lockdown of human activities during the COVID-19 pandemic have significantly influenced the social life in China. However, understanding of the impact of this unique event on the emissions of different species is still insufficient, prohibiting the proper assessment of the environmental impacts of COVID-19 restrictions. Here we developed a multi-air pollutant inversion system to simultaneously estimate the emissions of NO_x, SO_2, CO, $PM_{2.5}$ and PM_{10} in China during COVID-19 restrictions with high temporal (daily) and horizontal (15km) resolutions. Subsequently, contributions of emission changes versus meteorology variations during COVID-19 lockdown were separated and quantified. The results demonstrated that the inversion system effectively reproduced the actual emission variations of multi-air pollutants in China during different periods of COVID-19 lockdown, which indicate that the lockdown is largely a nationwide road traffic control measure with NO_x emissions decreased substantially by ~40%. However, emissions of other air pollutants were found only decreased by ~10%, because power generation and heavy industrial processes were not halted during lockdown, and residential activities may actually have increased due to the stay-at-home orders. Consequently, although obvious reductions of $PM_{2.5}$ concentrations occurred over North China Plain (NCP) during lockdown period, the emission change only accounted for 8.6% of $PM_{2.5}$ reductions, and even led to substantial increases of O_3. The meteorological variation instead dominated the changes in $PM_{2.5}$ concentrations over NCP, which contributed 90% of the $PM_{2.5}$ reductions over most parts of NCP region. Meanwhile,

37   our results suggest that the local stagnant meteorological conditions together with inefficient reductions in $PM_{2.5}$ emissions

38   were the main drivers of the unexpected $PM_{2.5}$ pollution in Beijing during lockdown period. These results highlighted that

39   traffic control as a separate pollution control measure has limited effects on the coordinated control of O_3 and $PM_{2.5}$

40   concentrations under current complex air pollution conditions in China. More comprehensive and balanced regulations for

41   multiple precursors from different sectors are required to address O_3 and $PM_{2.5}$ pollution in China.

1 Introduction

43   A novel coronavirus disease (COVID-19) broke out in Wuhan at the end of 2019 but quickly spread across the whole

44   China within a month. To curb the spread of the virus, strict epidemic control measures were implemented by Chinese

45   governments to prevent large gatherings, including strict travel restriction, shutting down of non-essential industries, extended

46   holidays, closing of schools and entertainment houses (Cheng et al., 2020). These restrictions have had a significant impact on

47   the industrial activities and social life, as exemplified by the drop of China's industrial output by 15-30%

48   (https://data.stats.gov.cn/, last accessed on 22 Oct, 2022) and the dramatic decrease of traffic flow by 60–90% in major cities

49   of China during COVID-19 epidemic (http://jiaotong.baidu.com/, last accessed on 22 Oct, 2022), which provides us a natural

50   experiment to examine the responses of the emissions and air quality on the changes in human activities.

51   It has been well documented that the short-term stringent emission control targeted on power generator or heavy industry

52   enacted by Chinese government during certain societal events, such as the 2008 Olympics Games, 2014 Asia-Pacific Economic

53   Cooperation conference and 2015 China Victory Day Parade, is an effective way to reduce emissions and improve air quality

54   (Okuda et al., 2011; Wang et al., 2014; Tang et al., 2015; Zhang et al., 2016; Wu et al., 2020; Chu et al., 2018). However,

55   different from those stringent emission controls, the COVID-19 restrictions are inclined to affect emissions from sectors more

56   closely to social life whose influence on emissions has still not well been assessed. Previous studies suggest that the COVID-

57   19 restrictions have substantially reduced the China's anthropogenic emissions from almost all sectors (Zheng et al., 2021;

58   Huang et al., 2021; Xing et al., 2020). For example, by using a bottom-up method based on near-real-time activity data, Zheng

59   et al. (2021) reported that the emissions of NO_x, SO_2, CO and primary $PM_{2.5}$ decreased by 36%, 27%, 28% and 24% during

60   COVID-19 restrictions, mostly due to the reductions in industry and transportation sector. Xing et al. (2020), by using a

61   response model, estimated stronger COVID-19 shutdown effects on emissions over the North China Plain (NCP) with

62   emissions of NO_x, SO_2 and primary $PM_{2.5}$ dropped by 51%, 28% and 63%, respectively. Others argue that the COVID-19

63   restriction may mainly affect the emissions from transportation, light industry and manufacturing, while it has much smaller

64   effects on the emissions from the power generator and heavy industry because of their non-interruptible processes (Chu et al.,

65   2021; Hammer et al., 2021; Le et al., 2020; Zhao et al., 2020). Moreover, the residential emissions may even increase during

66   the COVID-19 lockdown due to the increased demanding for space heating and cooking with the stay-at-home orders.

67   Therefore, Le et al. (2020) only considered the NO_x reductions during COVID-19 restrictions in their investigation of the

68   severe haze during COVID-19 lockdown, and similarly, Hammer et al. (2021) only considered the emission reductions in the

69 transportation sector. This indicates that there has large uncertainty in the current understanding of the effects of COVID-19

70 restrictions on the emissions of different species.

71   Quantification of the emission changes of different species and different sectors during the COVID-19 lockdown is thus

72 necessary for the comprehensive understanding of the environmental impacts of COVID-19 restrictions. In particular, although

73 observations indeed show decreases of air pollutant concentrations during COVID-19 restrictions (Fan et al., 2020; Wang et

74 al., 2021; He et al., 2020; Shi and Brasseur, 2020), the air quality improvement is much smaller than the expected (Shi et al.,

75 2021; Diamond and Wood, 2020; Yan et al., 2022). Moreover, severe haze still occurred in northern China (Sulaymon et al.,

76 2021; Le et al., 2020) and O_3 concentrations even showed significant increases (Zhang et al., 2021; Li et al., 2020). A number

77 of studies were conducted to explain this anomalistic air quality change by analyzing the effects of emission changes,

78 meteorological variations and secondary production (Huang et al., 2021; Le et al., 2020; Hammer et al., 2021; Zhao et al.,

79 2020; Zhao et al., 2021; Sulaymon et al., 2021; Wang et al., 2020; Li et al., 2021). However, due to the unknown emission

80 changes during COVID-19 restrictions, the emission reduction scenarios that used to represent the COVID-19 shutdown effects

81 varied among different studies and did not consider the spatial and temporal heterogeneity of the emission changes, leading to

82 biases in the model simulation (Zhao et al., 2021; Li et al., 2021; Hammer et al., 2021; Zheng et al., 2021) and uncertainty in

83 the quantification of the contributions of different factors.

84   Pioneer studies by Zheng et al. (2021) and Forster et al. (2020) have derived multi-air pollutant emissions from social

85 activity data using a bottom-up method, but due to the lack of detailed social activity data, large uncertainties existed in their

86 estimates. The meteorologically and seasonally driven variability of the concentrations of air pollutants also prohibit drawing

87 fully quantitative conclusions on the changes of emissions based on observations alone (Levelt et al., 2022). The emission

88 inversion technique, which takes advantage of the chemical transport model (CTM) and real-time observations, provides an

89 attractive way to estimate the sector-specific and space-based emission changes during COVID-19 restrictions, as shown in

90 Zhang et al. (2020), Zhang et al. (2021), Feng et al. (2020) and Hu et al. (2022). However, these studies only inversed the

91 emissions of single species (e.g., NO_x and SO_2) without insights into multiple species. In view of this discrepancy, in this study

92 we developed a multi-air pollutant inversion system to simultaneously estimated the multi-air pollutant emissions in China,

93 including NO_x, SO_2, CO, $PM_{2.5}$ and PM_{10}, during the COVID-19 restrictions using an ensemble Kalman filter (EnKF) and

94 surface observations from the China National Environmental Monitoring Centre (CNEMC). Subsequently, the inversed

95 emission inventory was used to quantify the contributions of emission changes versus meteorology variations to the changes

96 in $PM_{2.5}$ and O_3 concentrations over the NCP region during the COVID-19 restrictions.

97 **2 Method and data**

98   We developed a high-resolution multi-air pollutant inversion system to estimate the daily emissions of NO_x, SO_2, CO,

99 $PM_{2.5}$ and PM_{10} in China from 1 Jan to 29 Feb 2020 when the COVID-19 pandemic was at its most serious and the effects of

100 the COVID-19 restrictions were most profound in China. This system uses the NAQPMS (Nested Air Quality Prediction

101 Modelling System) model as the forecast model and the EnKF coupled with the state argumentation method as the inversion
102 method. It has the capabilities of simultaneous inversion of multi-air pollutant emissions at high temporal (daily) and spatial
103 (15km) resolutions. An iteration inversion scheme was also developed in this study to address the large biases in the a priori
104 emissions. In order to better characterize the emission changes during the COVID-19 restrictions, the whole time period was
105 divided into three periods according to different control phases of COVID-19 and the timing of the Chinese Lunar New Year:
106 before lockdown (P1, January 1-20), lockdown (P2, January 21-February 9) and after back-to-work day (P3, February 10-29).
107 Emission changes in different regions of China were also analyzed, including the North China Plain (NCP), Northeast China
108 (NE), Southeast China (SE), Southwest China (SW), Northwest China (NW) and Central regions (defined in Fig. 1) to
109 investigate the responses of emissions to the COVID-19 restrictions in different regions. In the following sections, we briefly
110 introduce each component of the inversion system.

2.1 Chemical transport model and its configuration

112   The NAQPMS model was used as the forecast model to represent the atmospheric chemistry in this study, which has been
113 used in previous inversion studies (Tang et al., 2011; Tang et al., 2013; Kong et al., 2019; Wu et al., 2020), where detailed
114 descriptions of NAQPMS are available. The Weather Research and Forecasting Model (WRF)(Skamarock, 2008) is used to
115 provide the meteorological inputs to the NAQPMS model.
116   Figure 1 shows the modelling domain of this study with a high horizontal resolution of 15 km. The a priori emission
117 inventory used in this study includes monthly anthropogenic emissions from the HTAP_v2.2 emission inventory for the base
118 year of 2010 (Janssens-Maenhout et al., 2015), biomass burning emissions from the Global Fire Emissions Data base (GFED)
119 version 4 (Randerson et al., 2017; Van Der Werf et al., 2010), biogenic volatile organic compound (BVOC) emissions from
120 MEGAN-MACC (Sindelarova et al., 2014), marine volatile organic compound emissions from the POET database (Granier et
121 al., 2005), soil NO_x emissions from the Regional Emission inventory in Asia (Yan et al., 2003) and lightning NO_x emissions
122 from Price et al. (1997). Chemical top and boundary conditions were provided by the global CTM MOZART (Model for
123 Ozone and Related Chemical Tracers) (Brasseur et al., 1998; Hauglustaine et al., 1998). We assumed no monthly variations in
124 the a priori emission inventory and used January's emission inventory for the whole simulation period so that the emission
125 variation was solely derived from the surface observations. A two-week free run of NAQPMS was conducted as a spin-up
126 time. For each day's meteorological simulation, a 36-h free run of WRF was conducted, of which the first 12-h simulation was
127 a spin-up run and the next 24-h simulation provided the meteorological inputs to NAQPMS. Initial and boundary conditions
128 for the meteorological simulation were provided by the National Center for Atmospheric Research/National Center for
129 Environment Prediction (NCAR/NCEP) 1° ×1° reanalysis data. Evaluation results for the WRF simulation are available in
130 Text S1 in Supplement.

2.2 Surface Observations

The hourly concentrations of NO_2, SO_2, CO, $PM_{2.5}$ and PM_{10} from CNEMC were used in this study to estimate the emissions during COVID-19. The spatial distributions of these observation sites are shown in Fig. 1, which contains 1436 observation sites covering most regions of China. Before assimilation, outliers of observations were first filtered out using the automatic outlier detection method developed by Wu et al. (2018) to prevent the adverse effects of the outliers on data assimilation. Then, the hourly concentrations were averaged to the daily values for the inversions of daily emissions.

The observation error is one of the key inputs to the data assimilation, which together with the background error determine the relative weights of the observation and background values on the analysis. The observation error includes measurement error and representativeness error. The measurement error of each species was designated according to the officially released documents of the Chinese Ministry of Ecology and Environmental Protection (HJ 193-2013 and HJ 654-2013, available at http://www.cnemc.cn/jcgf/dqhj/, last accessed on 22 Oct 2022), which is 5% for $PM_{2.5}$ and PM_{10} and 2% for SO_2, NO_2 and CO. A representativeness error arises from the different spatial scales that the discrete observation data and model simulation represent, which was estimated based on the previous study by Li et al. (2019) and Kong et al. (2021). It should be noted that the NO_2 measurement from CNEMC is made by the chemiluminescent analyser with a molybdenum converter. Due to the interference of HNO_3, PAN and alkyl nitrates (AN), the NO_2 concentrations can be overestimated (Dunlea et al., 2007; Lamsal et al., 2008) that may lead to spurious decreases in NO_x emissions during the lockdown period. Previous studies usually use chemical transport model to simulate NO_x, HNO_3, PAN and AN to produce correction factors (CFs) for the NO_2 measurements (Cooper et al., 2020; He et al., 2022) using the following relationship proposed by Lamsal et al. (2008):

$$CF = \frac{[NO_2]}{[NO_2]+0.95[PAN]+0.35[HNO_3]+\sum[AN]} \tag{1}$$

but the calculation of CF could be affected by the simulation errors in the model caused by uncertainties in emission inventory or other error sources, which may contaminate the observations. Therefore, similar to Feng et al. (2020), we did not correct the NO_2 measurement in our inversion of NO_x emissions since there were large uncertainties in the NO_x emissions during the COVID-19 pandemic that possibly led to erroneous CF. Since the EnKF considered the errors in observations through the use of observation error covariance matrix, the chemiluminescence monitor interference to NO_2 measurement were treated as the observation error during the assimilation. A sensitivity inversion experiment was also conducted based on the corrected NO_2 measurement using CF, which suggests that the chemiluminescence monitor interference only have small impacts on the inversed NO_x emission in terms of magnitude and its variation during COVID-19 pandemic. Detailed results of the sensitivity experiment are available in Text S2 in Supplement.

2.3 Inversion estimation scheme

The EnKF coupled with the state augmentation method was used in this study to constrain the emissions of multiple species. EnKF is an advanced data assimilation method proposed by Evensen (1994) that features representation of the uncertainties of the model state by a stochastic ensemble of model realizations. Different from the mass balance method used

163 in Zhang et al. (2020) and Zhang et al. (2021) that has difficulties in accounting for nonlinear relationship between emissions
164 and concentrations and is more suitable for short-lived species (e.g. NO_x) under relatively coarse (>1°) resolutions (Streets et
165 al., 2013), the EnKF can consider the indirect relationship between emissions and concentrations caused by complex physical
166 and chemical processes in the atmosphere through the use of flow-dependent background error covariance produced by
167 ensemble CTM forecasts (Evensen, 2009; Miyazaki et al., 2012). Compared with the four-dimensional variational assimilation
168 method used in Hu et al. (2022), the EnKF method has comparable computational cost (Skachko et al., 2014) but is more easily
169 implemented without the need to develop complicated adjoint models for complex CTMs. The state augmentation method is
170 a commonly used parameter estimation method (Tandeo et al., 2020), in which the emissions of multi species are treated as
171 state variable and are simultaneously updated according to the relationship between the emissions and concentrations of related
172 species. Due to the chemical reactions in the atmosphere, the concentrations of different species are interrelated with each
173 other. For example, the ambient $PM_{2.5}$ is not only primarily emitted, but also formed secondarily through reactions with several
174 gaseous precursors, such as NO_2 and SO_2. This means that the estimations of $PM_{2.5}$ emission by single inversed estimation
175 method could be biased if the errors in NO_2 and SO_2 emissions were not corrected synchronously. Therefore, it is beneficial
176 to do the multi-species inversion estimation which can provide more constraints on the atmospheric chemical system and lead
177 to more reasonable inversion results. Meanwhile, the use of EnKF method coupled with the state augmentation method allows
178 the estimations of multi-species emissions almost without additional computational cost.

179   Appropriate estimation of the uncertainty in emissions and chemical concentrations is important for the performance of
180 inversion estimation using EnKF. Since the source emission data over mainland China in HTAP_v2.2 inventory is obtained
181 from the MIX inventory (Li et al., 2017b) , the uncertainties of emissions of different species, including PMF, PMC, BC, OC,
182 NO_x, CO, SO_2, NH_3 and NMVOC (nonmethane volatile organic compounds), were obtained from Li et al. (2017b) and Streets
183 et al. (2003), which were represented by an ensemble of perturbed emissions generated by multiplying the a priori emissions
184 with a perturbation factor $\beta_{i,s}$:

185 $$E_{i,s} = \beta_{i,s} \circ E_s^p, \ i = 1,2, \cdots N_{ens} \tag{2}$$

186 where $E_{i,s}$ represents the vector of the ith member of perturbed emissions for species s, E_s^p represents the a priori emissions
187 for this species, $\circ$ denotes the schur product and N_{ens} denotes the ensemble size. In this way, the adjustment of emissions is
188 equivalent to the adjustment of perturbation factors.

189   In terms of the uncertainty in chemical concentrations, considering that emission uncertainty is the major contributor to
190 the uncertainties in air quality modelling, especially during the COVID-19 period when emissions changed rapidly,
191 uncertainties in chemical variables were obtained through ensemble simulations driven by perturbed emissions. The ensemble
192 size was chosen as 50 to maintain the balance between the filter performance and computational cost. After the ensemble
193 simulations, emissions of multiple species were updated using a deterministic form of EnKF (DEnKF) proposed by Sakov and
194 Oke (2008), which is formulated by

195 $$\overline{x^a} = \overline{x^b} + P_e^b H^T (H P_e^b H^T + R)^{-1} (y^o - H \overline{x^b}) \tag{3}$$

6

196 $\quad \overline{x^b} = \frac{1}{N}\sum_{i=1}^{N} x_i^b \; ; X_i^b = x_i^b - \overline{x^b}$ $\hfill$ (4)

197 $\quad \mathbf{P_e^b} = \frac{1}{N-1}\sum_{i=1}^{N} X_i^b \left(X_i^b\right)^T$ $\hfill$ (5)

198 where x denotes the state variables; b the background state (a priori); a the analysis state (posteriori); $\mathbf{P_e^b}$ the ensemble-

199 estimated background error covariance matrix and N the ensemble size. y^o represents the vector of observations with an error

200 covariance matrix of $\mathbf{R}$. $\mathbf{H}$ is the linear observational operator that maps the m-dimensional state vector x to a p- (number of

201 observations) dimensional observational vector ($\mathbf{H}\overline{x^b}$). The state variables were defined as follows according to state

202 augmentation method during the assimilation:

203 $\quad x_i = [c_i, \; \beta_i]^T, i = 1,2, \cdots N_{ens}$ $\hfill$ (6)

204 $\quad c_i = [PM_{2.5}, PM_{10-2.5}, \; NO_2, \; SO_2, CO]_i$ $\hfill$ (7)

205 $\quad \beta_i = [\beta_{PMF}, \beta_{BC}, \; \beta_{OC}, \; \beta_{PMC}, \beta_{NO_x}, \beta_{SO_2}, \beta_{CO}]_i$ $\hfill$ (8)

206 where x_i represents the ith member of the assimilated state variable, which consists of the fields of chemical variables c_i

207 and emission perturbation factors β_i. Detailed descriptions of the model state variables are summarized in Table 1. The use

208 of PM$_{10\text{-}2.5}$ (PM$_{10}$ minus PM$_{2.5}$) values was aimed to avoid the potential cross-correlations between PM$_{2.5}$ and PM$_{10}$ (Peng et

209 al., 2018; Ma et al., 2019). Moreover, to prevent spurious correlations between non- or weakly related variables, similar to Ma

210 et al. (2019) and Miyazaki et al. (2012), state variable localization was used during assimilation, with observations of one

211 particular species only used in the updates of the same species' emission rate. Corresponding relationship between the chemical

212 observations and adjusted emissions is summarized in Table 1. The PM$_{2.5}$ observations were one exception and were used to

213 update the emissions of PMF (fine mode unspeciated aerosol), BC (black carbon) and OC (organic carbon) since the

214 observations of speciated PM$_{2.5}$ were not available in this study. The lack of speciated PM$_{2.5}$ observations may lead to

215 uncertainties in the estimated emissions of PMF, BC and OC. Therefore, we only analyzed the emissions of PM$_{2.5,}$ which were

216 the sum of the emissions of these three species. Similarly, only PM$_{10}$ emissions were analyzed in this study, which includes

217 the emissions of PM$_{2.5}$ and PMC (coarse mode unspeciated aerosol).

218 $\quad\quad$ Due to the strict control measures implemented during the last decades, the emissions in China decreased dramatically

219 from 2010 to 2020, especially for SO$_2$. Thus, there are large biases in the a priori estimates of emissions in China (Zheng et

220 al., 2018), which would lead to incomplete adjustments of the a priori emissions and degrade the performance of assimilation.

221 Therefore, an iteration inversion scheme was developed in this study to address the large biases of SO$_2$ emissions. As illustrated

222 in Fig. 2, the main idea of the iteration inversion scheme is to update the ensemble mean of the state variable using the inversion

223 results of the kth iteration and corresponding simulations. The state variable used in the $(k + 1)th$ inversions is written as

224 follows:

225 $\quad x_i^{k+1} = \left[c^k + c_i^e - \overline{c^e}, \beta^k + \beta_i^e - \overline{\beta^e}\right]^T$ $\hfill$ (9)

226 where c^k represents the simulation results using the inversed emissions of the kth iteration, c_i^e represents the ith member

227 of ensemble simulations with an ensemble mean of $\bar{c^e}$, β^k represents the perturbation factors of the kth iteration, and

228 β_i^e represents the ith member of the ensemble of perturbation factors with a mean value of $\overline{\beta^e}$.

229 　　Using this method, the problems of large biases in the a priori emissions were well addressed as exemplified in Fig. 3 for

230 SO_2 emissions. It can be clearly seen that due to the large positive biases in the a priori SO_2 emissions, the model still has large

231 positive biases (NMB = 30.9–220.5%) and errors (RMSE = 8.7–23.0 $\mu g/m^3$) in simulated SO_2 concentration over all regions

232 of China even after assimilation (first iteration). However, the biases and errors continued to decrease with the increasing of

233 iteration times till the fourth iteration in which there were no significant improvement in SO_2 simulations compared to those

234 in third iteration. These results suggested that the iteration inversion method used in this study can well constrain the a priori

235 emission with large biases and, in this application, conducting three iteration is enough for constraining the emission. Besides

236 SO_2 emissions, the iteration inversion scheme was also applied to the emissions of other species. Meanwhile, to reduce the

237 influences of random model errors (e.g., errors in meteorological inputs) on the estimation of the variation in emissions, a 15-

238 day running average was performed on our daily inversion results after the inversion estimation.

239 **2.4 Quantification of the effects of emission changes and meteorological variations**

240 　　In previous studies, the meteorological-induced (MI) changes were usually determined by the CTM with a fixed emission

241 input setting and a varying meteorological input. Then, the difference between the MI changes and total changes in air pollutant

242 concentrations is defined as emission-induced (EI) changes. Another approach to estimate EI changes is to perform simulations

243 with a fixed meteorological input setting and varying emission inputs. Then, the MI changes are defined as the difference

244 between EI changes and total changes in air pollutant concentrations. Due to the nonlinear effects of atmospheric chemical

245 systems, these two methods yield different results. Thus, both methods were used in this study to account for the nonlinear

246 effects. The averaged results of these two methods are used to represent the impacts of emission changes and meteorological

247 variation on the air quality changes during the COVID-19 restrictions. In total, three scenario experiments were designed based

248 on our inversion results (Table 2). The first scenario simulation used the varying meteorological and emission inputs from the

249 P1 to P2 period, which represents the real-world scenario and is used to estimate the total changes in air pollutant concentrations

250 induced by emissions and meteorological changes from the P1 to P2 period (BASE scenario). The second scenario experiment

251 used the varying meteorological inputs but replaced the emissions during the P2 period with those during the P1 period, which

252 was used to estimate the MI changes using the first method (MET change scenario). The third scenario experiment used the

253 varying emissions input and replaced the meteorological input during the P2 period with that during the P1 period, which was

254 used to estimate the EI changes using the second method (EMIS change scenario). Based on the first method, the MI and EI

255 changes can be estimated as follows:

256 $MI_{MET\ change\ scenario} = conc_{p2,MET\ change\ scenario} - conc_{p1,MET\ change\ scenario}$ （10）

257 $EI_{MET\ change\ scenario} = conc_{p2,BASE\ scenario} - conc_{p1,BASE\ scenario} - MI_{MET\ change\ scenario}$ （11）

where $MI_{MET\ change\ scenario}$ represents the MI changes estimated based on the results from the MET change scenario, $conc_{p1,MET\ change\ scenario}$ and $conc_{p2,MET\ change\ scenario}$ represent the averaged concentrations of air pollutants during the P1 and P2 periods under the MET change scenario, $EI_{MET\ change\ scenario}$ represents the EI changes estimated based on the results from the MET change scenario, and $conc_{p1,BASE\ scenario}$, $conc_{p2,BASE\ scenario}$ respectively represent the averaged concentrations of air pollutants during the P1 and P2 periods under the BASE scenario. Similarly, the MI and EI changes estimated based on the second method are formulated as follows:

$$EI_{EMIS\ change\ scenario} = conc_{p2,EMIS\ change\ scenario} - conc_{p1,EMIS\ change\ scenario} \qquad (12)$$

$$MI_{EMIS\ change\ scenario} = conc_{p2,BASE\ scenario} - conc_{p1,BASE\ scenario} - EI_{EMIS\ change\ scenario} \qquad (13)$$

Then, the estimations from these two methods are averaged to estimate the contributions of meteorological change and emission change to the changes in PM$_{2.5}$ and O$_3$ concentrations during the COVID-19 lockdown:

$$MI = (MI_{EMIS\ change\ scenario} + MI_{MET\ change\ scenario})/2 \qquad (14)$$

$$EI = (EI_{EMIS\ change\ scenario} + EI_{MET\ change\ scenario})/2 \qquad (15)$$

$$contri_{met} = \frac{MI}{MI+EI} \times 100 \qquad (16)$$

$$contri_{emis} = \frac{EI}{MI+EI} \times 100 \qquad (17)$$

where $contri_{met}$ and $contri_{emis}$ represent the relative contributions (%) of the meteorological variations and emission changes to the changes in air pollutant concentrations. Detailed definition of each notation used in the calculation of MI and EI is given in Table 3.

3 Results

3.1 Validation of the inversion results

We firstly validate our inversion system by using a cross-validation method, in which 20% of observation sites were withheld from the emission inversion and used as the validation datasets. Figure S1–6 showed the concentrations of different air pollutants in China from 1st Jan to 29th Feb 2020 obtained from observations at validation sites and simulations using a priori and a posteriori emission. Commonly used statistical evaluation indices, including correlation coefficient (R), mean bias error (MBE), normalized mean bias (NMB) and root of mean square error (RMSE) are summarized in Table S1. The validation results suggest that the posteriori simulation agreed well with the observed concentrations for all species. The large biases in the a priori simulation of PM$_{2.5}$, PM$_{10}$, SO$_2$ and CO were almost completely removed in the a posteriori simulation with NMB about -3.9–15.7% for PM$_{2.5}$, -3.1–11.6% for PM$_{10}$, -12.6–5.3% for NO$_2$, -9.5–6.2% for SO$_2$ and -10–7.6% for CO (Table S1). RMSE values were also significantly reduced in the a posteriori simulation which were 9.1–32.2 μg/m^3 for PM$_{2.5}$, 12.6–42.4 μg/m^3 for PM$_{10}$, 5.1–12.3 μg/m^3 for NO$_2$, 1.2–5.6 μg/m^3 for SO$_2$ and 0.10–0.46 mg/m^3 for CO. Moreover, the inversion emission considerably improved the fit to the observed time evolution of air pollutants' concentrations. The R values

were improved for all species in the a posteriori simulation that were up to 0.74–0.94 for $PM_{2.5}$, 0.63 – 0.92 for PM_{10}, 0.76–0.94 for NO_2, 0.23–0.79 for SO_2 and 0.63–0.92 for CO. These results suggest that our inversion results have excellent performance in representing the magnitude and variation of these species' emission in China during COVID-19 restrictions. Model performance in simulating O_3 concentration is relatively poor compared to other species although improvement was remarkable in NCP, NE and SE regions. This would be due to the use of outdated emission inventory for base year 2010 and that the emission of non-mental volatile organic compounds (NMVOC), another important precursor for O_3, were not constrained in this study. As shown in fig. S7, the NMVOC emissions for base year 2010 were generally lower than those for 2018 except over the SW regions. Considering the increasing trend of NMVOC emissions in China (Li et al., 2019), the underestimates of NMVOC emissions for base year 2020 could be larger. This is in line with the negative biases in the simulated O_3 concentrations over these regions.

3.2 Emission changes of multi-species during COVID-19 restrictions

3.2.1 Unbalanced emission changes between NO_x and other species

The control of COVID-19 began on 23rd January when the Chinese government declared the first level of national responses to public health emergencies, one day before the 2020 Chinese New Year Eve. Figure 4 shows the time evolution of the normalized emission anomaly for different species in China from 1st January to 29th February. The temporal variation in the emission varied largely between NO_x and other species. Due to the combined effects of the Spring Festival and COVID-19 lockdown, NO_x emissions decreased continuously at the beginning of January until approximately one week after the implementation of the COVID-19 lockdown, with estimated decreases in NO_x emissions of up to 42.5% from the P1 to P2 period (Table 4). Subsequently, the NO_x emissions stabilized with small fluctuations until the official back-to-work day when the NO_x emissions began to increase due to easing of the control measures and the resumption of business. According to inversion estimation, NO_x emissions recovered by 3.9% during the P3 period. These results indicate that the temporal variation in our estimated NO_x emissions agreed well with the timing of the Spring Festival and different control stages of COVID-19. However, for other species (i.e., $PM_{2.5}$, PM_{10}, SO_2 and CO), although their emissions generally decreased from 1st January to the end of the 2020 Spring Festival holiday, they showed much smaller reductions than the NO_x emissions. The emission reduction for these species was only approximately 7.9-12.1% (Table 4). This is consistent with the inversion results by Hu et al. (2022) who found that SO_2 emissions in China decreased only by 9.2% during COVID-19 lockdown. In addition, the emissions of these species quickly rebounded to their normal level just one week after the end of the Spring Festival holiday. As estimated by our inversion results, the SO_2 emissions recovered by 7.2% during the P3 period, which was only 2.5% lower than that during the P1 period. The $PM_{2.5}$ and PM_{10} emissions during the P3 period were 3.3% and 43.6% higher, respectively, than those during the P1 period.

Similar results were found in different regions of China (Fig. 5 and Table 5), where the NO_x emissions decreased much more than other species. In addition, unlike the uniform decreases in NO_x emissions in different regions of China (~40%),

10

320 there was apparent spatial heterogeneity in the emission changes in $PM_{2.5}$, PM_{10}, SO_2 and CO (Table 5 and Fig. 6). For example,

321 from the P1 to P2 period, the $PM_{2.5}$ emissions decreased by over 20% in the Central region but only by 8.8% in the NE region.

322 The $PM_{2.5}$ emissions even increased by 5.5% in the NCP region. This may be due to the increased emissions from industry

323 and fireworks according to the field measurements conducted by previous studies (Li et al., 2022; Ma et al., 2022; Zuo et al.,

324 2022; Dai et al., 2020). Based on the measurement of stable Cu and Si isotopic signature and distinctive metal ratios in Beijing

325 and Hebei, Zuo et al. (2022) analyzed the variations in the $PM_{2.5}$ sources during the COVID-19 pandemic, who reported that

326 the primary $PM_{2.5}$ emissions did not decrease in Beijing and Hebei, and that the PM-associated industrial emissions may

327 actually increase during the lockdown period. The increased industrial heat sources detected by Li et al. (2022) based on VIIRS

328 active fire data also supported the increased industrial emissions over the NCP region during lockdown period. Meanwhile,

329 consistent with the field measurements in Beijing and Tianjin conducted by Ma et al. (2022) and Dai et al. (2020), substantial

330 high levels of potassium (K^+) and magnesium (Mg^{2+}) ion were found over the NCP region during the Spring Festival according

331 to the aerosol chemical composition measurements obtained from CNEMC (Fig. S8). Since K^+ and Mg^{2+} are two important

332 fingerprints of the firework emissions, the high levels of K^+ and Mg^{2+} suggest that the emissions from fireworks during Spring

333 Festival were also a potential contributor to the increased of $PM_{2.5}$ emissions over the NCP region. In contrast, the SW and

334 central regions exhibited relatively larger emission reductions for these species (Fig. 5 and Table 5) by 12.6–25.9% and 10.6–

335 23.7%, respectively. The emission rebound during the P3 period was more prominent in the SE, central and SW regions (Fig.

336 5 and Fig. 7), where emissions recovered by 6.0–16.4% for NO_x, 7.5–19.8% for SO_2, 7.4–13.1% for CO, 12.3–47.7% for $PM_{2.5}$

337 and 28.6–135.9% for PM_{10} (Table 5). This result is consistent with the earlier degradation of the response level to the COVID-

338 19 virus (from the first level to the second or third level) over these regions (Table S2). In contrast, there were decreases in

339 emissions in the NCP, NE and NW regions. $PM_{2.5}$ emissions were reduced by 9.9% in the NCP region and by 19.2% in the

340 NE region from the P2 to P3 period (Table 5). Moreover, we found that the PM_{10} emissions surged in the NW and central

341 regions, where the PM_{10} emissions during the P3 period were almost two times larger than those during the P2 period (Table

342 5). However, this finding may be related to the enhanced dust emissions over these two regions rather than the effects of

343 returning to work according to the decreased $PM_{2.5}/PM_{10}$ ratios during the P3 period. According to Fig.S9, the $PM_{2.5}/PM_{10}$

344 ratio was relatively stable during the P1 and P2 period, but it decreased substantially during the P3 period, from 0.81 to 0.48

345 over the NW region and from 0.77 to 0.53 over the Central region. A lower $PM_{2.5}/PM_{10}$ ratio commonly suggests that the PM_{10}

346 is more likely to be attributed to natural sources such as dust (Wang et al., 2015; Fan et al., 2021). Moreover, the NW and

347 Central region are typical source areas of dust in China, therefore the increasing of PM_{10} emissions over NW and Central

348 regions may be mainly related to the enhanced dust emissions. This demonstrates the necessity to consider changes in natural

349 emissions during COVID-19 restrictions. Thus, to reduce the effects of natural emissions on our findings, the same analysis

350 was performed for the emissions over southeast China (Fig. S10) where emissions were dominated by anthropogenic sources,

351 which shows consistent results with the findings above (Fig. S11 and Table S3).

3.2.3 Explanations for the emission changes during COVID-19 restrictions

Two explanations may help clarify the unbalanced emission changes between NO_x and other species. First, the COVID-19 lockdown policy has led to dramatic decreases in transportation activities throughout China; however, as shown in Fig. 4, the relative contributions of the transportation sector to the emissions of SO_2 (2.4%), CO (18.5%), $PM_{2.5}$ (6.1%) and PM_{10} (4.7%) are much smaller than those for NO_x emissions (34.3%) (Zheng et al., 2018; Li et al., 2017a). Thus, the reduction in traffic activities can only substantially decrease NO_x emissions. Reductions in CO emissions (-10.6%) were relatively larger than those for SO_2 (-9.7%) and $PM_{2.5}$ (-7.9%) emissions, which is consistent with the relatively larger contributions of the transportation sector to CO emissions. However, the differences in the percentage decreases in emissions of CO, SO_2 and $PM_{2.5}$ is not as significant as the differences in their transportation share (18% versus 2% and 6%). This may be on the one hand due to the uncertainty in the estimated relative contributions of different sectors to the total emissions of CO, SO_2 and $PM_{2.5}$, on the other hand were possibly due to the uncertainty in the emission inversions, especially considering that the decreasing trend of CO, SO_2 and $PM_{2.5}$ were not significant. Also, other factors beyond transportation may have influenced the reductions of anthropogenic emissions during P2 period. For example, the PM_{10} emissions showed the largest reductions among these four species, which is related in part to the reduced dust emissions due to shutting down of construction sites during the lockdown period (Li et al., 2020). Second, as shown in Fig. 4, the industrial and residential sectors are the major contributors to the anthropogenic emissions of SO_2, CO, $PM_{2.5}$ and PM_{10} in China, together contributing 77.6%, 78.3%, 86.5% and 86.3%, respectively, to their total emissions. The much smaller reductions of these species' emissions were thus in line with the fact that there were no intentional restrictions on heavy industry during the COVID-19 restrictions. A large number of non-interruptible processes, such as steel, glass, coke, refractory, petrochemical, electric power, and especially heating, cannot be stopped during the COVID-19 lockdown. According to statistical data from the National Bureau of Statistics of China (Fig. S12), the industrial and power sectors did not show similar reductions in their activity levels as those seen in the transportation sector. Power generation and steel production even showed increases in many provinces, which corresponds well with the emission increases over these regions. In addition, since people were required to stay at home, residential emissions were likely increased due to the increased energy consumption for heating or cooking. Therefore, our inversion results supported the views that the emissions of species related to industrial and residential activities did not decline much during the lockdown period, and that the COVID-19 lockdown policy was largely a traffic control measure with small influences on other sectors.

3.3 Investigation of air quality change over the NCP region during COVID-19 restrictions

Using the inversion results, we reassessed the environmental impacts of the COVID-19 restrictions on the air pollution over NCP region. The NCP region was chosen because it is the key target region of air pollution control in China and where unexpected severe haze occurred. A major caveat in previous studies that explored the impacts of COVID-19 lockdowns on air quality is the uncertainty in the emission changes during COVID-19 restrictions. The inversion results enable us give a more reliable assessment of the environmental impacts of COVID-19 restrictions. Figure 8 shows the observed changes in

384 PM$_{2.5}$ and O$_3$ concentrations over the NCP region from the P1 to P2 period. The observations showed consistent reductions in
385 PM$_{2.5}$ concentrations over the NCP region (by 13.6 μg/m^3). However, substantial increases in PM$_{2.5}$ concentrations were
386 observed in the Beijing area (by 31.2 μg/m^3). In contrast to the widespread reductions in PM$_{2.5}$ concentrations, the O$_3$
387 concentrations significantly increased over the whole NCP region (by 28.3 μg/m^3) and the Beijing area (by 16.8 μg/m^3). The
388 simulations based on our inversion results reproduced the observed changes in PM$_{2.5}$ and O$_3$ concentrations over the NCP
389 region well, although the O$_3$ concentrations were underestimated in all regions (Fig. S6) and the changes in PM$_{2.5}$ and O$_3$
390 concentrations were slightly overestimated by 1.6 and 2.6 μg/m^3 in the simulation (Fig. 8).

391   As detailed in the Sect 2.4, the simulated changes in air pollutant concentrations before and after lockdown were
392 decomposed into meteorological-induced (MI) changes and emission-induced (EI) changes through two different scenarios to
393 account for the nonlinearity of the atmospheric chemical system. According to Fig. S13, the differences in calculated MI and
394 EI based on different scenarios were small for PM$_{2.5}$ concentrations, which were about 2 μg/m^3 in this application, while they
395 were relatively larger for O$_3$, which were around 5 μg/m^3 over the Beijing and NCP region (Fig. S14). In addition, the sign
396 of calculated MI using different scenarios were opposite although both suggested weak contributions of meteorological
397 variation to the changes of O$_3$ concentrations. This suggests that the calculated MI and EI changes of O$_3$ concentrations could
398 be more sensitive to the used scenarios, which may be associated with the stronger chemical nonlinearity of the O$_3$
399 concentrations. Figure 9 shows the mean results of the calculated MI and EI changes using the two different scenarios. It shows
400 that the meteorological variation dominated the changes in PM$_{2.5}$ concentrations over the NCP region, which contributed 90%
401 of the PM$_{2.5}$ reductions over most parts of the NCP region. Moreover, this variation made significant contributions (57.9%) to
402 the increases in PM$_{2.5}$ concentrations over the Beijing area. This finding suggested that meteorological variations played an
403 irreplaceable role in the occurrence of the unexpected PM$_{2.5}$ pollution around the Beijing area. Compared with the
404 meteorological conditions before lockdown (Fig. 10), there were increases in relative humidity over northern China, which
405 facilitated the reactions for aerosol formation and growth. Wind speed also decreased over the Beijing area accompanied by
406 an anomalous south wind, which facilitated aerosol accumulation and the transportation of air pollutants from the polluted
407 industrial regions of the Hebei Province to Beijing. The increases in boundary layer height from the P1 to P2 period were also
408 much smaller in the Beijing area than in other areas of the NCP. Thus, the Beijing area has exhibited distinct meteorological
409 variations from other areas of the NCP region, which correspond well to the different changes in PM$_{2.5}$ concentrations over the
410 Beijing area.

411   The emission changes contributed slightly to the PM$_{2.5}$ reductions over the NCP region (8.6%). This is because, on the
412 one hand, the large reductions in NO$_x$ emissions (by 44.4%) only reduced nitrate by approximately 10–30% due to the nonlinear
413 effects of chemical reactions (Fig. 11), and on the other hand, the emissions of primary PM$_{2.5}$ and its precursors from other
414 sectors changed little during the COVID-19 restrictions (Table 5). The emission changes contributed more to the increased
415 PM$_{2.5}$ concentrations over the Beijing area (42.1%). This is mainly associated with the increases in primary PM$_{2.5}$ emissions
416 around the Beijing area, as seen in Fig. 6, possibly due to the increased emissions from the industry as we mentioned before
417 (Zuo et al., 2022) and the increased firework emissions during the Spring Festival as shown by the rapid increases in

418 concentrations of K^+ and Mg^{2+} measured by CNEMC (Fig. S15). Therefore, our results suggested that the unexpected $PM_{2.5}$

419 pollution during lockdown period was mainly driven by unfavorable meteorological conditions together with small changes

420 or even increases in primary $PM_{2.5}$ emissions. This finding is in line with previous results of Le et al. (2020) but different from

421 those of Huang et al. (2021), who suggested that enhanced secondary aerosol formation was the main driver of severe haze

422 during the COVID-19 restrictions. To investigate it, we further analyzed the changes in the concentrations of secondary

423 inorganic aerosols (SIAs). First, we evaluated our model results against the observed SIA concentrations, which showed that

424 the model results using our inversion emissions well reproduced the observed concentrations of SIAs over the NCP region

425 (Fig. 12) with mean bias (MB) ranging from -5.14 to 5.45 $\mu g/m^3$ and correlation coefficient (R) ranging from 0.59 to 0.80. The

426 observed increases in SIA concentrations over the Beijing area, especially for sulfate concentrations, were also captured in our

427 simulations (Fig. 11), although underestimation occurred due to the uncertainty in simulating SIA concentrations. Through

428 sensitivity experiments, we found that the increases in SIA concentrations were still driven by meteorological variations (Fig.

429 13). In fact, the emission reductions only led to a 10% decrease in SIA concentrations over the NCP region. This finding

430 suggests that the enhanced secondary aerosol formation was likely mainly driven by the unfavorable meteorological conditions

431 associated with higher temperature and relative humidity instead of the emission reductions during the lockdown period. This

432 is in line with the observation evidences from Ma, T et al (2022) who emphasized that the increased temperature and relative

433 humidity promoted the formation of secondary pollutants during the COVID-19 restrictions.

434   In terms of O_3 concentrations, the emission changes subsequently became the dominant contributor to the O_3 increases

435 by more than 100% in the Beijing area and by 96.0% over the NCP region. This result is mainly because the lockdown period

436 occurred in midwinter when photochemical O_3 formation was minimal; thus, the large increase in O_3 is expected solely from

437 the effect of the reduced titration reaction associated with the large reductions in NO_x emissions. Although the higher

438 temperature and slower wind speed during the lockdown period were favorable for the increases in O_3 concentrations, their

439 contributions were much smaller than those of emission changes (Fig. 9). These results suggested that control measures, such

440 as COVID-19 restrictions, were inefficient for air pollution mitigation in China considering the high economic cost of the

441 COVID-19 restrictions.

442   We also compared our results with previous studies that differentiated the contributions of meteorology and emission to

443 the $PM_{2.5}$ and O_3 concentrations. Before comparisons, it should be noted that it is difficult to directly compare our results with

444 previous studies due the altered definition of meteorological contribution, different reference period that used to quantify the

445 meteorological contributions and different targeted region. For example, in Song et al. (2021), the reference period used to

446 determine the meteorological contribution is the corresponding period of COVID-19 pandemic in 2019. Le et al. (2020) used

447 the multiyear climatology as the reference period. In Wang et al. (2020) and Sulaymon et al. (2021), the MI changes of $PM_{2.5}$

448 concentrations were defined as the difference between the modeled concentrations in high-pollution days and those in low-

449 pollution days under hypothetical emission reduction scenario. Zhao et al. (2020) used a similar reference period to ours to

450 determine the MI changes but they used the outdated emission inventory. Table 6 summarized the results from the selected

451 studies over Beijing and Beijing-Tianjin-Hebei region. Note that some studies only provided the relative changes in the

modeled PM$_{2.5}$ concentrations. It shows that due to the uncertainties in emission changes during COVID-19 pandemic, the EI changes estimated by Zhao et al. (2020) were possibly overestimated compared to our studies (55% versus 24.7%). Both Sulaymon et al. (2021) and Wang et al. (2020) suggested negative EI changes during COVID-19 period in Beijing. This because they presumed that the emissions were largely reduced during COVID-19 lockdown which may deviate from the real changes of emissions according to our inversion results. Meanwhile, although they used same method and reference period, their results differed largely (-2.7 versus -13.4 $\mu g/m^3$) due to the different emission reduction scenario they assumed. Le et al. (2020) only considered the emission reductions of NO$_x$ in their sensitivity simulations without considerations of other species, therefore their calculated EI changes may be underestimated compared to our results (almost 0% versus 24.7%). However, the calculated MI changes were consistent between our study and Le et al. (2020). In terms of O$_3$, the calculated EI changes by our study were also higher than that calculated by Zhao et al. (2020) in Beijing (85.7% versus 70%). These results suggested that the EI and MI changes calculated by our study could be more reasonable, considering that the emissions of different species were well constrained which could better represent the temporal variation and spatial heterogeneity of emission changes during COVID-19.

4 Conclusions and discussions

The COVID-19 pandemic is an unprecedented event that significantly influenced the social activity and associated emissions of air pollutants. Our results provide a quantitative assessment of the influences of COVID-19 restrictions on multi-air pollutant emissions in China. Otherwise, understanding of the relationship between air quality and human activities may be biased. The inversion results provide important evidences that the COVID-19 lockdown policy was largely a traffic control measure with substantially reducing impacts on NO$_x$ emissions but much smaller influences on the emissions of other species and other sectors. Traffic control has widely been considered to be the normal protocol in implementing regulations in many cities of China, but its effectiveness on air pollution control is still disputed (Han and Naeher, 2006; Zhang et al., 2007; Chen et al., 2021; Cai and Xie, 2011; Chowdhury et al., 2017; Li et al., 2017c). Thus, the COVID-19 restrictions provided us with a real nationwide traffic control scenario to investigate the effectiveness of traffic control on the mitigation of air pollution in China. The results suggested that traffic control as a separate pollution control measure has limited effects on the coordinated control of high concentrations of O$_3$ and PM$_{2.5}$ under the current air pollution conditions in China. In this case, the PM$_{2.5}$ concentrations were slightly reduced, while leading to substantial increases in O$_3$ concentrations. Severe haze was also not avoided during the COVID-19 restrictions due to unbalanced emission changes from other sectors and unfavorable meteorological conditions. China is now facing major challenges in both controlling PM$_{2.5}$ and controlling emerging O$_3$ pollution. The tragic COVID-19 pandemic has revealed the limitation of the road traffic control measure in the coordinated control of PM$_{2.5}$ and O$_3$. More comprehensive regulations for multiple precursors from different sectors are required in the future to address O$_3$ and PM$_{2.5}$ pollution in China.

Finally, there are certain limitations that should be aware of in our inversion work. Firstly, the COVID-19 restrictions were initiated during the Spring Festival of China which would also influence the air pollutant emissions in China. However, the inversion method used in this study did not differentiate the contributions of the Spring Festival from the COVID-19 restrictions. Similarly, the effects of natural emission changes were not differentiated in this study, which would lead to uncertainty in quantifying the effects of the COVID-19 restrictions on air pollutant emissions. Secondly, the overestimations of NO_2 measurement induced by chemiluminescence monitor interference were not directly corrected in our study due to the lack of synchronous observations of HNO_3, PAN and AN, thus the estimated NO_x emissions could be slightly overestimated according to the sensitivity run with corrected NO_2 measurement using CFs (Fig. S16–18). Meanwhile, the sensitivity results suggest that the inversed NO_x emissions may even drop faster if the NO_2 measurement were corrected over the SE and SW regions (Fig. S19). Thirdly, the use of outdated emission inventory as the a priori emission would also be a potential limitation in our work although the iteration inversion method was used. A sensitivity inversion run was thus conducted based on the a priori emission for a more recent year of 2018 to test the influence of the a priori emission inventory. This new emission inventory is comprised of the anthropogenic emissions obtained from HTAPv3 (Crippa et al., 2023), the biogenic, soil and oceanic emissions obtained from the CAMS global emission inventory (https://ads.atmosphere.copernicus.eu/cdsapp#!/dataset/cams-global-emission-inventories?tab=overview, last access: March 15, 2023) and the biomass burning emissions obtained from the Global Fire Assimilation System (GFAS) (Kaiser et al., 2012). Detailed steps of the new inversion estimation were same as those elucidated in Sect.2. The results suggest that the inversion results based on the 2010 and 2018 inventory were broadly close to each other, while the inversion results based on 2018 inventory were relatively higher than those based on 2010 inventory, reflecting the uncertainty in our inversion results caused by the choice of a priori emission inventory (Fig. S20–22). However, the sensitivity run consistently showed that the NO_x emissions decreased much larger than other species (Fig. S23–24). This suggests that the choice of a priori emission inventory may not obviously influence the main conclusion of our study, but can lead to uncertainty in the magnitude of the inversion results which should be aware of by potential readers.

517 **Tables**

518 **Table 1. Corresponding relationship between the chemical observations and adjusted emissions**

Species	Descriptions	Observations that used for inversions of this species
BC	black carbon	$PM_{2.5}$
OC	organic carbon	$PM_{2.5}$
PMF	fine mode unspeciated aerosol	$PM_{2.5}$
PMC	coarse mode unspeciated aerosol	$PM_{10} - PM_{2.5}$
NO_x	nitrogen oxide	NO_2
SO_2	sulfur dioxide	SO_2
CO	carbon monoxide	CO

519

520 <mark>**Table 2. Configuration of simulation scenarios**</mark>

Scenarios	Meteorology input	Emission input	Purpose
BASE scenario	varied meteorological condition from pre lockdown to lockdown period	varied emission from pre-lockdown to lockdown period	To estimate the total changes of air pollutant concentrations induced by emission and meteorological change
MET change scenario	varied meteorological condition from pre-lockdown to lockdown period	constant emissions during pre-lockdown and lockdown period	To estimate the impacts of meteorological changes on the air pollutants
EMIS change scenario	constant meteorological during pre-lockdown and lockdown period	varied emission from pre-lockdown to lockdown period	To estimate the impacts of emission changes on the air pollutants

521
522
523
524
525
526
527

528

notation	description
MI	meteorological-induced changes in air pollutant concentrations
EI	emission-induced changes in air pollutant concentrations
$MI_{MET\ change\ scenario}$	meteorological-induced changes in air pollutant concentrations calculated by the MET change scenario
$EI_{MET\ change\ scenario}$	emission-induced changes in air pollutant concentrations calculated by total changes minus $MI_{MET\ change\ scenario}$
$EI_{EMIS\ change\ scenario}$	emission-induced changes in air pollutant concentrations calculated by the EMIS change scenario
$MI_{EMIS\ change\ scenario}$	meteorological-induced changes in air pollutant concentrations calculated by total changes minus $EI_{EMIS\ change\ scenario}$
$conc_{p1,BASE\ scenario}$	averaged concentrations of air pollutants during P1 period under the BASE scenario
$conc_{p2,BASE\ scenario}$	averaged concentrations of air pollutants during P2 period under the BASE scenario
$conc_{p1,MET\ change\ scenario}$	averaged concentrations of air pollutants during P1 period under the MET change scenario
$conc_{p2,MET\ change\ scenario}$	averaged concentrations of air pollutants during P2 period under the MET change scenario
$conc_{p1,EMIS\ change\ scenario}$	averaged concentrations of air pollutants during P1 period under the EMIS change scenario
$conc_{p2,EMIS\ change\ scenario}$	averaged concentrations of air pollutants during P2 period under the EMIS change scenario
$contri_{met}$	relative contributions of the meteorological variations to the changes in air pollutant concentrations
$contri_{emis}$	relative contributions of the emission changes to the changes in air pollutant concentrations

531

532

533

534

535

536 **Table 4. Inversion estimated emissions of different air pollutants in China and their changes between different periods during**
537 **COVID-19.**

	NO_x	SO_2	CO	$PM_{2.5}$	PM_{10}
P1 (Gg/day)	72.9	23.8	1160.2	44.5	75.5
P2 (Gg/day)	41.9	21.5	1037.4	40.9	66.4
P3 (Gg/day)	44.8	23.2	1078.2	45.9	108.4
(P2-P1)/P1	-42.5%	-9.7%	-10.6%	-7.9%	-12.1%
(P3-P2)/P1	3.9%	7.2%	3.6%	11.2%	55.7%
(P3-P1)/P1	-38.6%	-2.5%	-7.0%	3.3%	43.6%

538
539
540
541
542
543
544
545
546
547
548
549
550
551
552
553
554
555
556
557
558
559
560

561 **Table 5. Inversion estimated emission changes of different air pollutants over different regions in China between different periods**
562 **during COVID-19 restrictions**

	NO_x	$PM_{2.5}$	PM_{10}	SO_2	CO
NCP					
(P2-P1)/P1	-44.4%	5.5%	2.8%	-1.6%	-4.3%
(P3-P2)/P1	-0.8%	-9.9%	31.8%	-5.9%	-10.0%
(P3-P1)/P1	-45.2%	-4.3%	34.7%	-7.5%	-14.3%
NE					
(P2-P1)/P1	-41.8%	-8.8%	-3.5%	-3.2%	-10.9%
(P3-P2)/P1	-6.0%	-19.2%	23.7%	-2.9%	-6.6%
(P3-P1)/P1	-47.8%	-28.0%	20.2%	-6.1%	-17.5%
SE					
(P2-P1)/P1	-41.4%	-9.5%	-24.4%	-19.4%	-3.5%
(P3-P2)/P1	10.2%	12.3%	28.6%	19.8%	13.1%
(P3-P1)/P1	-31.2%	2.8%	4.2%	0.3%	9.7%
SW					
(P2-P1)/P1	-43.5%	-12.6%	-25.9%	-17.5%	-23.8%
(P3-P2)/P1	6.0%	47.7%	33.1%	7.5%	7.4%
(P3-P1)/P1	-37.5%	35.1%	7.2%	-10.0%	-16.4%
NW					
(P2-P1)/P1	-38.5%	-4.0%	-8.3%	14.2%	-2.6%
(P3-P2)/P1	-21.1%	4.9%	145.3%	-4.1%	-7.2%
(P3-P1)/P1	-59.6%	0.9%	136.9%	10.1%	-9.8%
Central					
(P2-P1)/P1	-43.8%	-23.7%	-15.7%	-10.6%	-17.4%
(P3-P2)/P1	16.4%	24.4%	135.9%	18.5%	8.4%
(P3-P1)/P1	-27.4%	0.7%	120.3%	7.9%	-9.0%

563

564

565

Table 6. Calculated MI and EI changes in PM$_{2.5}$ concentrations during COVID-19 pandemic by previous studies

	MI changes	EI changes	Region	Reference period	Method	Reference
1	26.79 μg/m^3	-21.84 μg/m^3	Beijing	January 23-March 10, 2019 versus January 23-March 10, 2020	observation-based wind-decomposition method	Song et al. (2021)
2	Around 20 μg/m^3	-2.7 μg/m^3	Beijing	January 01 to February 29, 2020	CTM with hypothetical emission reduction scenario	Sulaymon et al. (2021)
3	Around 45 μg/m^3	-13.4 μg/m^3	Beijing	January 01 to February 29, 2020	CTM with hypothetical emission reduction scenario	Wang et al. (2020)
4	31.3%	Around 0%	Beijing-Tianjin-Hebei	January 01 to February 13, 2020	CTM sensitivity simulations using different emission rates and multiyear climatology	Le et al. (2020)
5	Around 5%	Around 55%	Beijing	January 16-22, 2020 versus January 26 to February 1, 2020	CTM with fixed emission inventory for 2017	Zhao et al. (2020)
6	17.5 μg/m^3 (34.0%)	12.7 μg/m^3 (24.7%)	Beijing	January 1-20, 2020 versus January 21 to February 9, 2020	CTM with inversion emission inventory	This study

570   **Figure 1: Modeling domain of the ensemble simulation overlay the distributions of observation sites from CNEMC. Different colours**
571   **denote the different regions in mainland of China, namely North China Plain (NCP), Northeast China (NE), Southwest China (SW),**
572   **Southeast China (SE), Northwest China (NW) and Central.**
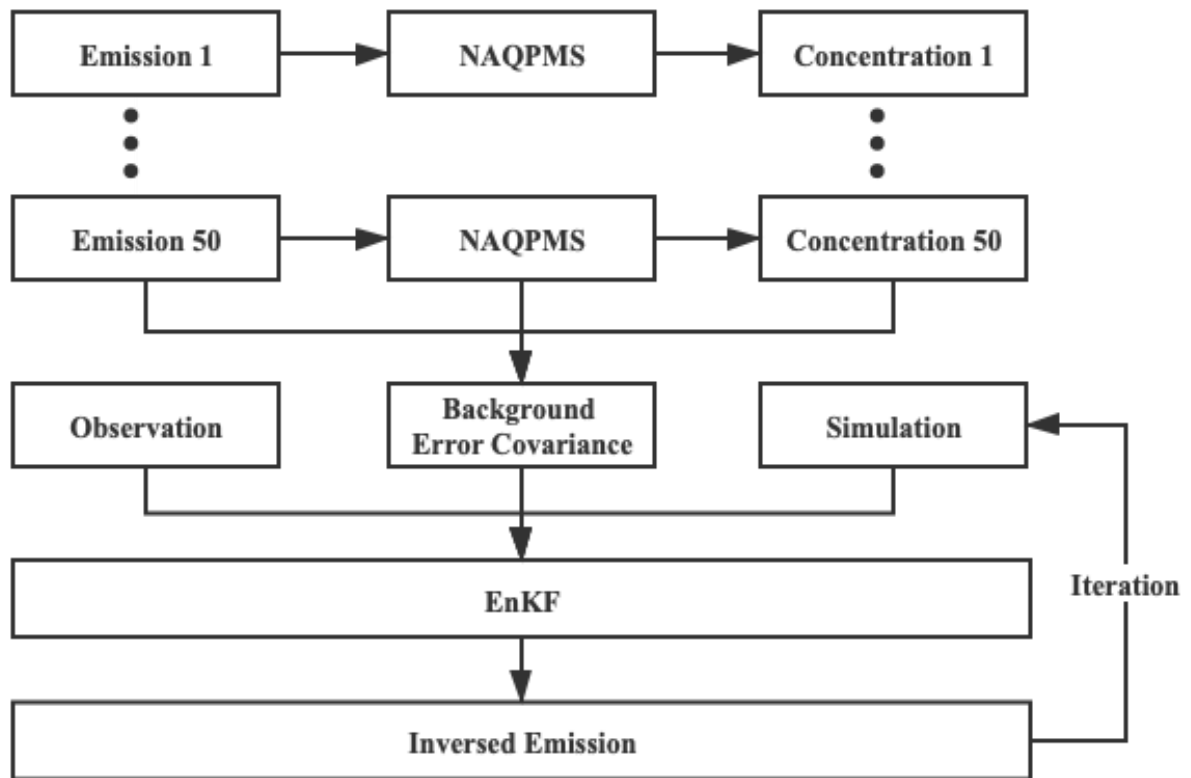
573

574 **Figure 2: Illustration of the iteration inversion scheme used in this study.**

575
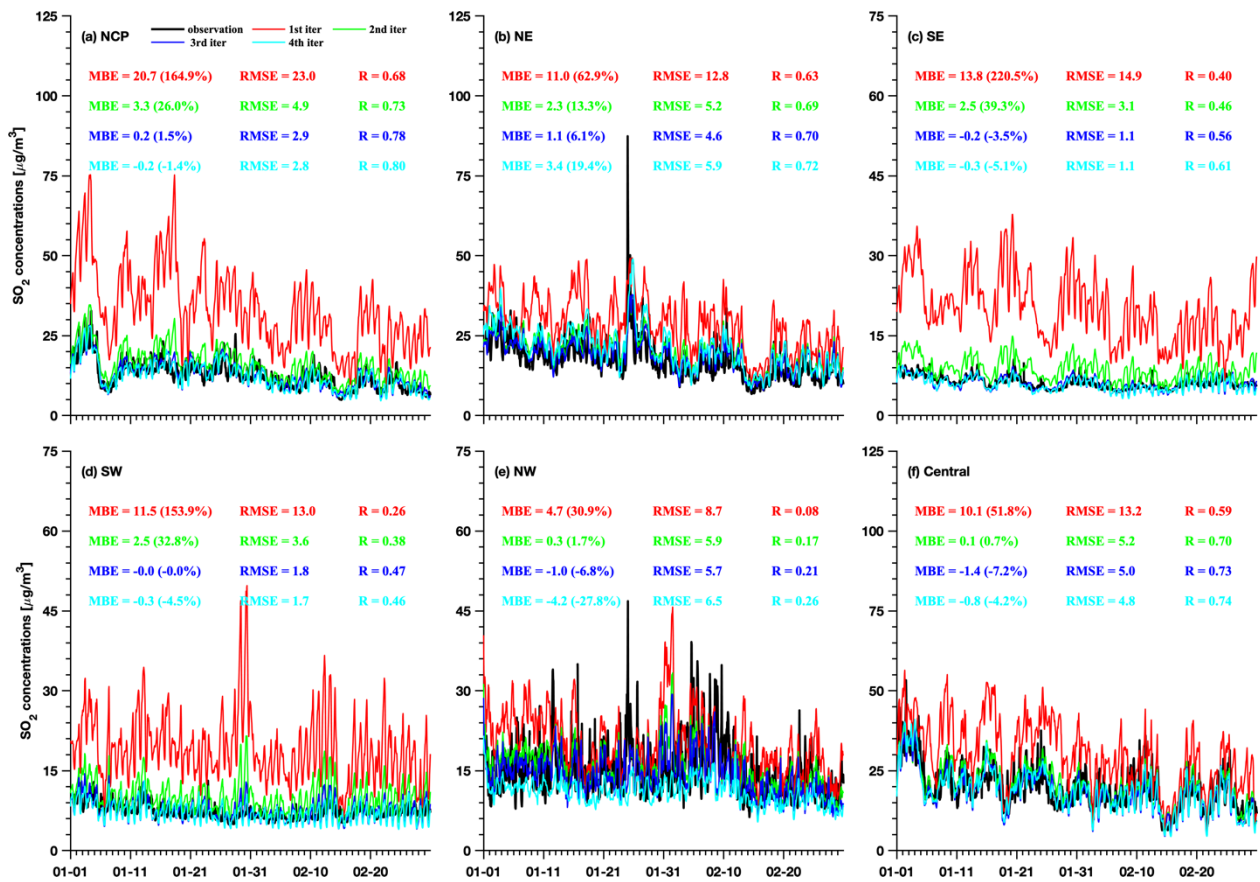
Figure 3: Comparisons of the observed and simulated mean SO₂ concentrations using emissions of different iteration time at validation sites over (a) NCP region, (b) NE region, (c) SE region, (d) SW region, (e) NW region and (f) Central region.

24
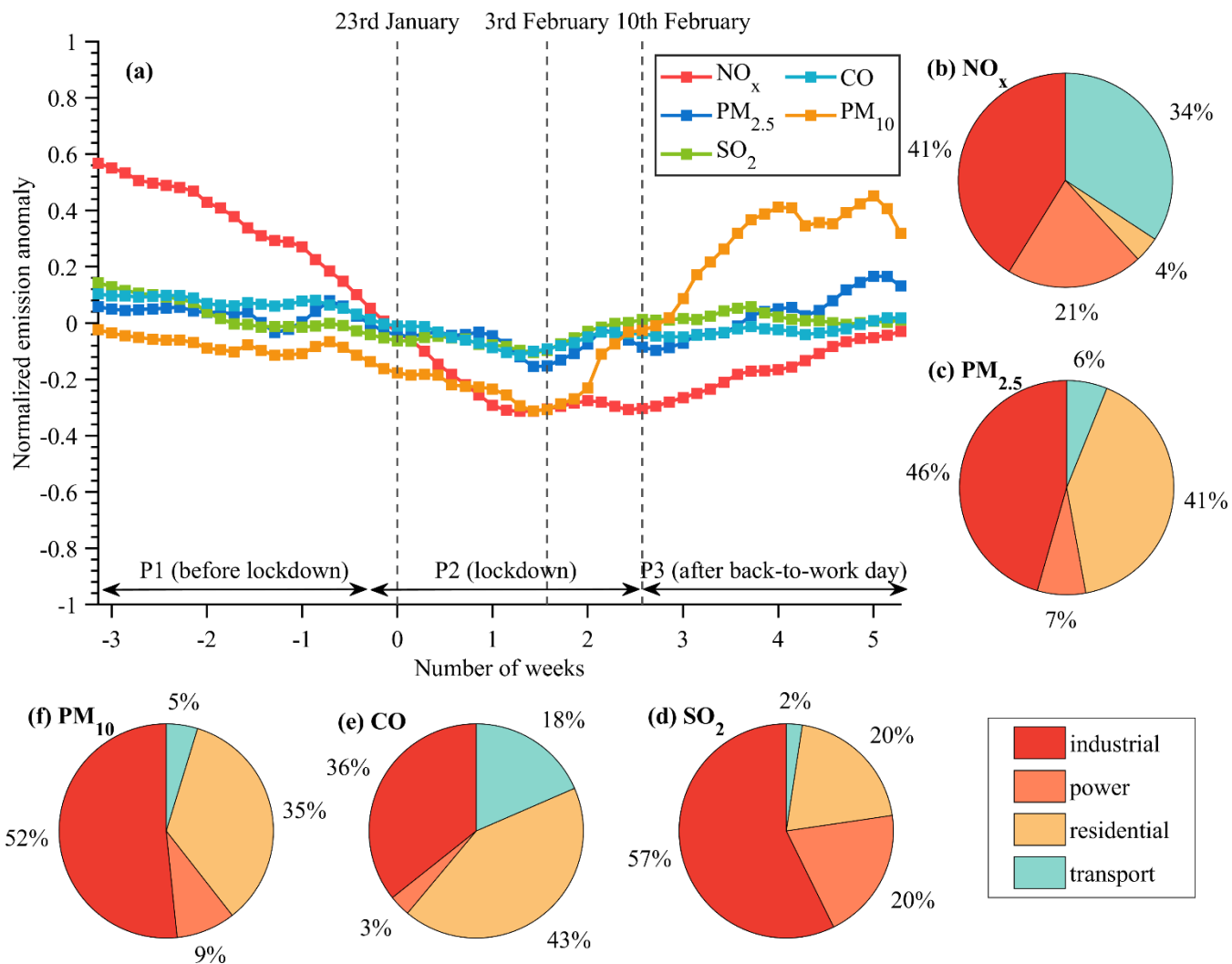
Figure 4: (a) Time series of normalized emission anomalies estimated by inversion results for different species in China from 1st January to 29th February 2020, and (b-f) Relative contributions of different sectors to the total anthropogenic emissions of NO_x, $PM_{2.5}$, PM_{10}, CO and SO_2 obtained from Zheng et al. (2018). The normalized emission anomaly is calculated by the emission anomaly divided by the average emissions during the whole period.

25
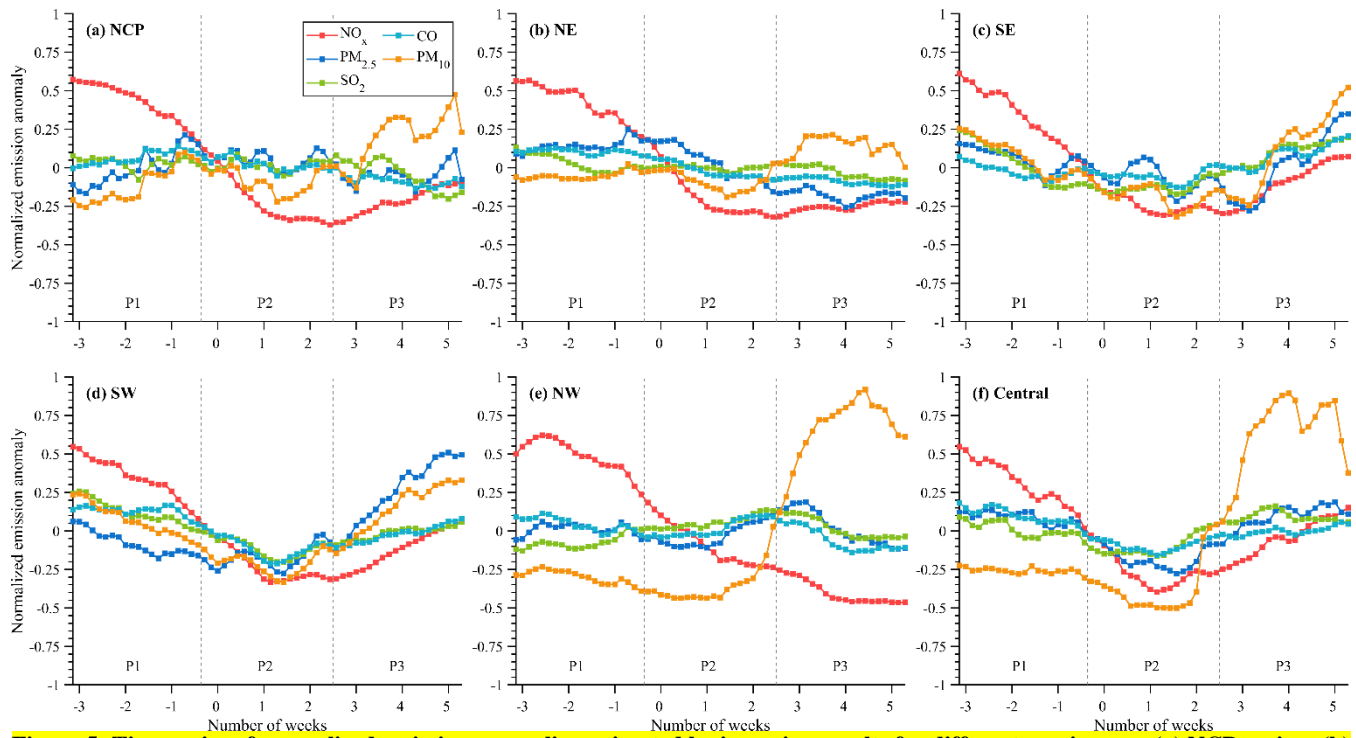
587
588 **Figure 5: Time series of normalized emission anomalies estimated by inversion results for different species over (a) NCP region, (b)**
589 **NE region, (c) SE region, (d) SW region, (e) NW region and (f) Central region from 1st January to 29th February 2020.**
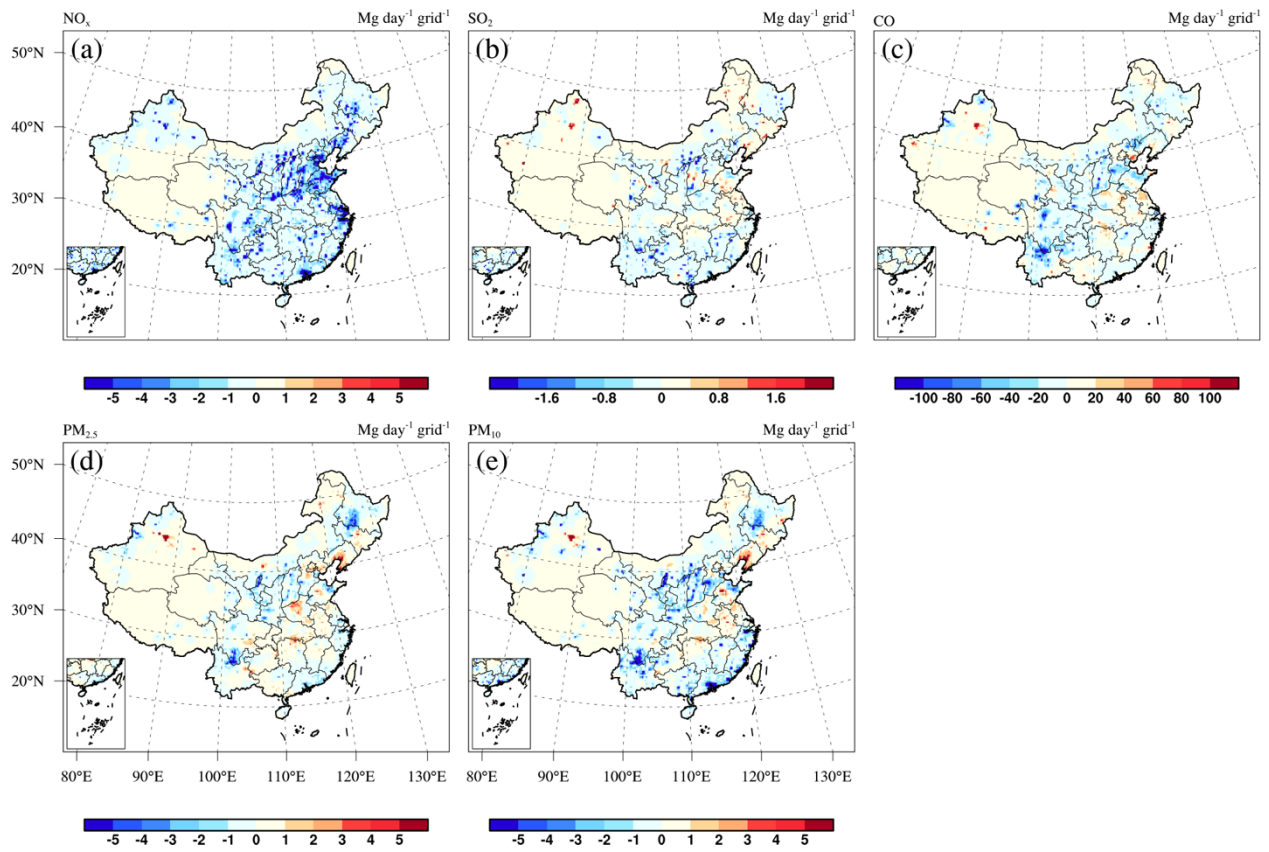
590

591   **Figure 6: The inversion estimated emission changes of (a) NO$_x$, (b) SO$_2$, (c) CO, (d) PM$_{2.5}$ and (e) PM$_{10}$ in China from P1 to P2 period.**

592
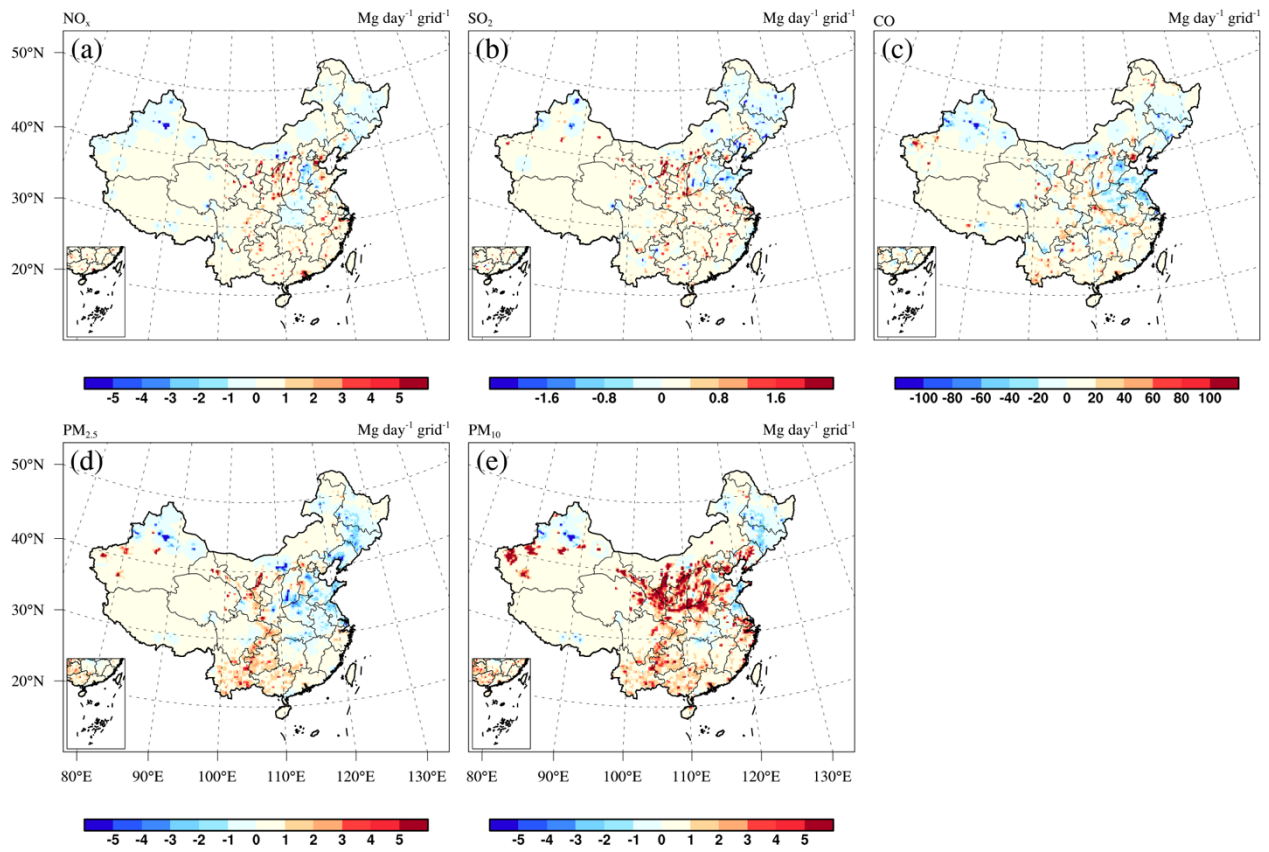
Figure 7: The inversion estimated emission changes of (a) NO$_x$, (b) SO$_2$, (c) CO, (d) PM$_{2.5}$ and (e) PM$_{10}$ in China from P2 to P3 period.

594

595
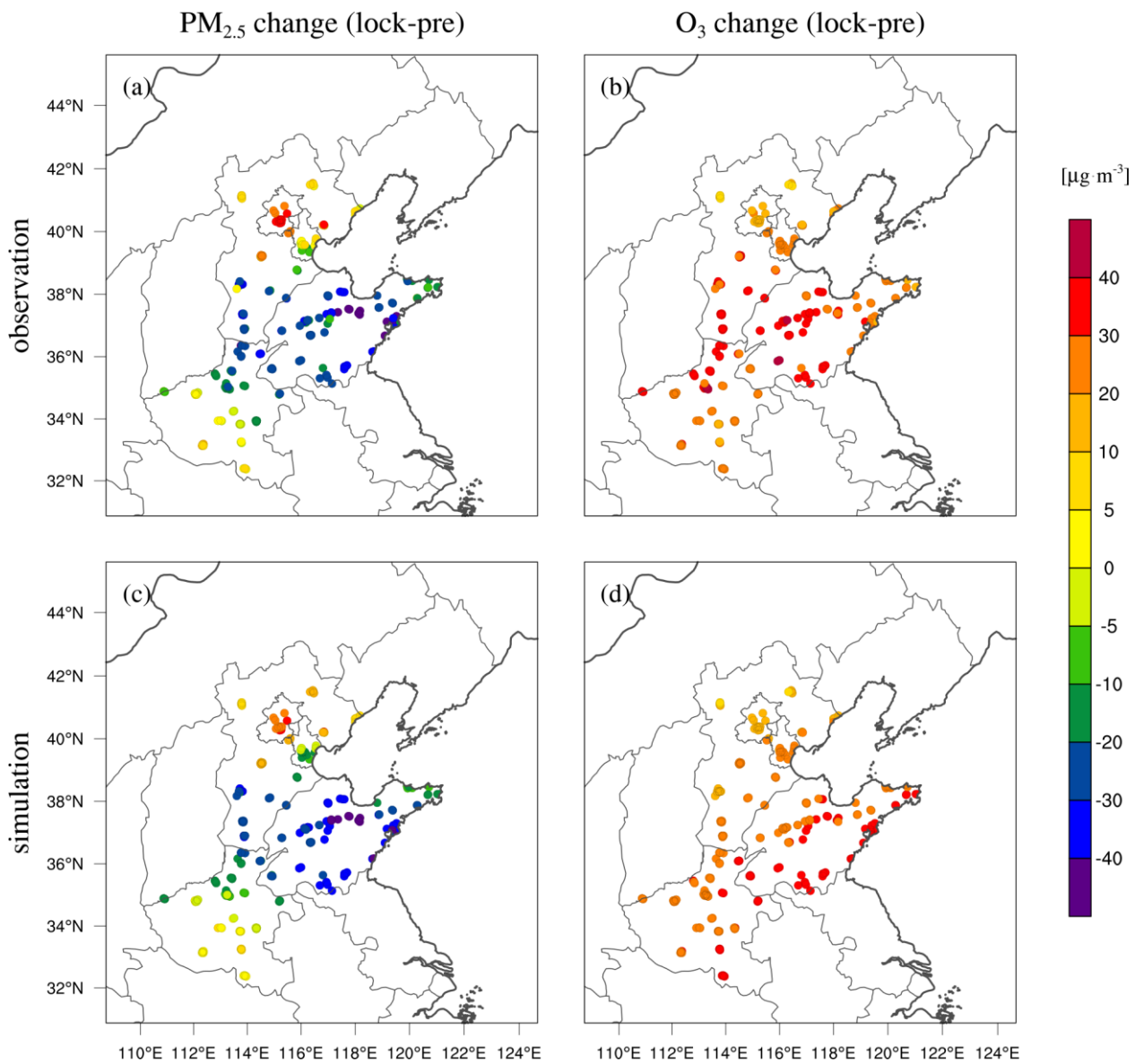
Figure 8: Changes in the observed and simulated concentrations of (a, c) PM$_{2.5}$ and (b, d) O$_3$ over the NCP region from the pre
lockdown period (P1) to the lockdown period (P2).

598
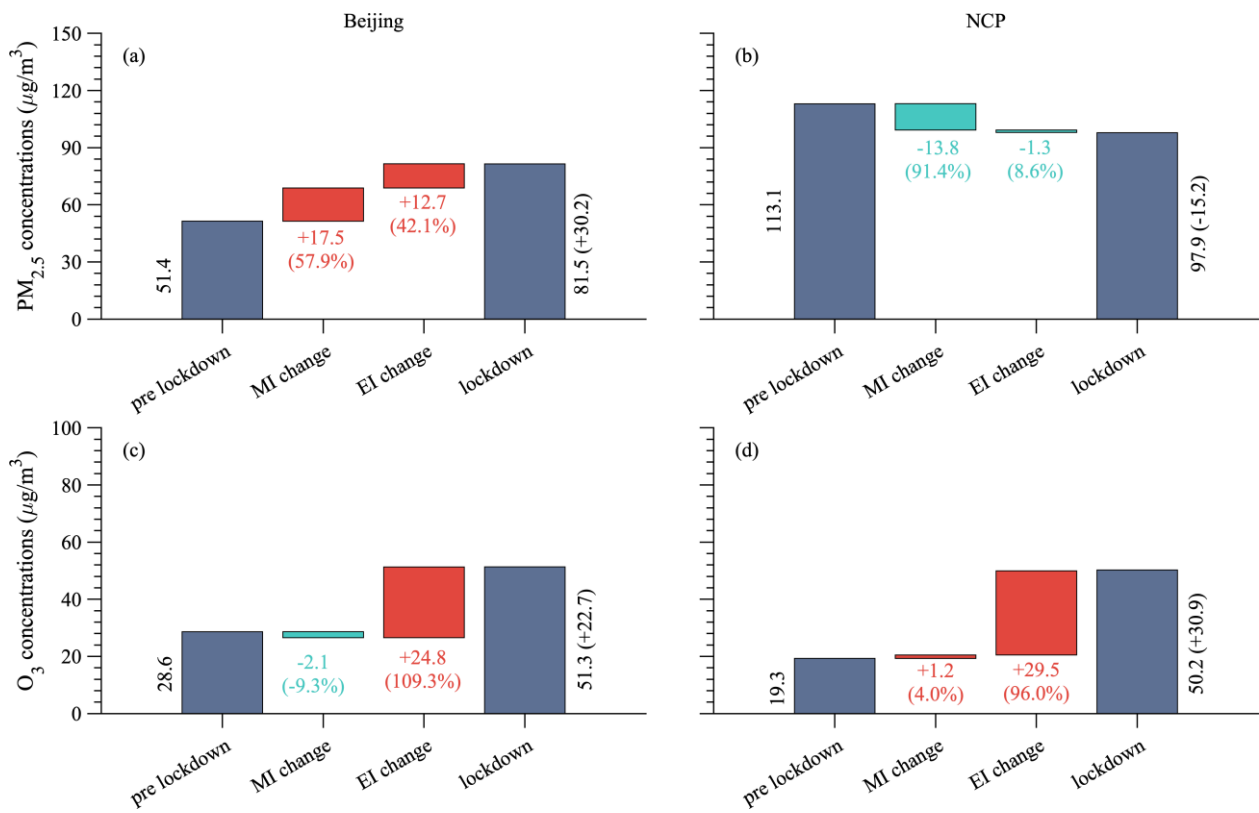
Figure 9: Contributions of the meteorological variations and emission changes to the changes in (a, b) PM$_{2.5}$ and (c, d) O$_3$
concentrations over Beijing and the NCP region from the pre lockdown period (P1) to the lockdown period (P2).
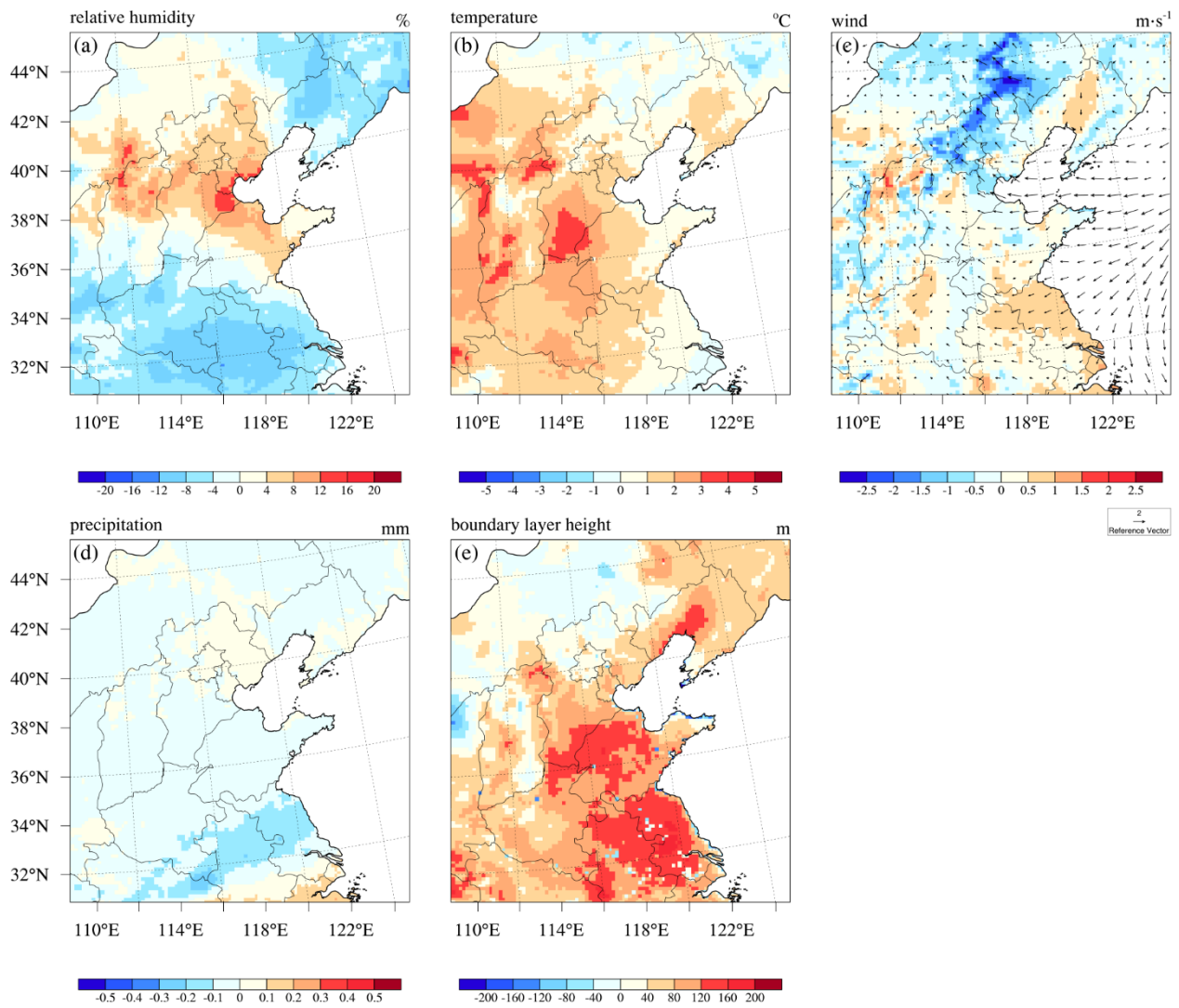
Figure 10: Changes in the (a) relative humidity, (b) temperature, (c) wind speed, (d) precipitation and (e) boundary layer height over the NCP region from P1 to P2 period obtained from WRF simulations.
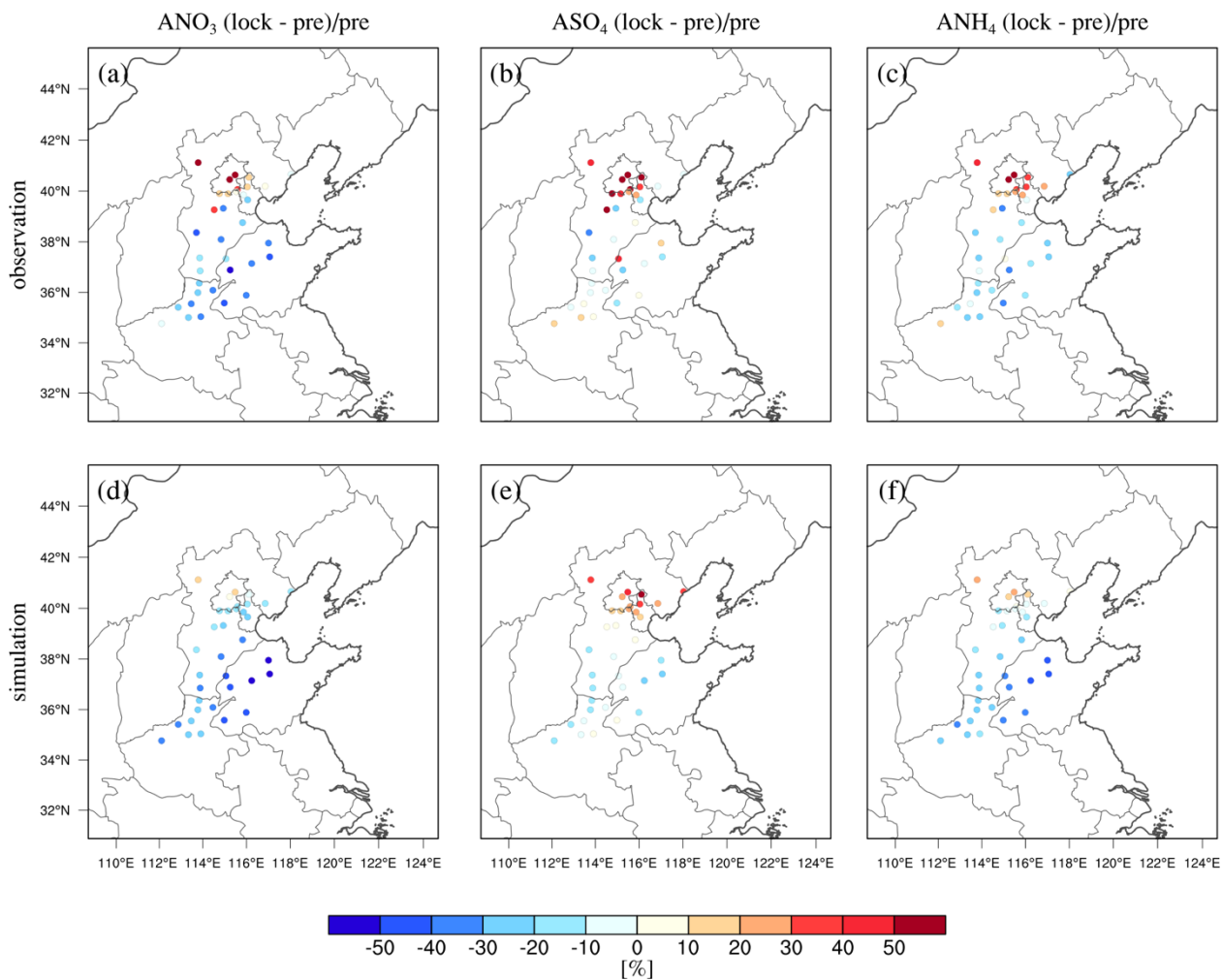
Figure 11: Relative changes in the simulated and observed concentrations of (a) ANO_3, (b) ASO_4, (c) ANH_4 over NCP region from P1 to P2 period.

612
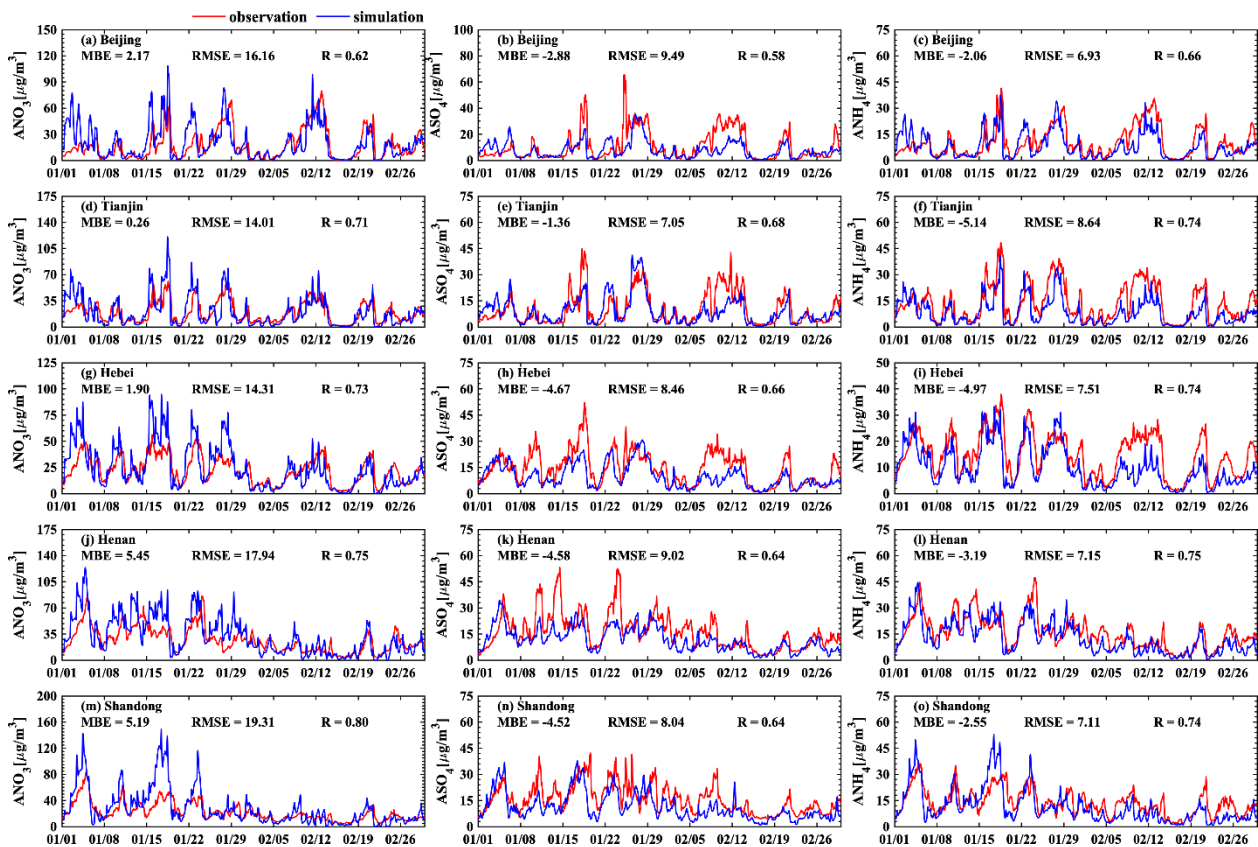
Figure 12: Time series of observed and simulated concentrations of ANO₃, ASO₄ and ANH₄ in (a-c) Beijing, (b-f) Tianjin, (g-i) Heibei, (j-l) Henan and (m-o) Shangdong province from 1st January to 29th February 2020.

615

616

617
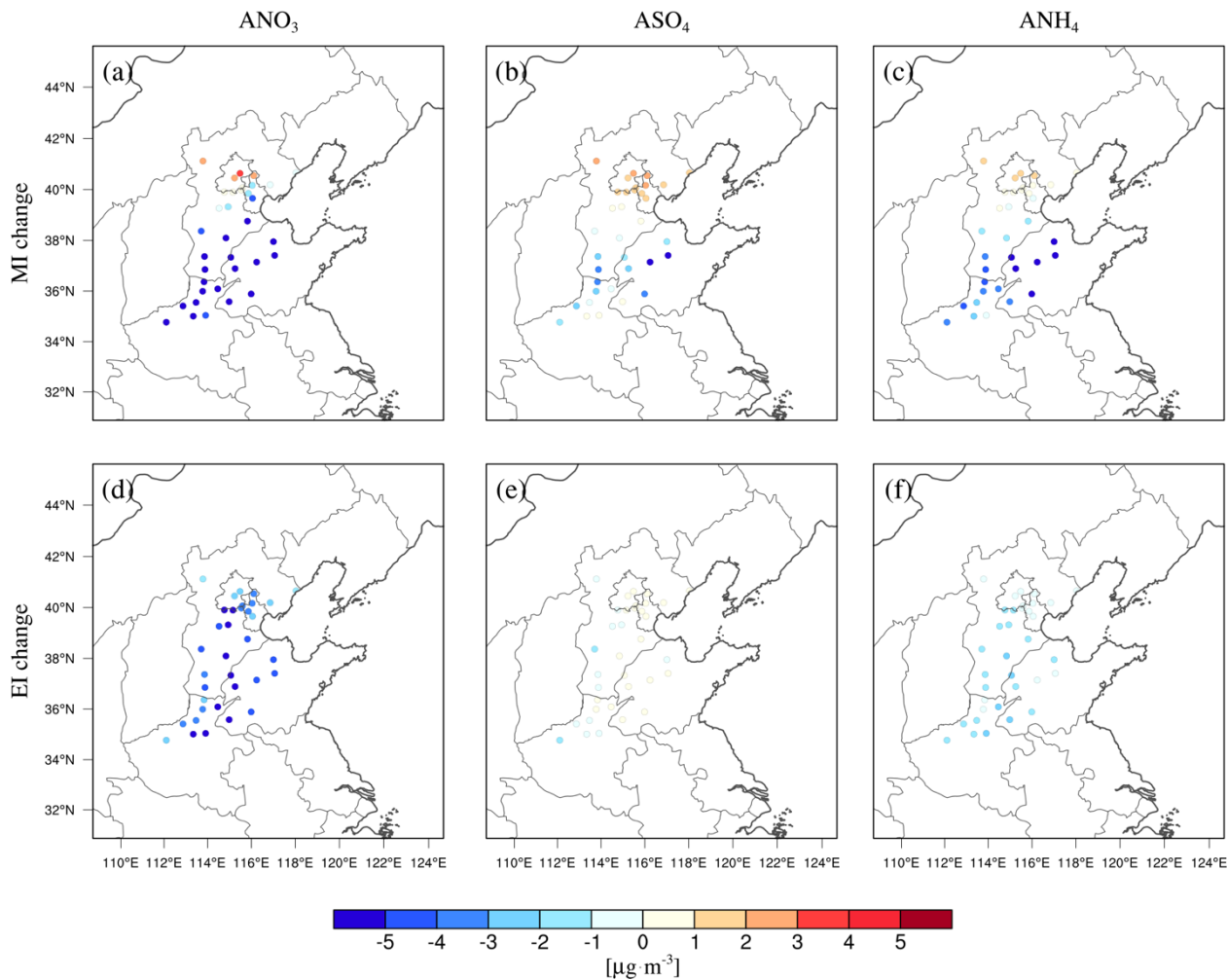
Figure 13: Meteorology-induced (MI) changes in the concentrations of (a) ANO₃, (b) ASO₄ and (c) ANH₄, as well as Emission-induced (EI) changes in the concentrations of (d) ANO₃, (e) ASO₄ and (f) ANH₄.

620

Data availability

The hourly surface observations can be obtained from China National Environmental Monitoring Centre (http://www/cnemc.cn/en); The inversion estimated emissions of multi-air pollutants in China during COVID-19 lockdown period and the NAQPMS simulation results are available from the corresponding authors on request.

636 **References**

637 Brasseur, G. P., Hauglustaine, D. A., Walters, S., Rasch, P. J., Muller, J. F., Granier, C., and Tie, X. X.: MOZART, a global chemical transport
638   model for ozone and related chemical tracers 1. Model description, J. Geophys. Res.-Atmos., 103, 28265-28289,
639   https://doi.org/10.1029/98jd02397, 1998.

640 Cai, H. and Xie, S.: Traffic-related air pollution modeling during the 2008 Beijing Olympic Games: The effects of an odd-even day traffic
641   restriction scheme, Sci. Total Environ., 409, 1935-1948, https://doi.org/10.1016/j.scitotenv.2011.01.025, 2011.

642 Chen, Z., Hao, X., Zhang, X., and Chen, F.: Have traffic restrictions improved air quality? A shock from COVID-19, J. Clean Prod., 279,
643   123622, https://doi.org/10.1016/j.jclepro.2020.123622, 2021.

644 Cheng, C., Barceló, J., Hartnett, A. S., Kubinec, R., and Messerschmidt, L.: COVID-19 Government Response Event Dataset (CoronaNet
645   v.1.0), Nat. Hum. Behav., 4, 756-768, https://doi.org/10.1038/s41562-020-0909-7, 2020.

646 Chowdhury, S., Dey, S., Tripathi, S. N., Beig, G., Mishra, A. K., and Sharma, S.: "Traffic intervention" policy fails to mitigate air pollution
647   in megacity Delhi, Environ. Sci. Policy, 74, 8-13, https://doi.org/10.1016/j.envsci.2017.04.018, 2017.

648 Chu, B., Zhang, S., Liu, J., Ma, Q., and He, H.: Significant concurrent decrease in PM2.5 and NO2 concentrations in China during COVID-
649   19 epidemic, J. Environ. Sci., 99, 346-353, https://doi.org/10.1016/j.jes.2020.06.031, 2021.

650 Chu, K. K., Peng, Z., Liu, Z. Q., Lei, L. L., Kou, X. X., Zhang, Y., Bo, X., and Tian, J.: Evaluating the Impact of Emissions Regulations on
651   the Emissions Reduction During the 2015 China Victory Day Parade With an Ensemble Square Root Filter, J. Geophys. Res.-Atmos., 123,
652   4122-4134, https://doi.org/10.1002/2017jd027631, 2018.

653 Cooper, M. J., Martin, R. V., McLinden, C. A., and Brook, J. R.: Inferring ground-level nitrogen dioxide concentrations at fine spatial
654   resolution applied to the TROPOMI satellite instrument, Environ. Res. Lett., 15, 12, https://doi.org/10.1088/1748-9326/aba3a5, 2020.

655 Crippa, M., Guizzardi, D., Butler, T., Keating, T., Wu, R., Kaminski, J., Kuenen, J., Kurokawa, J., Chatani, S., Morikawa, T., Pouliot, G.,

656   Racine, J., Moran, M. D., Klimont, Z., Manseau, P. M., Mashayekhi, R., Henderson, B. H., Smith, S. J., Suchyta, H., Muntean, M., Solazzo,

657   E., Banja, M., Schaaf, E., Pagani, F., Woo, J. H., Kim, J., Monforti-Ferrario, F., Pisoni, E., Zhang, J., Niemi, D., Sassi, M., Ansari, T., and

658   Foley, K.: HTAP_v3 emission mosaic: a global effort to tackle air quality issues by quantifying global anthropogenic air pollutant sources,

659   Earth Syst. Sci. Data Discuss., 2023, 1-34, https://doi.org/10.5194/essd-2022-442, 2023.

660 Dai, Q., Liu, B., Bi, X., Wu, J., Liang, D., Zhang, Y., Feng, Y., and Hopke, P. K.: Dispersion Normalized PMF Provides Insights into the

661   Significant Changes in Source Contributions to PM2.5 after the COVID-19 Outbreak, Environ. Sci. Technol., 54, 9917-9927,

662   https://doi.org/10.1021/acs.est.0c02776, 2020.

663 Diamond, M. S. and Wood, R.: Limited Regional Aerosol and Cloud Microphysical Changes Despite Unprecedented Decline in Nitrogen

664   Oxide Pollution During the February 2020 COVID-19 Shutdown in China, Geophys. Res. Lett., 47, e2020GL088913,

665   https://doi.org/10.1029/2020gl088913, 2020.

666 Dunlea, E. J., Herndon, S. C., Nelson, D. D., Volkamer, R. M., San Martini, F., Sheehy, P. M., Zahniser, M. S., Shorter, J. H., Wormhoudt,

667   J. C., Lamb, B. K., Allwine, E. J., Gaffney, J. S., Marley, N. A., Grutter, M., Marquez, C., Blanco, S., Cardenas, B., Retama, A., Villegas,

668   C. R. R., Kolb, C. E., Molina, L. T., and Molina, M. J.: Evaluation of nitrogen dioxide chemiluminescence monitors in a polluted urban

669   environment, Atmos. Chem. Phys., 7, 2691-2704, https://doi.org/10.5194/acp-7-2691-2007, 2007.

670 Evensen, G.: Sequential data assimilation with a nonlinear quasi-geostrophic model using Monte Carlo methods to forecast error statistics,

671   J. Geophys. Res.-Oceans, 99, 10143-10162, https://doi.org/10.1029/94JC00572, 1994.

672 Fan, C., Li, Y., Guang, J., Li, Z. Q., Elnashar, A., Allam, M., and de Leeuw, G.: The Impact of the Control Measures during the COVID-19

673   Outbreak on Air Pollution in China, Remote Sens., 12, 23, https://doi.org/10.3390/rs12101613, 2020.

674 Fan, H., Zhao, C., Yang, Y., and Yang, X.: Spatio-Temporal Variations of the $PM_{2.5}/PM_{10}$ Ratios and Its Application to Air Pollution Type

675   Classification in China, Front. Environ. Sci., 9, https://doi.org/10.3389/fenvs.2021.692440, 2021.

676 Feng, S., Jiang, F., Wang, H., Wang, H., Ju, W., Shen, Y., Zheng, Y., Wu, Z., and Ding, A.: NOx Emission Changes Over China During the

677   COVID-19 Epidemic Inferred From Surface NO2 Observations, Geophys. Res. Lett., 47, e2020GL090080, 10.1029/2020gl090080, 2020.

678 Forster, P. M., Forster, H. I., Evans, M. J., Gidden, M. J., Jones, C. D., Keller, C. A., Lamboll, R. D., Le Quere, C., Rogelj, J., Rosen, D.,

679   Schleussner, C. F., Richardson, T. B., Smith, C. J., and Turnock, S. T.: Current and future global climate impacts resulting from COVID-

680   19, Nat. Clim. Chang., 10, 913-+, https://doi.org/10.1038/s41558-020-0883-0, 2020.

681 Granier, C., Lamarque, J., Mieville, A., Muller, J., Olivier, J., Orlando, J., Peters, J., Petron, G., Tyndall, G., and Wallens, S.: POET, a

682   database of surface emissions of ozone precursors, 2005.

683 Hammer, M. S., van Donkelaar, A., Martin, R. V., McDuffie, E. E., Lyapustin, A., Sayer, A. M., Hsu, N. C., Levy, R. C., Garay, M. J.,

684   Kalashnikova, O. V., and Kahn, R. A.: Effects of COVID-19 lockdowns on fine particulate matter concentrations, Sci. Adv., 7,

685   https://doi.org/10.1126/sciadv.abg7670, 2021.

686 Han, X. L. and Naeher, L. P.: A review of traffic-related air pollution exposure assessment studies in the developing world, Environ. Int., 32,

687   106-120, https://doi.org/10.1016/j.envint.2005.05.020, 2006.

688 Hauglustaine, D. A., Brasseur, G. P., Walters, S., Rasch, P. J., Muller, J. F., Emmons, L. K., and Carroll, C. A.: MOZART, a global chemical

689   transport model for ozone and related chemical tracers 2. Model results and evaluation, J. Geophys. Res.-Atmos., 103, 28291-28335,

690   https://doi.org/10.1029/98jd02398, 1998.

691 He, G. J., Pan, Y. H., and Tanaka, T.: The short-term impacts of COVID-19 lockdown on urban air pollution in China, Nat. Sustain, 3, 9,

692   https://doi.org/10.1038/s41893-020-0581-y, 2020.

693 He, T. L., Jones, D. B. A., Miyazaki, K., Bowman, K. W., Jiang, Z., Chen, X., Li, R., Zhang, Y., and Li, K.: Inverse modelling of Chinese
694   NOx emissions using deep learning: integrating in situ observations with a satellite-based chemical reanalysis, Atmos. Chem. Phys., 22,
695   14059-14074, https://doi.org/10.5194/acp-22-14059-2022, 2022.

696 Hu, Y., Zang, Z., Ma, X., Li, Y., Liang, Y., You, W., Pan, X., and Li, Z.: Four-dimensional variational assimilation for SO2 emission and its
697   application around the COVID-19 lockdown in the spring 2020 over China, Atmos. Chem. Phys., 22, 13183-13200,
698   https://doi.org/10.5194/acp-22-13183-2022, 2022.

699 Huang, X., Ding, A., Gao, J., Zheng, B., Zhou, D., Qi, X., Tang, R., Wang, J., Ren, C., Nie, W., Chi, X., Xu, Z., Chen, L., Li, Y., Che, F.,
700   Pang, N., Wang, H., Tong, D., Qin, W., Cheng, W., Liu, W., Fu, Q., Liu, B., Chai, F., Davis, S. J., Zhang, Q., and He, K.: Enhanced
701   secondary pollution offset reduction of primary emissions during COVID-19 lockdown in China, Natl. Sci. Rev., 8,
702   https://doi.org/10.1093/nsr/nwaa137, 2021.

703 Janssens-Maenhout, G., Crippa, M., Guizzardi, D., Dentener, F., Muntean, M., Pouliot, G., Keating, T., Zhang, Q., Kurokawa, J., Wankmuller,
704   R., van der Gon, H. D., Kuenen, J. J. P., Klimont, Z., Frost, G., Darras, S., Koffi, B., and Li, M.: HTAP_v2.2: a mosaic of regional and
705   global emission grid maps for 2008 and 2010 to study hemispheric transport of air pollution, Atmos. Chem. Phys., 15, 11411-11432,
706   https://doi.org/10.5194/acp-15-11411-2015, 2015.

707 Kaiser, J. W., Heil, A., Andreae, M. O., Benedetti, A., Chubarova, N., Jones, L., Morcrette, J. J., Razinger, M., Schultz, M. G., Suttie, M.,
708   and van der Werf, G. R.: Biomass burning emissions estimated with a global fire assimilation system based on observed fire radiative
709   power, Biogeosciences, 9, 527-554, https://doi.org/10.5194/bg-9-527-2012, 2012.

710 Kong, L., Tang, X., Zhu, J., Wang, Z., Pan, Y., Wu, H., Wu, L., Wu, Q., He, Y., Tian, S., Xie, Y., Liu, Z., Sui, W., Han, L., and Carmichael,
711   G.: Improved Inversion of Monthly Ammonia Emissions in China Based on the Chinese Ammonia Monitoring Network and Ensemble
712   Kalman Filter, Environ. Sci. Technol., 53, 12529-12538, https://doi.org/10.1021/acs.est.9b02701, 2019.

713 Kong, L., Tang, X., Zhu, J., Wang, Z., Li, J., Wu, H., Wu, Q., Chen, H., Zhu, L., Wang, W., Liu, B., Wang, Q., Chen, D., Pan, Y., Song, T.,
714   Li, F., Zheng, H., Jia, G., Lu, M., Wu, L., and Carmichael, G. R.: A 6-year-long (2013–2018) high-resolution air quality reanalysis dataset
715   in China based on the assimilation of surface observations from CNEMC, Earth Syst. Sci. Data, 13, 529-570, https://doi.org/10.5194/essd-
716   13-529-2021, 2021.

717 Lamsal, L. N., Martin, R. V., van Donkelaar, A., Steinbacher, M., Celarier, E. A., Bucsela, E., Dunlea, E. J., and Pinto, J. P.: Ground-level
718   nitrogen dioxide concentrations inferred from the satellite-borne Ozone Monitoring Instrument, J. Geophys. Res.-Atmos., 113,
719   https://doi.org/10.1029/2007JD009235, 2008.

720 Le, T. H., Wang, Y., Liu, L., Yang, J. N., Yung, Y. L., Li, G. H., and Seinfeld, J. H.: Unexpected air pollution with marked emission reductions
721   during the COVID-19 outbreak in China, Science, 369, 702-+, https://doi.org/10.1126/science.abb7431, 2020.

722 Levelt, P. F., Stein Zweers, D. C., Aben, I., Bauwens, M., Borsdorff, T., De Smedt, I., Eskes, H. J., Lerot, C., Loyola, D. G., Romahn, F.,
723   Stavrakou, T., Theys, N., Van Roozendael, M., Veefkind, J. P., and Verhoelst, T.: Air quality impacts of COVID-19 lockdown measures
724   detected from space using high spatial resolution observations of multiple trace gases from Sentinel-5P/TROPOMI, Atmos. Chem. Phys.,
725   22, https://doi.org/10319-10351, 10.5194/acp-22-10319-2022, 2022.

726 Li, B., Fan, J., Han, L., Sun, G., Zhang, D., and Zhang, P.: An Industrial Heat Source Extraction Method: BP Neural Network Using
727   Temperature Feature Template (in Chinese with English abstract), Journal of Geo-Information Science, 24, 533-545, 2022.

728 Li, F., Tang, X., Wang, Z., Zhu, L., Wang, X., Wu, H., Lu, M., Li, J., and Zhu, J.: Estimation of Representative Errors of Surface Observations
729   of Air Pollutant Concentrations Based on High-Density Observation Network over Beijing-Tianjin-Hebei Region, Chinese Journal of
730   Atmospheric Sciences, 43, 277-284, 2019.

731 Li, L., Li, Q., Huang, L., Wang, Q., Zhu, A., Xu, J., Liu, Z., Li, H., Shi, L., Li, R., Azari, M., Wang, Y., Zhang, X., Liu, Z., Zhu, Y., Zhang,
732   K., Xue, S., Ooi, M. C. G., Zhang, D., and Chan, A.: Air quality changes during the COVID-19 lockdown over the Yangtze River Delta
733   Region: An insight into the impact of human activity pattern changes on air pollution variation, Sci. Total Environ., 732, 139282,
734   https://doi.org/10.1016/j.scitotenv.2020.139282, 2020.

735 Li, M., Wang, T., Xie, M., Li, S., Zhuang, B., Fu, Q., Zhao, M., Wu, H., Liu, J., Saikawa, E., and Liao, K.: Drivers for the poor air quality
736   conditions in North China Plain during the COVID-19 outbreak, Atmos. Environ., 246, 118103,
737   https://doi.org/10.1016/j.atmosenv.2020.118103, 2021.

738 Li, M., Liu, H., Geng, G. N., Hong, C. P., Liu, F., Song, Y., Tong, D., Zheng, B., Cui, H. Y., Man, H. Y., Zhang, Q., and He, K. B.:
739   Anthropogenic emission inventories in China: a review, Natl. Sci. Rev., 4, 834-866, https://doi.org/10.1093/nsr/nwx150, 2017a.

740 Li, M., Zhang, Q., Kurokawa, J. I., Woo, J. H., He, K., Lu, Z., Ohara, T., Song, Y., Streets, D. G., Carmichael, G. R., Cheng, Y., Hong, C.,
741   Huo, H., Jiang, X., Kang, S., Liu, F., Su, H., and Zheng, B.: MIX: a mosaic Asian anthropogenic emission inventory under the international
742   collaboration framework of the MICS-Asia and HTAP, Atmos. Chem. Phys., 17, 935-963, https://doi.org/10.5194/acp-17-935-2017, 2017b.

743 Li, M., Zhang, Q., Zheng, B., Tong, D., Lei, Y., Liu, F., Hong, C. P., Kang, S. C., Yan, L., Zhang, Y. X., Bo, Y., Su, H., Cheng, Y. F., and
744   He, K. B.: Persistent growth of anthropogenic non-methane volatile organic compound (NMVOC) emissions in China during 1990-2017:
745   drivers, speciation and ozone formation potential, Atmos. Chem. Phys., 19, 8897-8913, https://doi.org/10.5194/acp-19-8897-2019, 2019.

746 Li, X., Zhang, Q., Zhang, Y., Zhang, L., Wang, Y. X., Zhang, Q. Q., Li, M., Zheng, Y. X., Geng, G. N., Wallington, T. J., Han, W. J., Shen,
747   W., and He, K. B.: Attribution of PM2.5 exposure in Beijing-Tianjin-Hebei region to emissions: implication to control strategies, Sci.
748   Bull., 62, 957-964, https://doi.org/10.1016/j.scib.2017.06.005, 2017c.

749 Ma, C. Q., Wang, T. J., Mizzi, A. P., Anderson, J. L., Zhuang, B. L., Xie, M., and Wu, R. S.: Multiconstituent Data Assimilation With WRF-
750   Chem/DART: Potential for Adjusting Anthropogenic Emissions and Improving Air Quality Forecasts Over Eastern China, J. Geophys.
751   Res.-Atmos., 124, 7393-7412, https://doi.org/10.1029/2019jd030421, 2019.

752 Ma, T., Duan, F. K., Ma, Y. L., Zhang, Q. Q., Xu, Y. Z., Li, W. G., Zhu, L. D., and He, K. B.: Unbalanced emission reductions and adverse
753   meteorological conditions facilitate the formation of secondary pollutants during the COVID-19 lockdown in Beijing, Sci. Total Environ.,
754   838, 8, https://doi.org/10.1016/j.scitotenv.2022.155970, 2022.

755 Miyazaki, K., Eskes, H. J., Sudo, K., Takigawa, M., van Weele, M., and Boersma, K. F.: Simultaneous assimilation of satellite NO2, O-3,
756   CO, and HNO3 data for the analysis of tropospheric chemical composition and emissions, Atmos. Chem. Phys., 12, 9545-9579,
757   https://doi.org/10.5194/acp-12-9545-2012, 2012.

758 Okuda, T., Matsuura, S., Yamaguchi, D., Umemura, T., Hanada, E., Orihara, H., Tanaka, S., He, K., Ma, Y., Cheng, Y., and Liang, L.: The
759   impact of the pollution control measures for the 2008 Beijing Olympic Games on the chemical composition of aerosols, Atmos. Environ.,
760   45, 2789-2794, https://doi.org/10.1016/j.atmosenv.2011.01.053, 2011.

761 Peng, Z., Lei, L. L., Liu, Z. Q., Su, J. N., Ding, A. J., Ban, J. M., Chen, D., Kou, X. X., and Chu, K. K.: The impact of multi-species surface
762   chemical observation assimilation on air quality forecasts in China, Atmos. Chem. Phys., 18, 18, https://doi.org/10.5194/acp-18-17387-
763   2018, 2018.

764 Price, C., Penner, J., and Prather, M.: NOx from lightning .1. Global distribution based on lightning physics, J. Geophys. Res.-Atmos., 102,
765   5929-5941, https://doi.org/10.1029/96jd03504, 1997.

766 Randerson, J. T., Van Der Werf, G. R., Giglio, L., Collatz, G. J., and Kasibhatla, P. S.: Global Fire Emissions Database, Version 4.1 (GFEDv4),
767   10.3334/ornldaac/1293, 2017.

768 Sakov, P. and Oke, P. R.: A deterministic formulation of the ensemble Kalman filter: an alternative to ensemble square root filters, Tellus

769   Ser. A-Dyn. Meteorol. Oceanol., 60, 361-371, https://doi.org/10.1111/j.1600-0870.2007.00299.x, 2008.

770 Skachko, S., Errera, Q., Ménard, R., Christophe, Y., and Chabrillat, S.: Comparison of the ensemble Kalman filter and 4D-Var assimilation

771   methods using a stratospheric tracer transport model, Geosci. Model Dev., 7, 1451-1465, https://doi.org/10.5194/gmd-7-1451-2014, 2014.

772 Shi, X. and Brasseur, G. P.: The Response in Air Quality to the Reduction of Chinese Economic Activities During the COVID-19 Outbreak,

773   Geophys. Res. Lett., 47, e2020GL088070, https://doi.org/10.1029/2020gl088070, 2020.

774 Shi, Z., Song, C., Liu, B., Lu, G., Xu, J., Van Vu, T., Elliott, R. J. R., Li, W., Bloss, W. J., and Harrison, R. M.: Abrupt but smaller than

775   expected   changes   in   surface   air   quality   attributable   to   COVID-19   lockdowns,   Sci.   Adv.,   7,   eabd6696,

776   https://doi.org/10.1126/sciadv.abd6696, 2021.

777 Sindelarova, K., Granier, C., Bouarar, I., Guenther, A., Tilmes, S., Stavrakou, T., Muller, J. F., Kuhn, U., Stefani, P., and Knorr, W.: Global

778   data set of biogenic VOC emissions calculated by the MEGAN model over the last 30 years, Atmos. Chem. Phys., 14, 9317-9341,

779   https://doi.org/10.5194/acp-14-9317-2014, 2014.

780 Skamarock, W. C.: A description of the advanced research WRF version 3, Ncar Technical, 113, 7-25, 2008.

781 Song, Y. S., Lin, C. Q., Li, Y., Lau, A. K. H., Fung, J. C. H., Lu, X. C., Guo, C., Ma, J., and Lao, X. Q.: An improved decomposition method

782   to differentiate meteorological and anthropogenic effects on air pollution: A national study in China during the COVID-19 lockdown

783   period, Atmos. Environ., 250, 9, https://doi.org/10.1016/j.atmosenv.2021.118270, 2021.

784 Streets, D. G., Bond, T. C., Carmichael, G. R., Fernandes, S. D., Fu, Q., He, D., Klimont, Z., Nelson, S. M., Tsai, N. Y., Wang, M. Q., Woo,

785   J. H., and Yarber, K. F.: An inventory of gaseous and primary aerosol emissions in Asia in the year 2000, J. Geophys. Res.-Atmos., 108,

786   23, https://doi.org/10.1029/2002JD003093, 2003.

787 Streets, D. G., Canty, T., Carmichael, G. R., de Foy, B., Dickerson, R. R., Duncan, B. N., Edwards, D. P., Haynes, J. A., Henze, D. K.,

788   Houyoux, M. R., Jacob, D. J., Krotkov, N. A., Lamsal, L. N., Liu, Y., Lu, Z., Martin, R. V., Pfister, G. G., Pinder, R. W., Salawitch, R. J.,

789   and Wecht, K. J.: Emissions estimation from satellite retrievals: A review of current capability, Atmos. Environ., 77, 1011-1042,

790   https://doi.org/10.1016/j.atmosenv.2013.05.051, 2013.

791 Sulaymon, I. D., Zhang, Y., Hopke, P. K., Hu, J., Zhang, Y., Li, L., Mei, X., Gong, K., Shi, Z., Zhao, B., and Zhao, F.: Persistent high PM2.5

792   pollution driven by unfavorable meteorological conditions during the COVID-19 lockdown period in the Beijing-Tianjin-Hebei region,

793   China, Environ. Res., 198, 111186, https://doi.org/10.1016/j.envres.2021.111186, 2021.

794 Tandeo, P., Ailliot, P., Bocquet, M., Carrassi, A., Miyoshi, T., Pulido, M., and Zhen, Y. C.: A Review of Innovation-Based Methods to Jointly

795   Estimate Model and Observation Error Covariance Matrices in Ensemble Data Assimilation, Mon. Weather Rev., 148, 3973-3994,

796   https://doi.org/10.1175/mwr-d-19-0240.1, 2020.

797 Tang, G., Zhu, X., Hu, B., Xin, J., Wang, L., Münkel, C., Mao, G., and Wang, Y.: Impact of emission controls on air quality in Beijing during

798   APEC 2014: lidar ceilometer observations, Atmos. Chem. Phys., 15, 12667-12680, https://doi.org/10.5194/acp-15-12667-2015, 2015.

799 Tang, X., Zhu, J., Wang, Z. F., and Gbaguidi, A.: Improvement of ozone forecast over Beijing based on ensemble Kalman filter with

800   simultaneous adjustment of initial conditions and emissions, Atmos. Chem. Phys., 11, 12901-12916, 10.5194/acp-11-12901-2011, 2011.

801 Tang, X., Zhu, J., Wang, Z. F., Wang, M., Gbaguidi, A., Li, J., Shao, M., Tang, G. Q., and Ji, D. S.: Inversion of CO emissions over Beijing

802   and its surrounding areas with ensemble Kalman filter, Atmos. Environ., 81, 676-686, https://doi.org/10.1016/j.atmosenv.2013.08.051,

803   2013.

van der Werf, G. R., Randerson, J. T., Giglio, L., Collatz, G. J., Mu, M., Kasibhatla, P. S., Morton, D. C., DeFries, R. S., Jin, Y., and van Leeuwen, T. T.: Global fire emissions and the contribution of deforestation, savanna, forest, agricultural, and peat fires (1997–2009), Atmos. Chem. Phys., 10, 11707-11735, https://doi.org/10.5194/acp-10-11707-2010, 2010.

Wang, P., Chen, K., Zhu, S., Wang, P., and Zhang, H.: Severe air pollution events not avoided by reduced anthropogenic activities during COVID-19 outbreak, Resour. Conserv. Recycl., 158, 104814, https://doi.org/10.1016/j.resconrec.2020.104814, 2020.

Wang, S., Gao, J., Zhang, Y., Zhang, J., Cha, F., Wang, T., Ren, C., and Wang, W.: Impact of emission control on regional air quality: An observational study of air pollutants before, during and after the Beijing Olympic Games, J. Environ. Sci., 26, 175-180, https://doi.org/10.1016/S1001-0742(13)60395-2, 2014.

Wang, Y. Q., Zhang, X. Y., Sun, J. Y., Zhang, X. C., Che, H. Z., and Li, Y.: Spatial and temporal variations of the concentrations of PM_{10}, $PM_{2.5}$ and PM_1 in China, Atmos. Chem. Phys., 15, 13585-13598, https://doi.org/10.5194/acp-15-13585-2015, 2015.

Wang, Z., Uno, I., Yumimoto, K., Itahashi, S., Chen, X., Yang, W., and Wang, Z.: Impacts of COVID-19 lockdown, Spring Festival and meteorology on the NO2 variations in early 2020 over China based on in-situ observations, satellite retrievals and model simulations, Atmos. Environ., 244, 117972, https://doi.org/10.1016/j.atmosenv.2020.117972, 2021.

Wu, H., Tang, X., Wang, Z., Wu, L., Li, J., Wang, W., Yang, W., and Zhu, J.: High-spatiotemporal-resolution inverse estimation of CO and NOx emission reductions during emission control periods with a modified ensemble Kalman filter, Atmos. Environ., 236, 117631, https://doi.org/10.1016/j.atmosenv.2020.117631, 2020.

Wu, H. J., Tang, X., Wang, Z. F., Wu, L., Lu, M. M., Wei, L. F., and Zhu, J.: Probabilistic Automatic Outlier Detection for Surface Air Quality Measurements from the China National Environmental Monitoring Network, Adv. Atmos. Sci., 35, 1522-1532, https://doi.org/10.1007/s00376-018-8067-9, 2018.

Xing, J., Li, S. W., Jiang, Y. Q., Wang, S. X., Ding, D., Dong, Z. X., Zhu, Y., and Hao, J. M.: Quantifying the emission changes and associated air quality impacts during the COVID-19 pandemic on the North China Plain: a response modeling study, Atmos. Chem. Phys., 20, 14347-14359, https://doi.org/10.5194/acp-20-14347-2020, 2020.

Yan, C., Shen, Y. C., Stolzenburg, D., Dada, L., Qi, X. M., Hakala, S., Sundstrom, A. M., Guo, Y. S., Lipponen, A., Kokkonen, T. V., Kontkanen, J., Cai, R. L., Cai, J., Chan, T., Chen, L. D., Chu, B. W., Deng, C. J., Du, W., Fan, X. L., He, X. C., Kangasluoma, J., Kujansuu, J., Kurppa, M., Li, C., Li, Y. R., Lin, Z. H., Liu, Y. L., Liu, Y. L., Lu, Y. Q., Nie, W., Pulliainen, J., Qiao, X. H., Wang, Y. H., Wen, Y. F., Wu, Y., Yang, G., Yao, L., Yin, R. J., Zhang, G., Zhang, S. J., Zheng, F. X., Zhou, Y., Arola, A., Tamminen, J., Paasonen, P., Sun, Y. L., Wang, L., Donahue, N. M., Liu, Y. C., Bianchi, F., Daellenbach, K. R., Worsnop, D. R., Kerminen, V. M., Petaja, T., Ding, A. J., Jiang, J. K., and Kulmala, M.: The effect of COVID-19 restrictions on atmospheric new particle formation in Beijing, Atmos. Chem. Phys., 22, 12207-12220, https://doi.org/10.5194/acp-22-12207-2022, 2022.

Yan, X. Y., Akimoto, H., and Ohara, T.: Estimation of nitrous oxide, nitric oxide and ammonia emissions from croplands in East, Southeast and South Asia, Glob. Change Biol., 9, 1080-1096, https://doi.org/10.1046/j.1365-2486.2003.00649.x, 2003.

Zhang, L., Shao, J., Lu, X., Zhao, Y., Hu, Y., Henze, D. K., Liao, H., Gong, S., and Zhang, Q.: Sources and Processes Affecting Fine Particulate Matter Pollution over North China: An Adjoint Analysis of the Beijing APEC Period, Environ. Sci. Technol., 50, 8731-8740, https://doi.org/10.1021/acs.est.6b03010, 2016.

Zhang, Q., Pan, Y., He, Y., Walters, W. W., Ni, Q., Liu, X., Xu, G., Shao, J., and Jiang, C.: Substantial nitrogen oxides emission reduction from China due to COVID-19 and its impact on surface ozone and aerosol pollution, Sci. Total Environ., 753, 142238, https://doi.org/10.1016/j.scitotenv.2020.142238, 2021.

841   Zhang, R. X., Zhang, Y. Z., Lin, H. P., Feng, X., Fu, T. M., and Wang, Y. H.: NOx Emission Reduction and Recovery during COVID-19 in

842   East China, Atmosphere, 11, 15, https://doi.org/10.3390/atmos11040433, 2020.

843   Zhang, W., Guo, J. H., Sun, Y. L., Yuan, H., Zhuang, G. S., Zhuang, Y. H., and Hao, Z. P.: Source apportionment for,urban PM10 and PM2.5

844   in the Beijing area, Chin. Sci. Bull., 52, 608-615, https://doi.org/10.1007/s11434-007-0076-5, 2007.

845   Zhao, X., Wang, G., Wang, S., Zhao, N., Zhang, M., and Yue, W.: Impacts of COVID-19 on air quality in mid-eastern China: An insight into

846   meteorology and emissions, Atmos. Environ., 266, 118750, https://doi.org/10.1016/j.atmosenv.2021.118750, 2021.

847   Zhao, Y. B., Zhang, K., Xu, X. T., Shen, H. Z., Zhu, X., Zhang, Y. X., Hu, Y. T., and Shen, G. F.: Substantial Changes in Nitrogen Dioxide

848   and Ozone after Excluding Meteorological Impacts during the COVID-19 Outbreak in Mainland China, Environ. Sci. Technol. Lett., 7,

849   402-408, https://doi.org/10.1021/acs.estlett.0c00304, 2020.

850   Zheng, B., Zhang, Q., Geng, G., Chen, C., Shi, Q., Cui, M., Lei, Y., and He, K.: Changes in China's anthropogenic emissions and air quality

851   during the COVID-19 pandemic in 2020, Earth Syst. Sci. Data, 13, 2895-2907, https://doi.org/10.5194/essd-13-2895-2021, 2021.

852   Zheng, B., Tong, D., Li, M., Liu, F., Hong, C. P., Geng, G. N., Li, H. Y., Li, X., Peng, L. Q., Qi, J., Yan, L., Zhang, Y. X., Zhao, H. Y.,

853   Zheng, Y. X., He, K. B., and Zhang, Q.: Trends in China's anthropogenic emissions since 2010 as the consequence of clean air actions,

854   Atmos. Chem. Phys., 18, 14095-14111, https://doi.org/10.5194/acp-18-14095-2018, 2018.

855   Zuo, P. J., Zong, Z., Zheng, B., Bi, J. Z., Zhang, Q. H., Li, W., Zhang, J. W., Yang, X. Z., Chen, Z. G., Yang, H., Lu, D. W., Zhang, Q. H.,

856   Liu, Q., and Jiang, G. B.: New Insights into Unexpected Severe PM2.5 Pollution during the SARS and COVID-19 Pandemic Periods in

857   Beijing, Environ. Sci. Technol., 56, 155-164, https://doi.org/10.1021/acs.est.1c05383, 2022.

Supplementary Material

Text S1: Evaluation of meteorological simulation

Performance of meteorological simulation is important for the inversion estimation since the meteorological parameters determine the transport process from the sources to the observation and influence the estimation of flow-dependent background error covariance. The air temperature, relative humidity and precipitation also affect the atmospheric chemistry and the removal of air pollutants. The meteorology simulation was evaluated against the daily observations from China Meteorological Administration (CMA) with spatial distribution of meteorological observation sites shown in Fig. S25. Figure S26–31 present the comparisons of simulated and observed regional mean daily meteorological parameters (i.e., u-wind, v-wind, temperature, relatively humidity and precipitation) over six regions of China from January to February 2020, with calculated evaluation statistics summarised in Table S4. In general, the simulation can well capture the main feathers of the observed meteorological conditions in all regions for our simulation period. All variables exhibited small RMSE values in all regions, that are around 1 m/s for wind speed, 1℃ for T, 10% for RH and 0.08–2.38mm for precipitation. Therefore, the WRF can generally well reproduce the meteorological conditions for all regions of China, which is adequate for our inversion estimates.

Text S2: Assessment of the influence of chemiluminescence monitor interference on the inversion of NO$_x$ emission

The NO$_2$ measurement from CNEMC is made by the chemiluminescent analyser with a molybdenum converter, which is subject to the positive bias induced by the interference of HNO$_3$, PAN and alkyl nitrates (AN) (Dunlea et al., 2007; Lamsal et al., 2008).To investigate the influence of the chemiluminescence monitor interference on the NO$_2$ measurement and its impact on the inversion of NO$_x$ emissions, a sensitivity inversion run was conducted based on the corrected NO$_2$ measurement using the corrected factors (Eq. (1)) proposed by Lamsal et al. (2008). In order to alleviate the effects of emission uncertainty on the CF calculations, the CF values were calculated based on the simulated NO$_2$, HNO$_3$, PAN and AN using the inversed emission inventory. Figure S16 shows the calculated CFs for NO$_2$ measurements over different regions of China during COVID-19 pandemic, which ranged from 0.75 to 0.99. The CF values over NCP, NE, NW and Central were stable throughout the COVID-19 pandemic, all larger than 0.9, suggesting that chemiluminescence monitor interference only has slight effects on the NO$_2$ measurement there. Over the SE and SW regions, there was a drop of CF values during the lockdown period, followed by an increase after the lockdown, suggesting that the decline of NO$_2$ concentrations during lockdown period may be larger.

As shown in Figure S17, the overestimations were lower than 3 μg/m^3 over different regions of China throughout the COVID-19 pandemic, which is smaller than the observation errors (~10 μg/m^3) we used in the assimilation, suggesting that the observation error caused by the chemiluminescence monitor interference were well considered in our assimilation. To better quantify the influences of chemiluminescence monitor interference on the inversed NO$_x$ emission, an additional inversion experiment was conducted based on the corrected NO$_2$ measurement using the calculated CFs. The results suggest the chemiluminescence monitor interference in the NO$_2$ observations had weak impacts on the inversed NO$_x$ emissions as seen in Fig. S18 and Fig. S19, which display the comparisons of the inversed NO$_x$ emission with and without correction in respect of the magnitude and change ratio during different stage of COVID-19 pandemic. The differences in the magnitude of inversed NO$_x$ emissions caused by correction were about 2–7% over the NCP, NE, NW and Central, and were about 10–13% over the SE and SW. The differences in the emission reductions of NO$_x$ were also small, which

36 was about 0.3 to 4.1 percentage points. These results indicate that due to the considerations of observation error in the EnKF, the

37 chemiluminescence monitor interference to the NO_2 measurement might not significantly influence our inversion results in this

38 application. However, the NO_x emissions could be slightly overestimated due to the positive biases in the NO_2 measurement, and the

39 inversed NO_x emissions may drop faster if the NO_2 measurement was corrected.

40 **Figures**

41

42
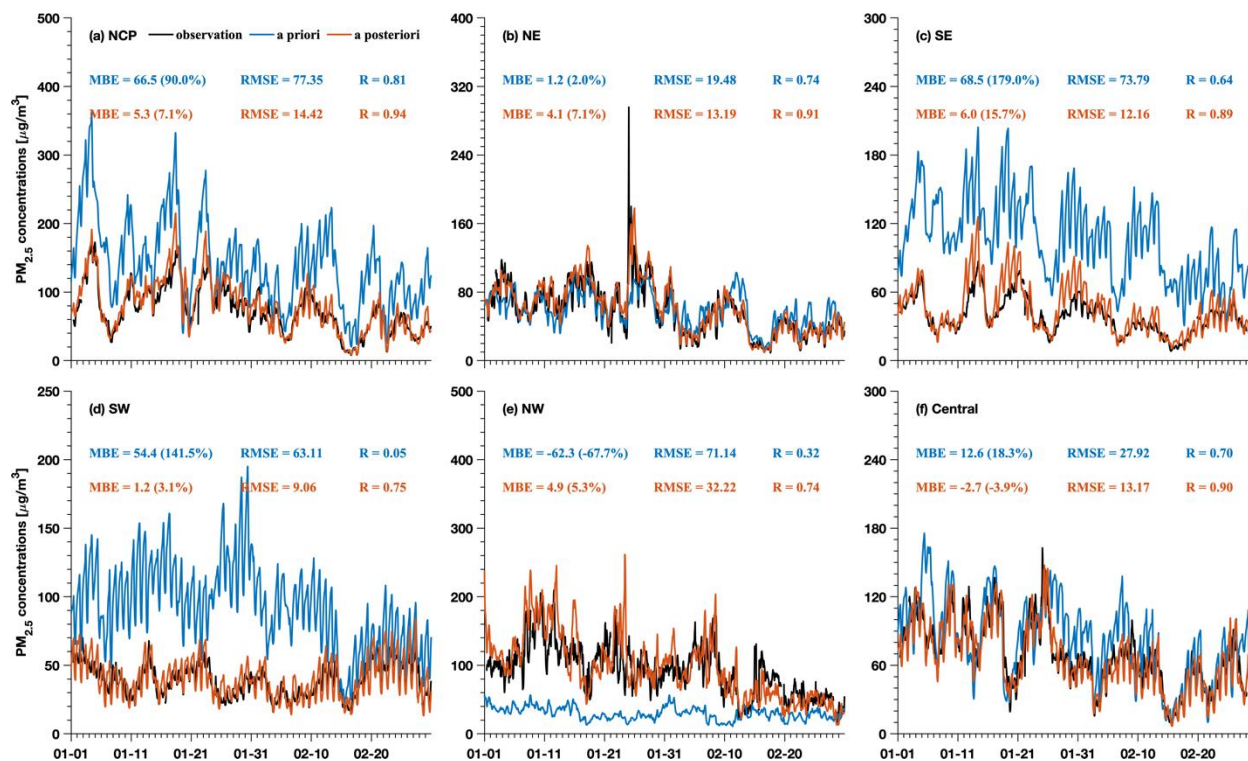
43 **Figure S1: Time series of $PM_{2.5}$ concentrations over (a) NCP, (b) NE, (c) SE, (d) SW, (e) NW and (f) Central regions from 1st Jan to 29th Feb**
44 **2020 obtained from observation (black line) and simulation using a priori (blue line) and a posteriori (orange line) emissions.**

45
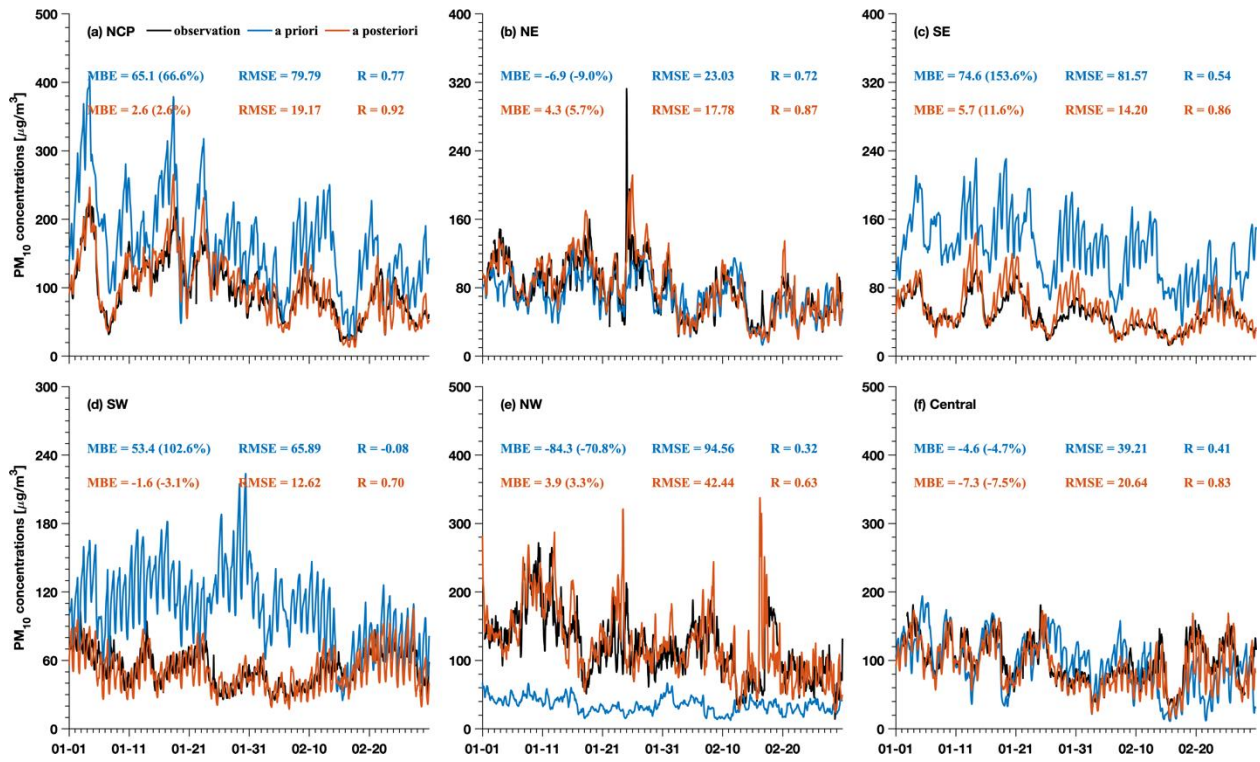
46   **Figure S2: Same as in Fig. S1 but for PM$_{10}$ concentrations.**

47
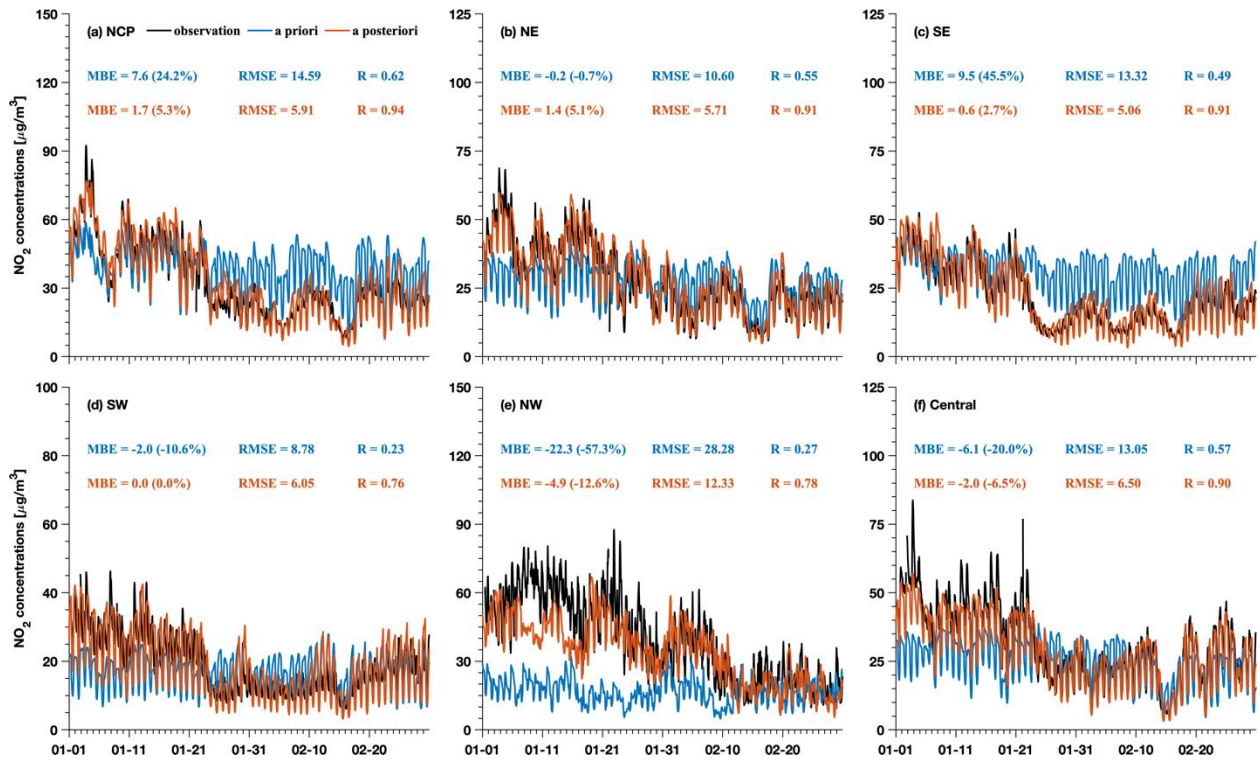
48   **Figure S3: Same as in Fig. S1 but for NO$_2$ concentrations.**

49
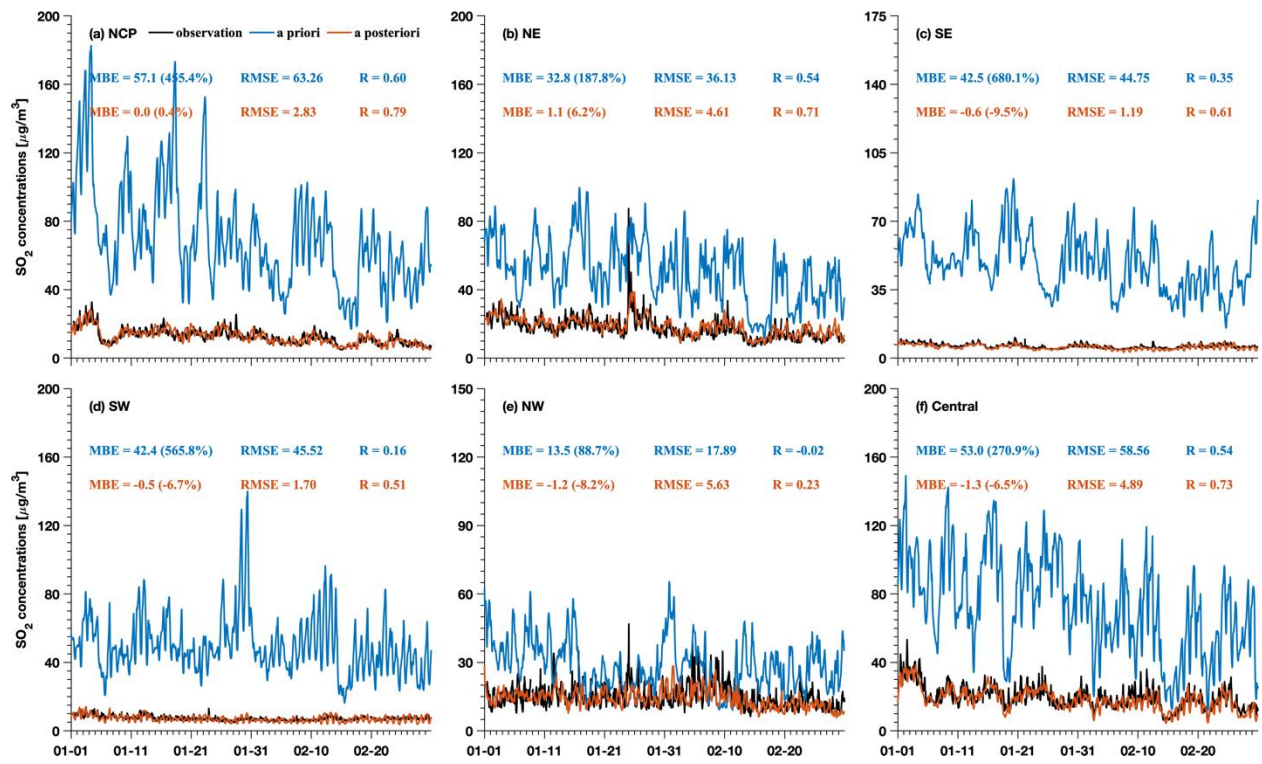
50 **Figure S4: Same as in Fig. S1 but for SO₂ concentrations.**

51
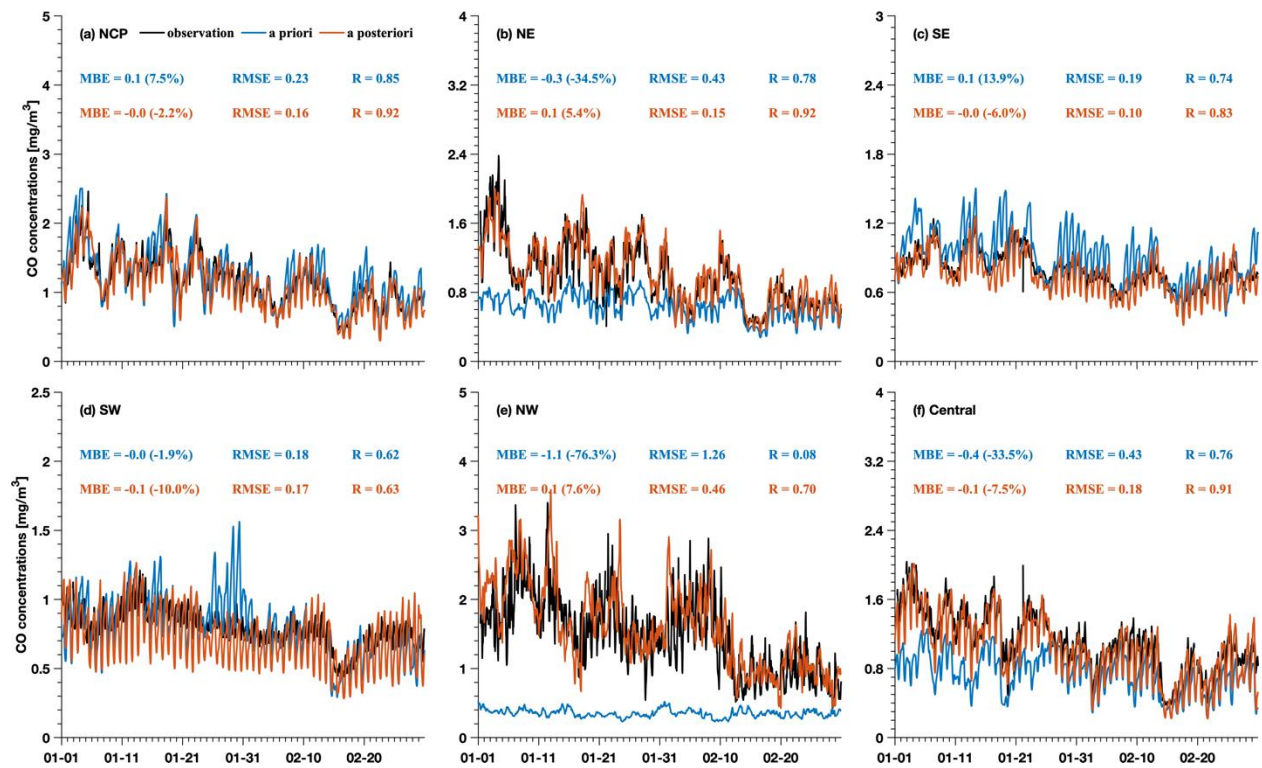
52 **Figure S5: Same as in Fig. S1 but for CO concentrations.**

(a) NCP — observation — a priori — a posteriori

MBE = -28.8 (-56.9%)   RMSE = 33.14   R = 0.61
MBE = -14.5 (-28.6%)   RMSE = 20.67   R = 0.78

(b) NE

MBE = -25.3 (-46.7%)   RMSE = 28.51   R = 0.58
MBE = -17.7 (-32.7%)   RMSE = 22.70   R = 0.64

(c) SE

MBE = -18.2 (-35.6%)   RMSE = 22.26   R = 0.74
MBE = -7.2 (-14.0%)   RMSE = 15.82   R = 0.79

(d) SW

MBE = 3.0 (6.2%)   RMSE = 10.46   R = 0.82
MBE = -5.7 (-11.8%)   RMSE = 11.73   R = 0.83

(e) NW

MBE = -4.7 (-9.3%)   RMSE = 21.40   R = 0.38
MBE = -18.9 (-37.6%)   RMSE = 25.40   R = 0.66

(f) Central

MBE = -14.8 (-29.3%)   RMSE = 22.22   R = 0.70
MBE = -17.9 (-35.3%)   RMSE = 23.69   R = 0.74

53

Figure S6: Same as in Fig. S1 but for O$_3$ concentrations.

55
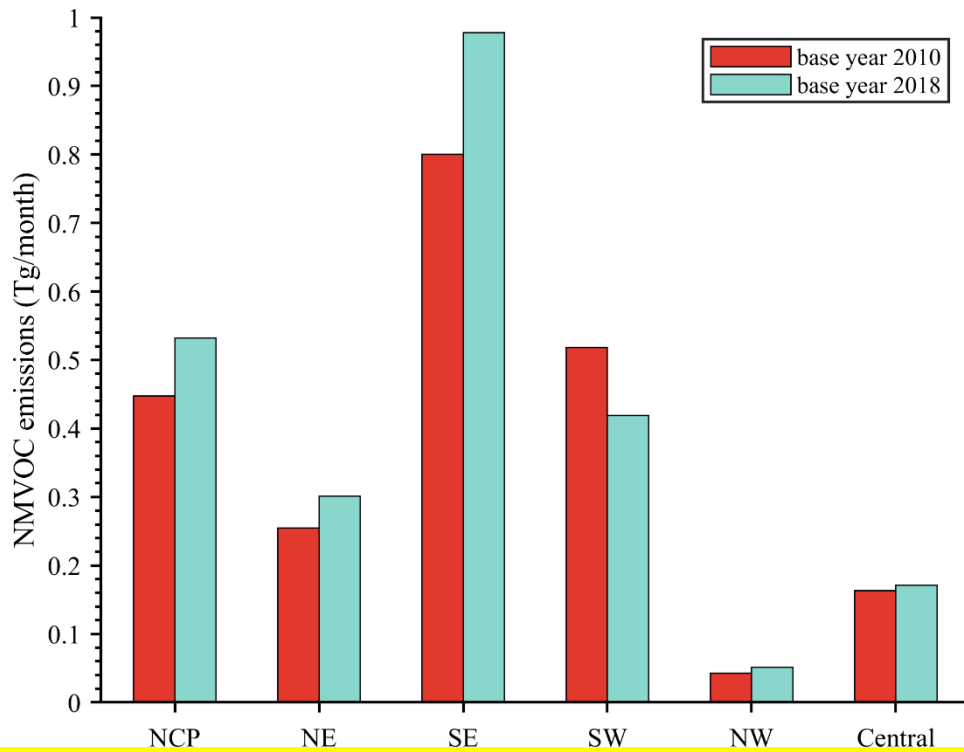
56
57 **Figure S7: comparisons of the NMVOC emissions for base year 2010 with those for 2018 over different regions of China.**

58
59

68
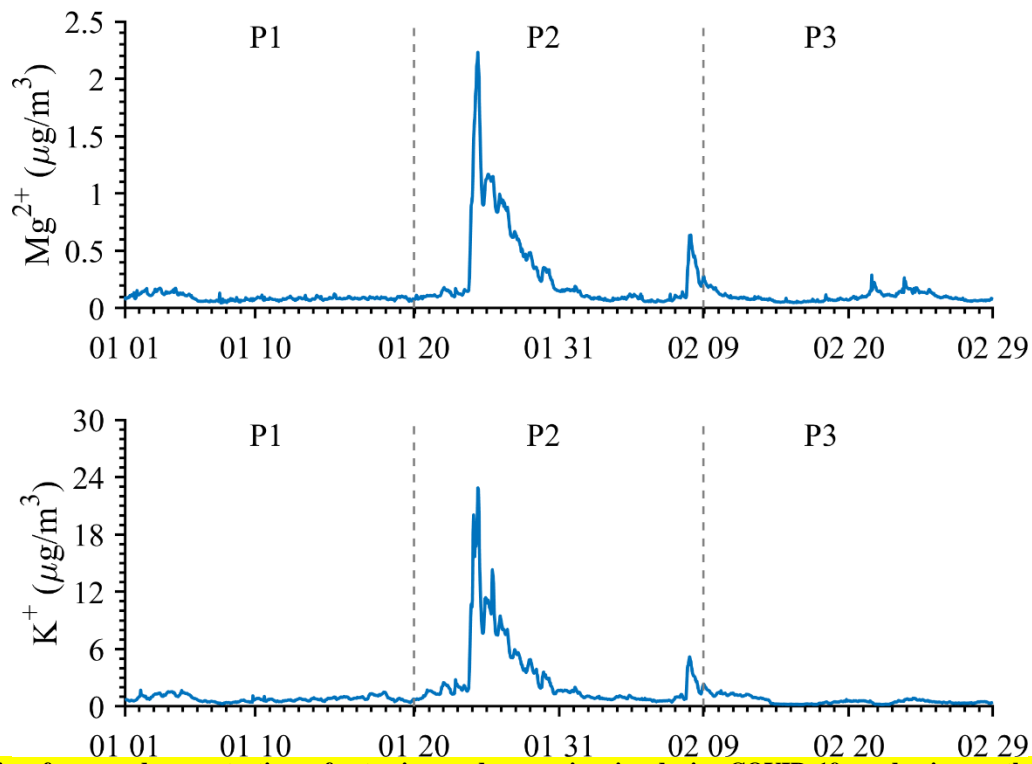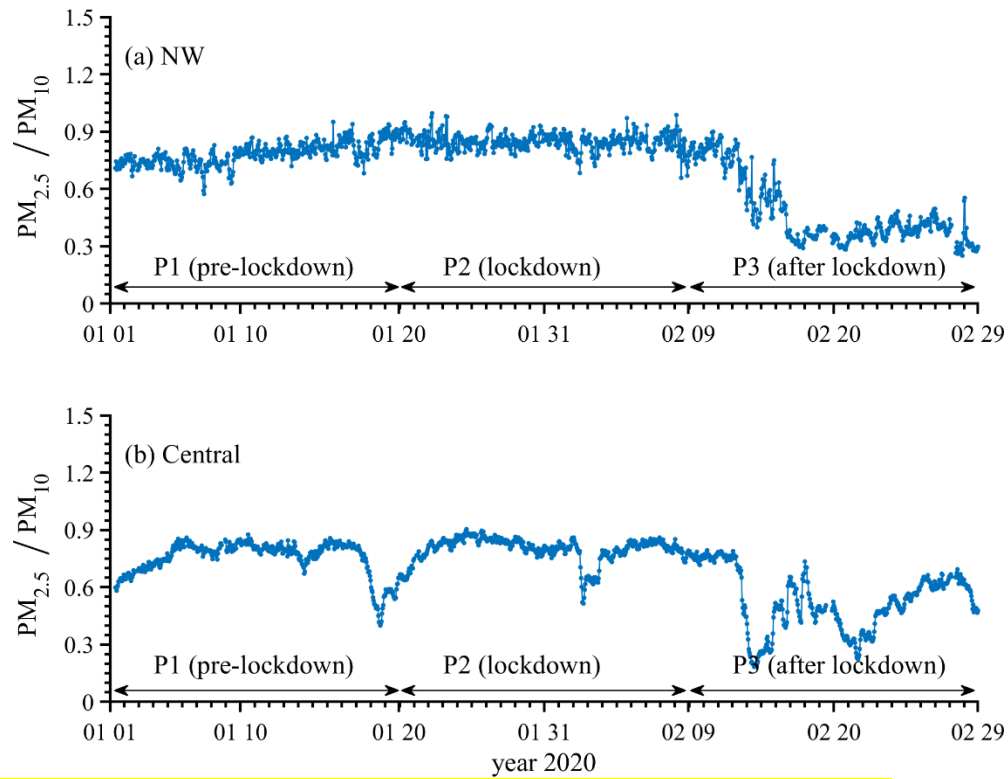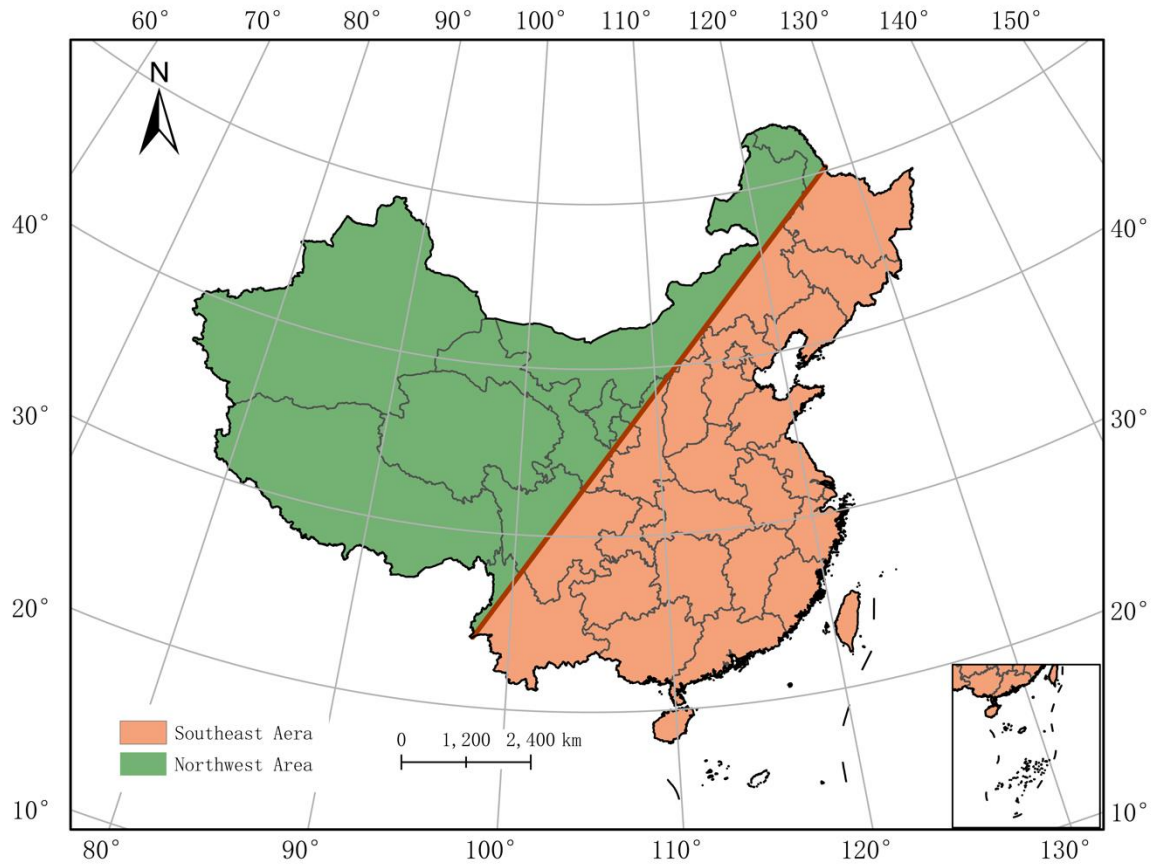
Figure S10: Geographical definition of southeast China (orange part) and northwest (green part) based on the Hu Huanyong Line. This line divides the China based on the population with population in east of this line (southeast China) accounts for 86.72% of the total population in China.

72

73
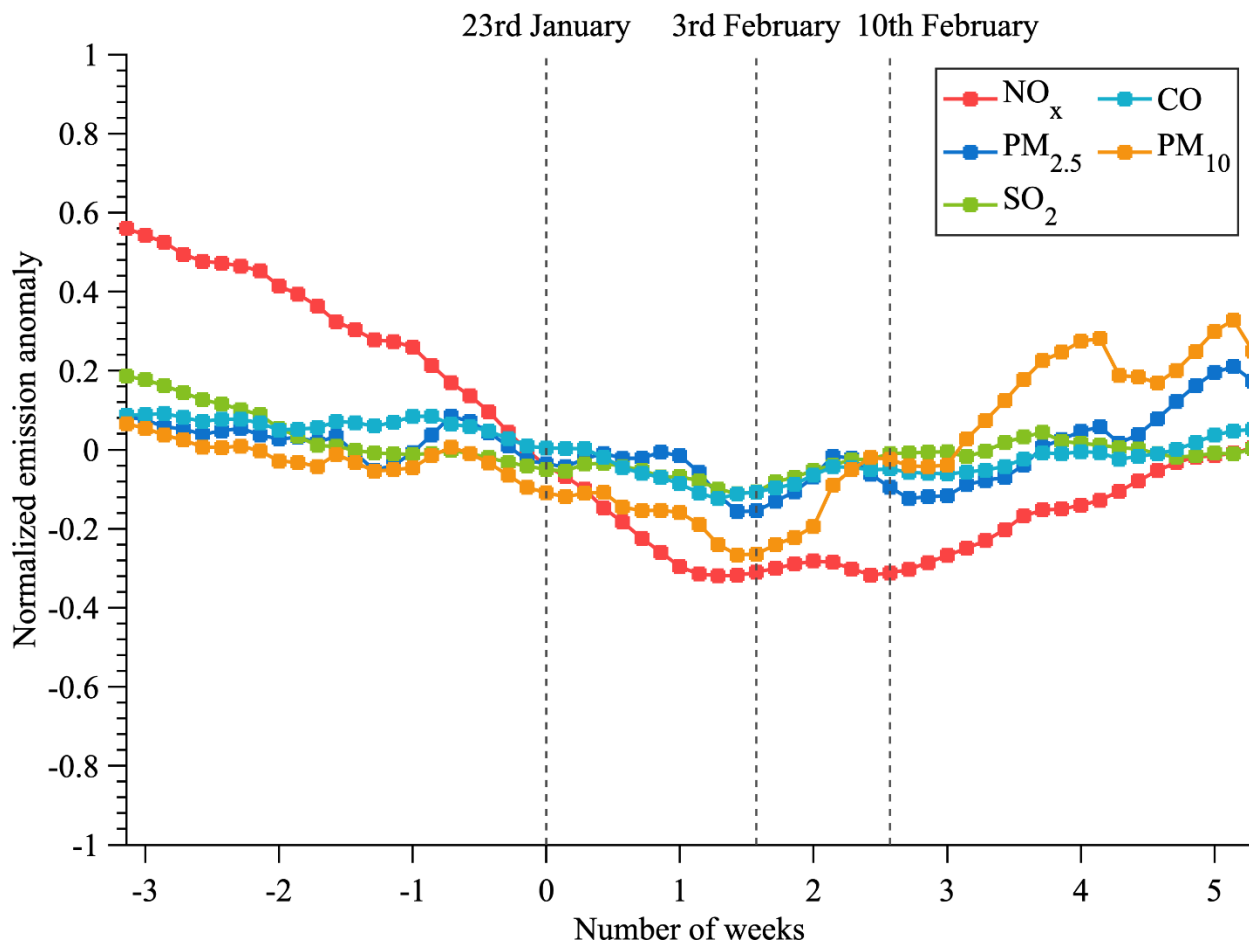
Figure S11: Time series of normalized emission anomaly estimated by inversion results for different species in southeast China (defined in Figure S10) from 1st January to 29th February 2020. The normalized emission anomaly is calculated by the emission anomaly divided by the averaged emission during the whole period.

77

78
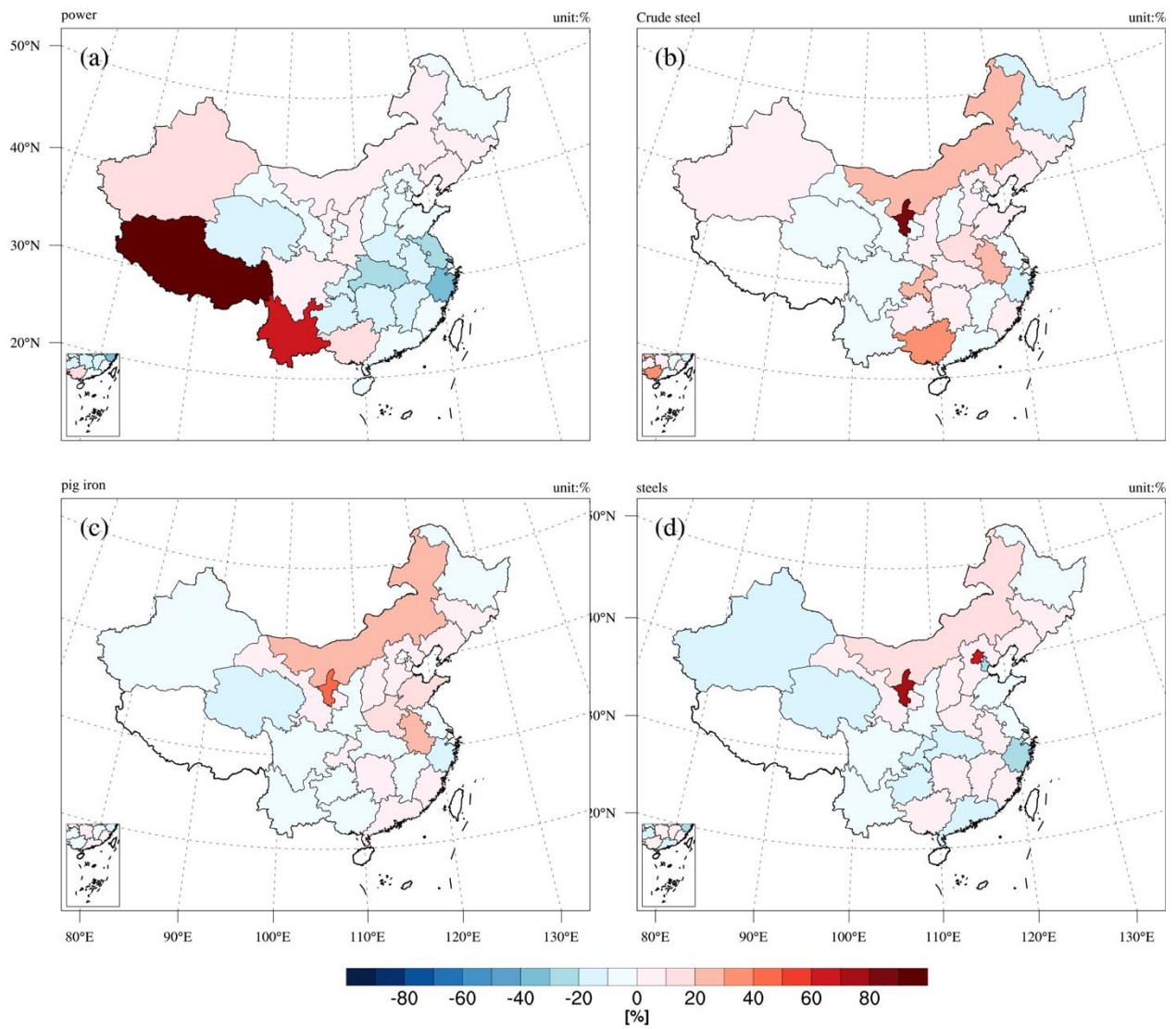
Figure S12: Changes in (a) thermal power generation, productions of (b) crude steel, (c) pig iron, and (d) steels in China in the first two months
of 2020 compared to those in 2019.

81

EMIS change scenario

(a) Beijing

51.4 +18.3 (60.7%) +11.9 (39.3%) 81.5 (+30.2)

(b) NCP

113.1 -14.2 (94.1%) -0.9 (5.9%) 97.9 (-15.2)

MET change scenario

(c) Beijing

51.4 +16.6 (55.1%) +13.6 (44.9%) 81.5 (+30.2)

(d) NCP

113.1 -13.4 (88.8%) -1.7 (11.2%) 97.9 (-15.2)
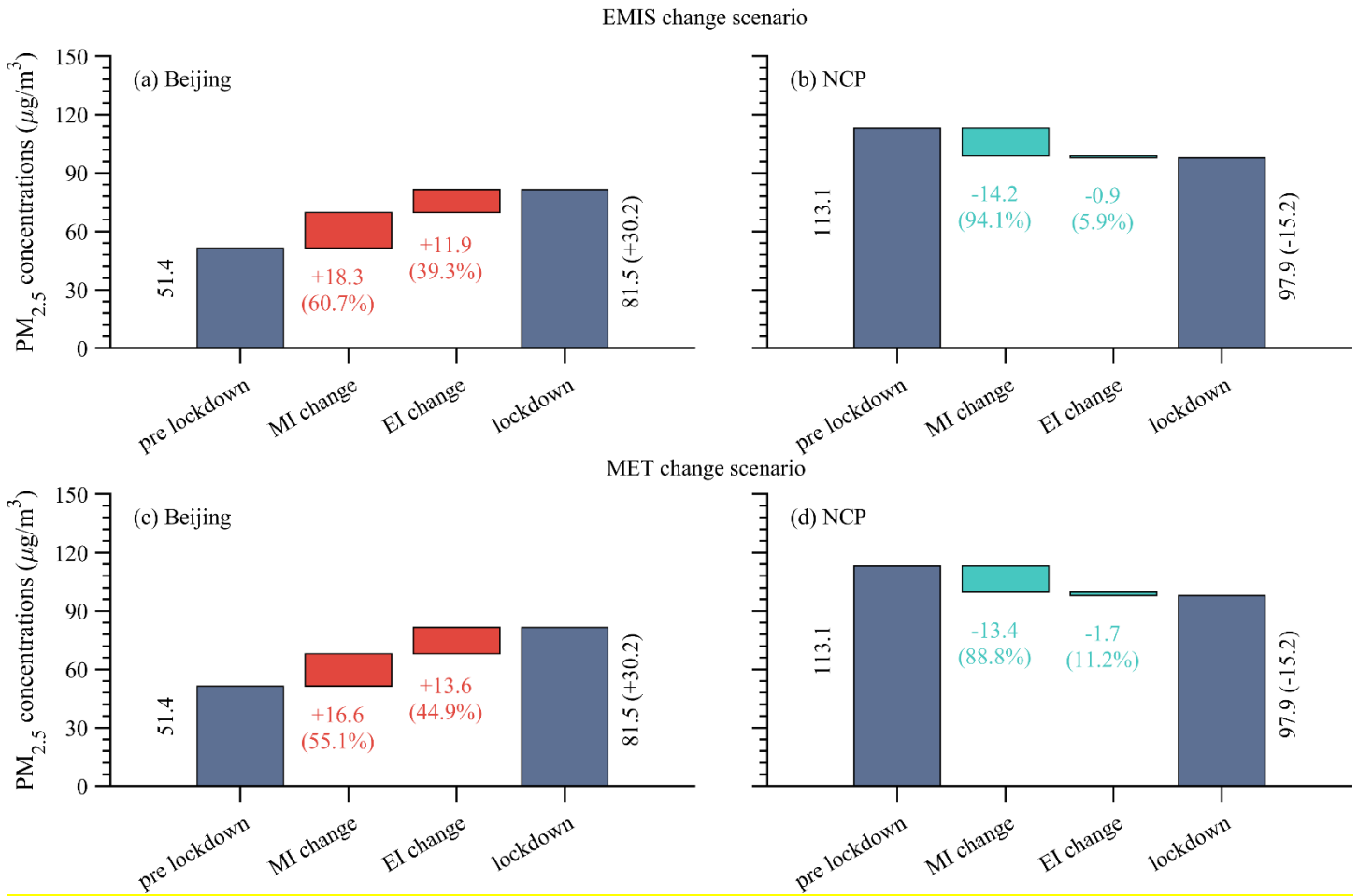
82
83 **Figure S13: The calculated MI and EI changes of PM$_{2.5}$ concentrations over the (a, c) Beijing and (b, d) the NCP region using the EMIS change**
84 **scenario (upper panel) and MET change scenario (lower panel).**

EMIS change scenario

(a) Beijing

(b) NCP

MET change scenario

(c) Beijing

(d) NCP
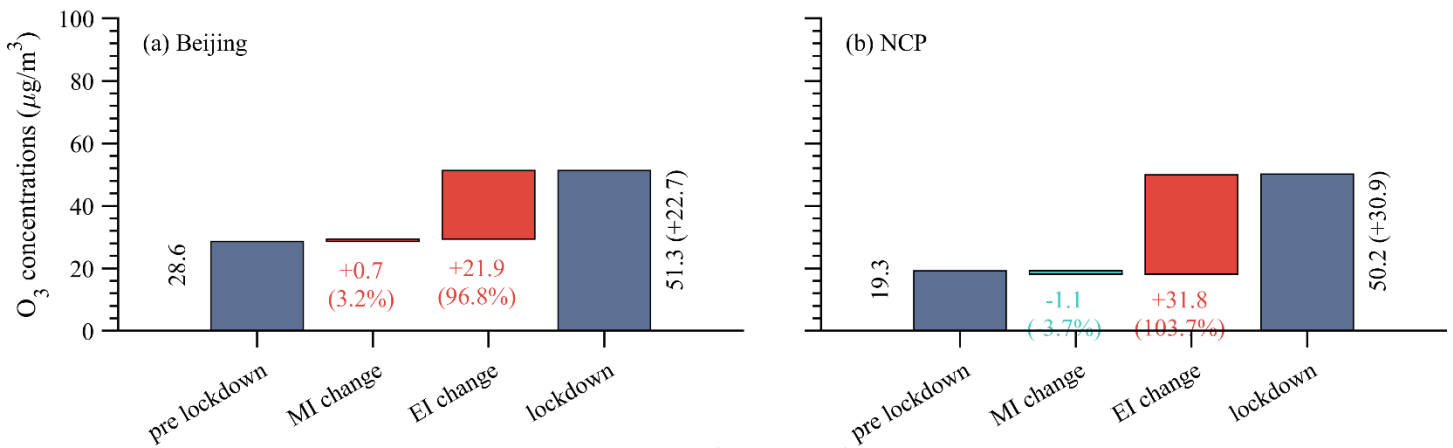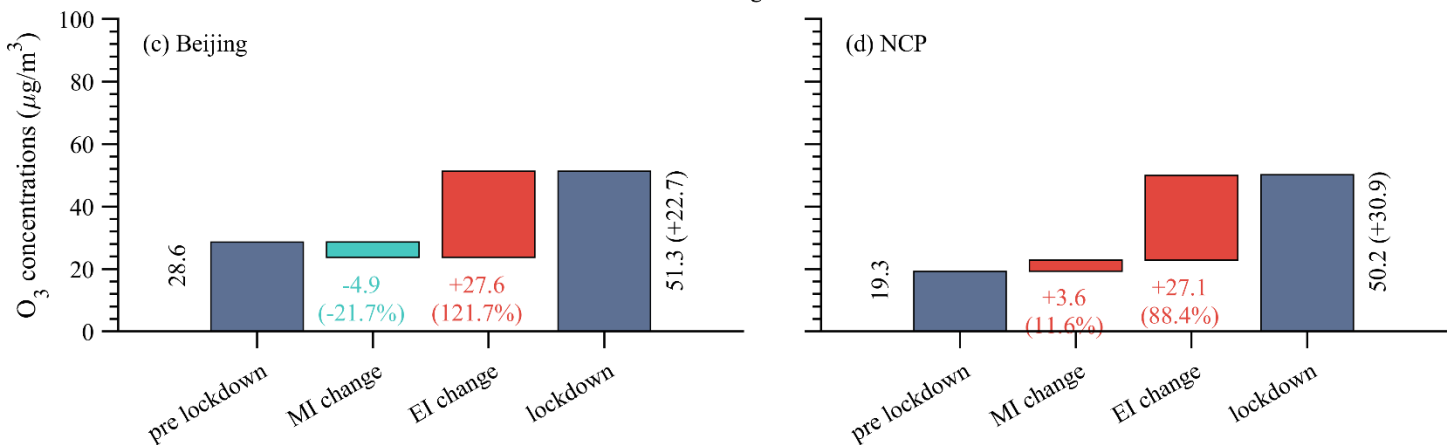
85
86 **Figure S14: The calculated MI and EI changes of O$_3$ concentrations over the (a, c) Beijing and (b, d) the NCP region using the EMIS change**
87 **scenario (upper panel) and MET change scenario (lower panel).**
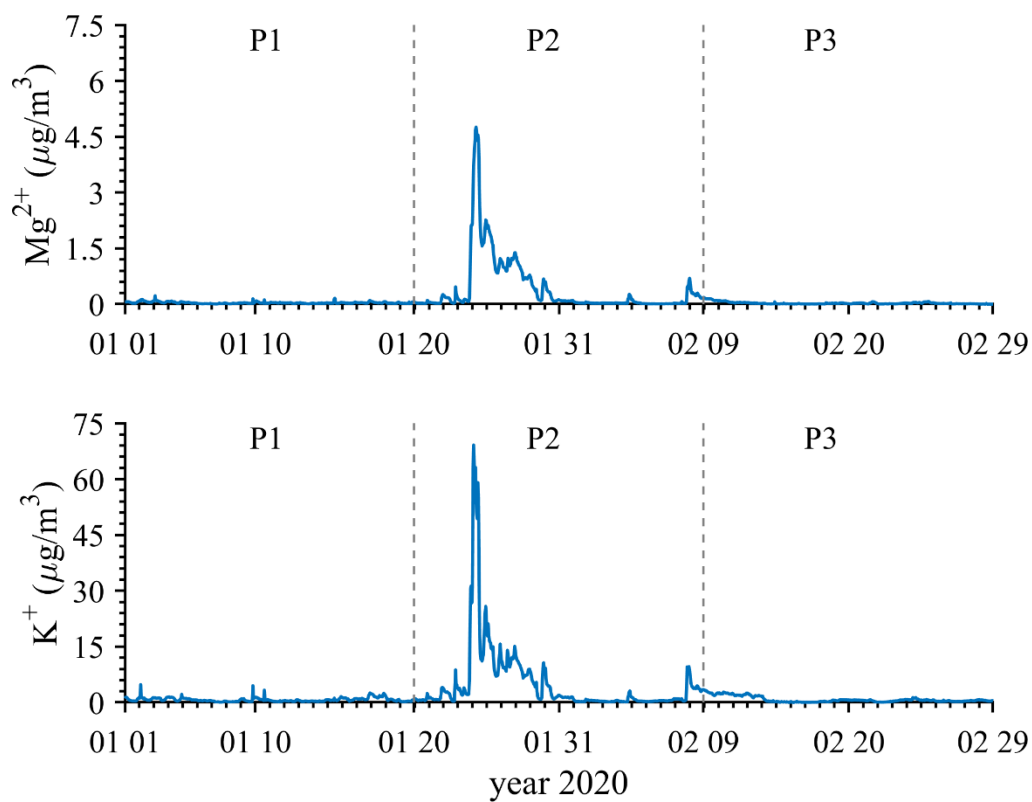
Figure S15: Timeseries of averaged concentrations of potassium and magnesium ion during COVID-19 pandemic over the Beijing. Measurements of potassium and magnesium ion were obtained from CNEMC.

92
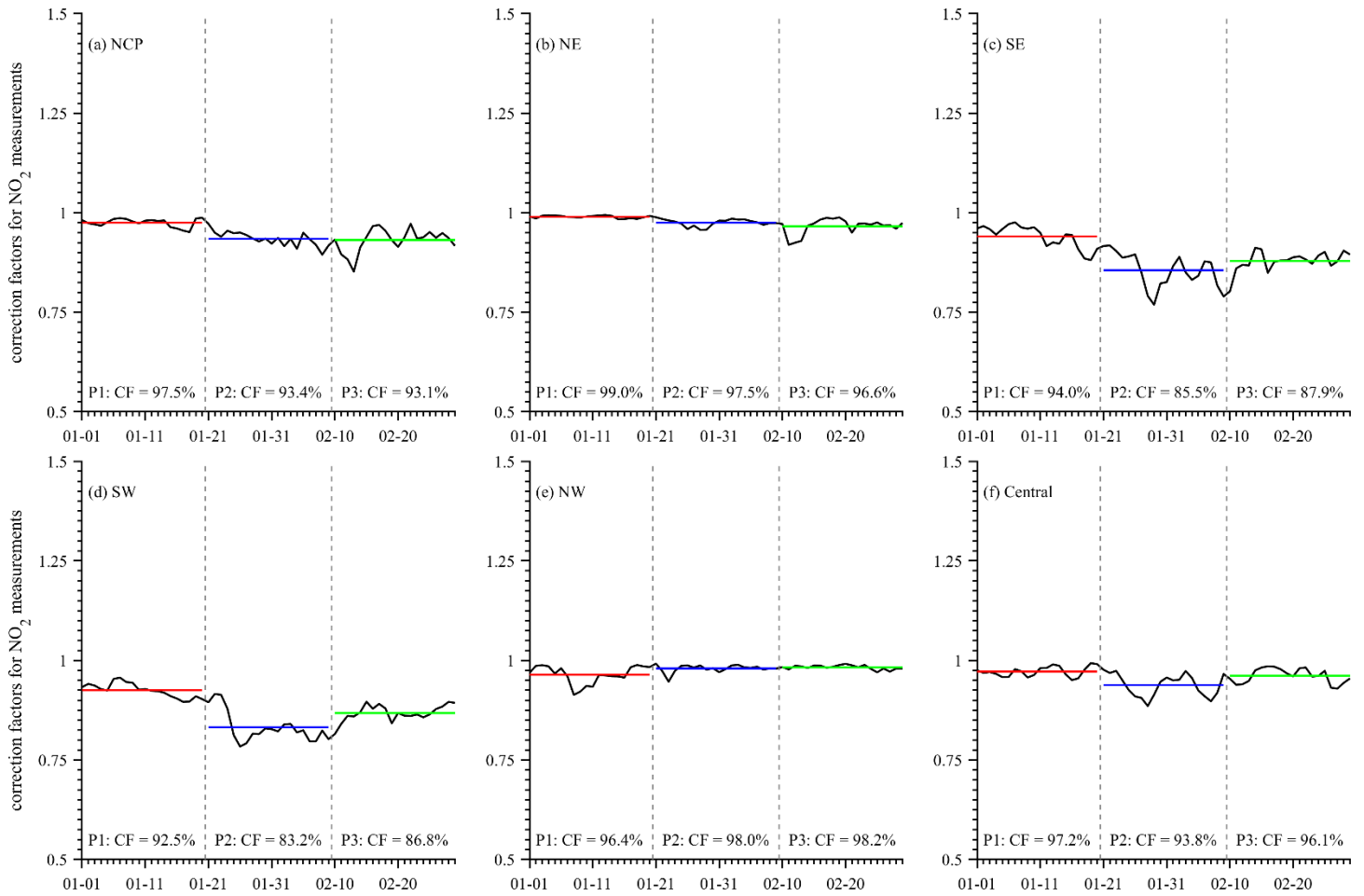
Figure S16: Time series of calculated CFs for NO$_2$ measurements over (a) NCP, (b) NE, (c) SE, (d) SW, (e) NW and (f) Central region during COVID-19 pandemic. The averaged CF values during different stages of COVID-19 pandemic are also labeled.

95

96
97 **Figure S17: the difference of NO₂ measurement before and after the corrections of chemiluminescence monitor interference over (a) NCP, (b)**
98 **NE, (c) SE, (d) SW, (e) NW and (f) Central during the COVID-19 period.**

99

100
101

102

103
104

105

106

107
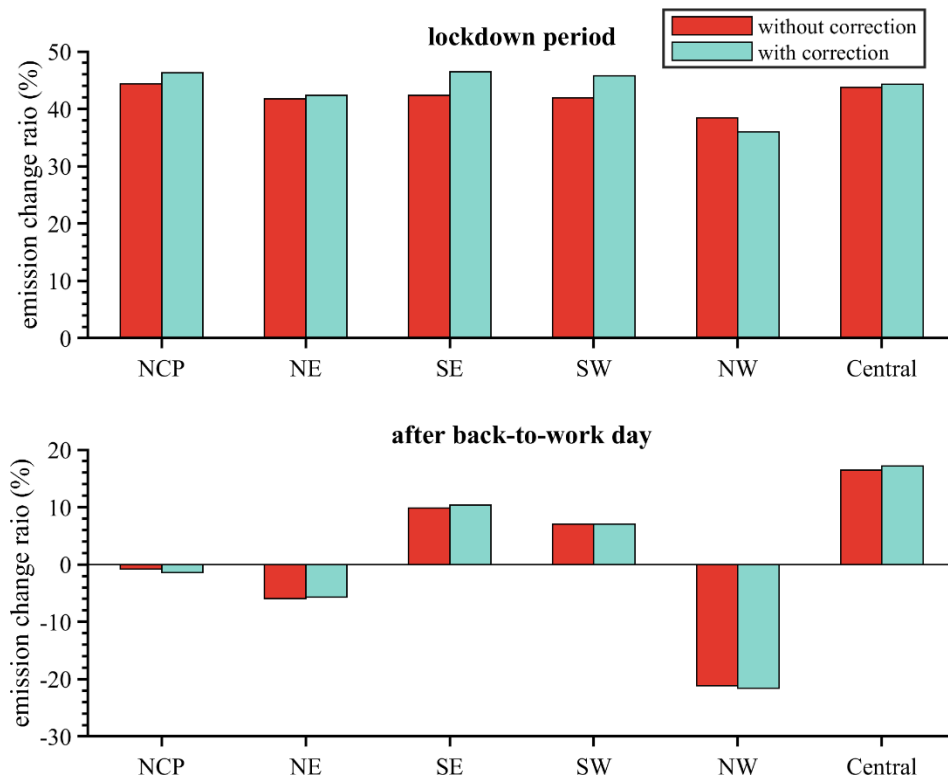
Figure S20: Comparisons of the inversion estimated total emissions of (a) NO$_x$, (b) SO$_2$, (c) CO, (d) PM$_{2.5}$ and (e) PM$_{10}$ before lockdown **based on the a priori emissions for 2010 (read) with those based on the a priori emissions for 2018 (blue).**
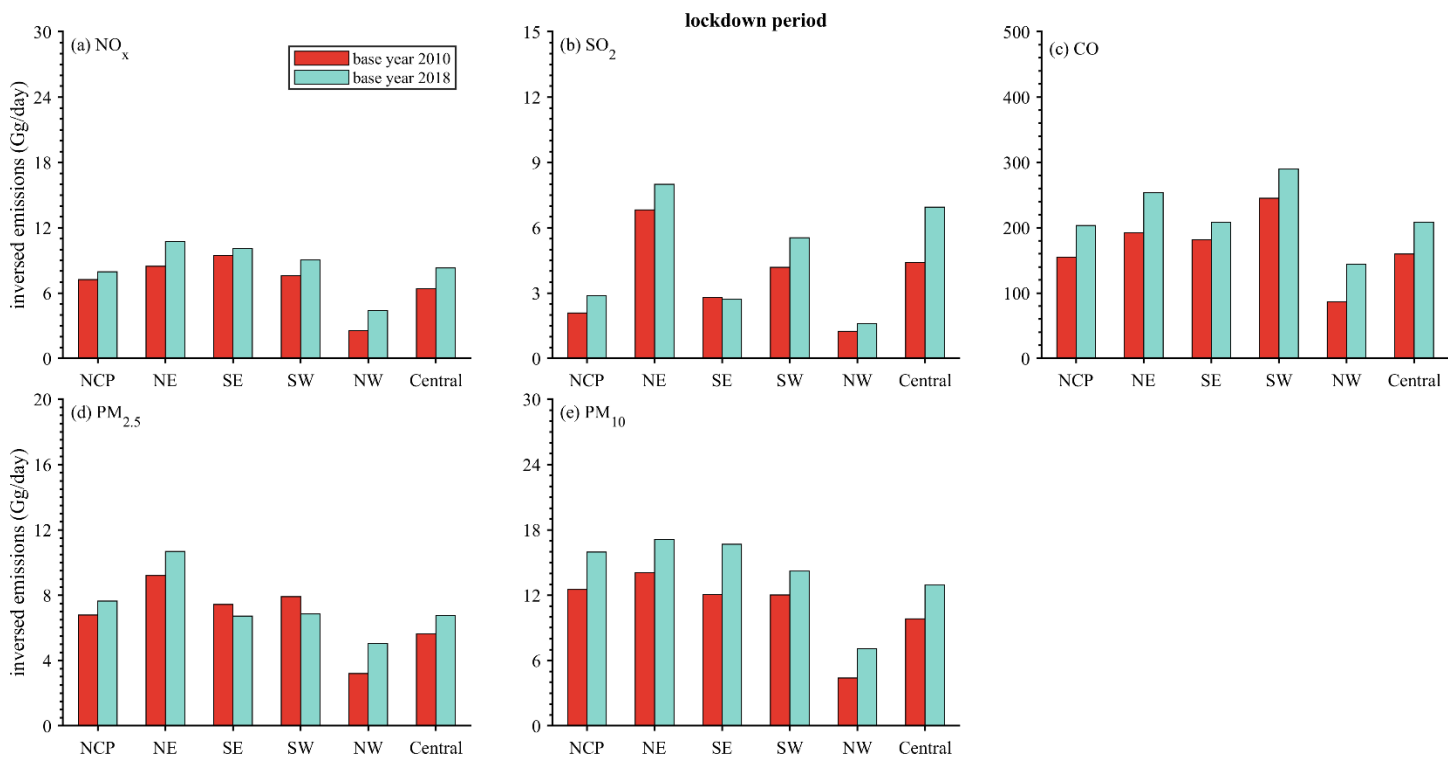
110

111

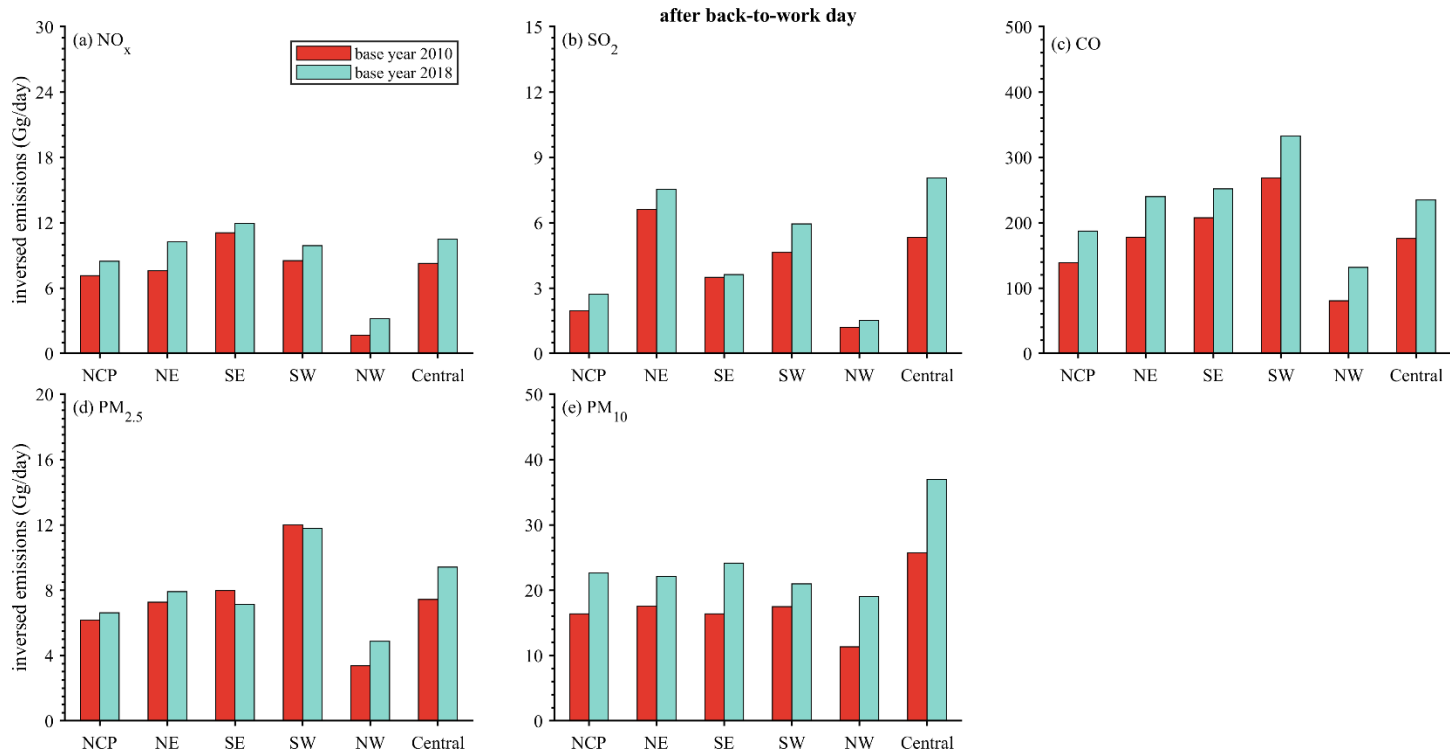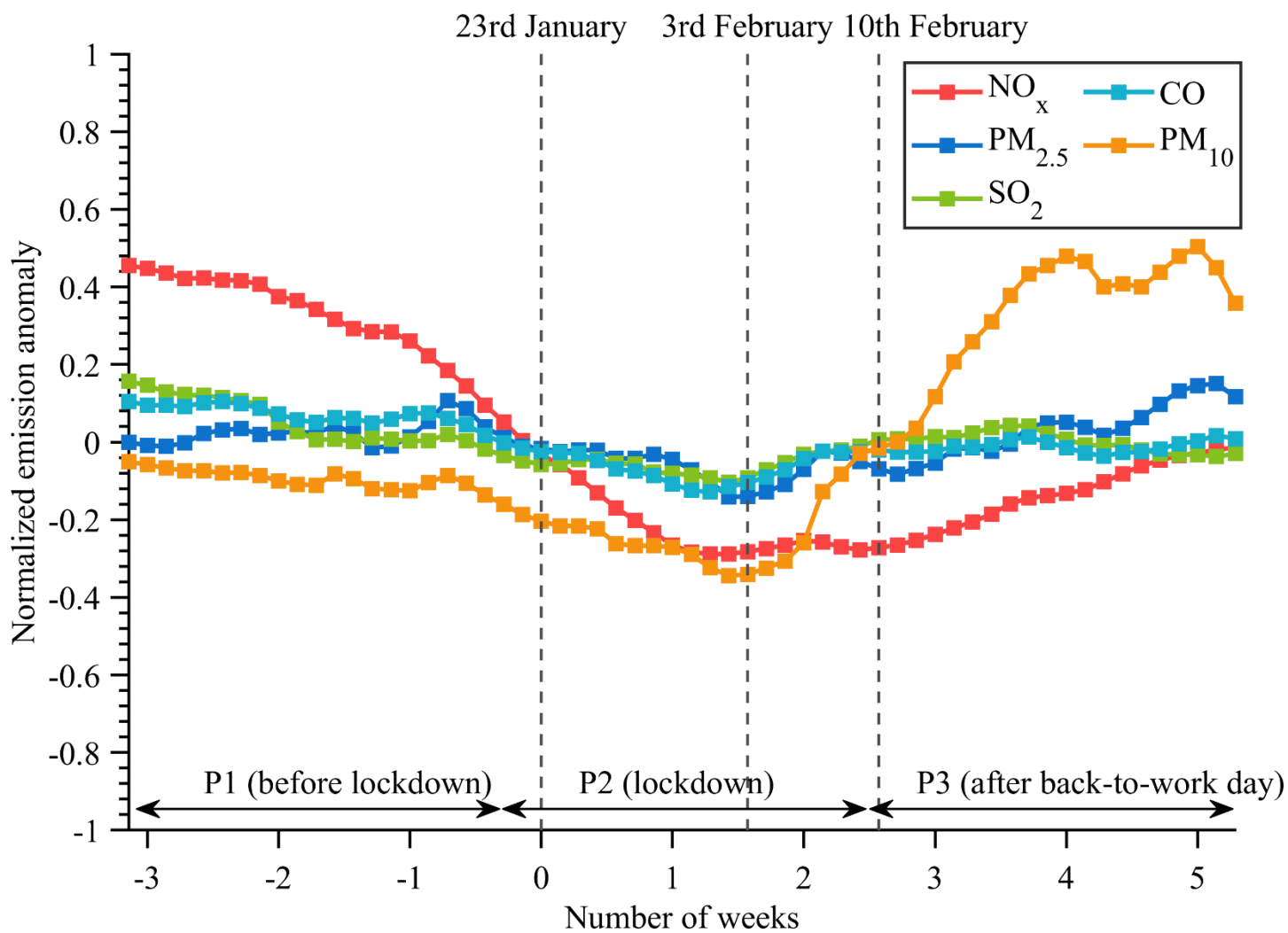**Figure S21: Same as Fig.S18 but for the lockdown period.**

113

114

115 **Figure S22: Same as Fig.S18 but for after back-to-work day.**

116

23rd January   3rd February 10th February

P1 (before lockdown)   P2 (lockdown)   P3 (after back-to-work day)
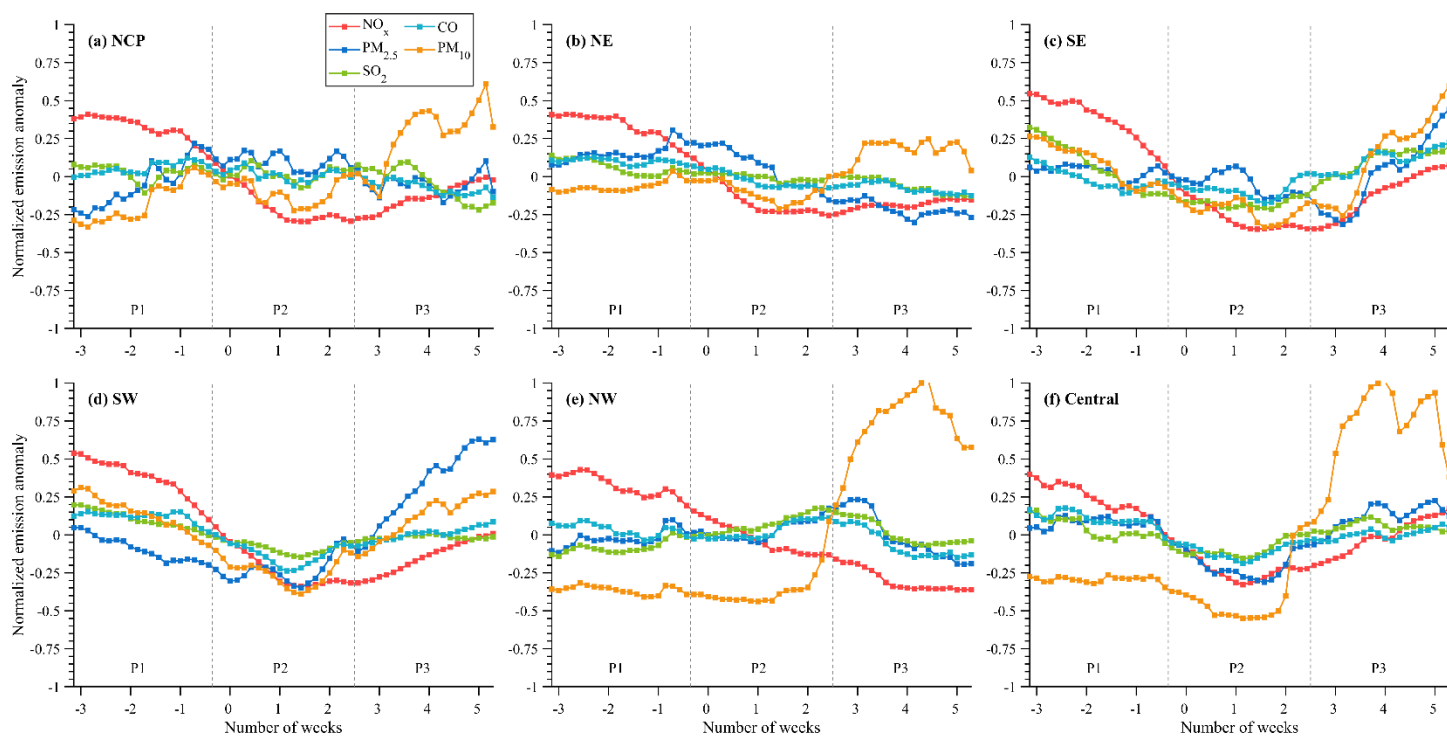
Figure S23: Time series of normalized emission anomalies estimated by inversion results for different species in China from 1st January to 29th February 2020 using the a priori emissions for 2018.

Figure S24: Time series of normalized emission anomalies estimated by inversion results for different species over (a) NCP region, (b) NE region, (c) SE region, (d) SW region, (e) NW region and (f) Central region from 1st January to 29th February 2020 using the a priori emissions for 2018.
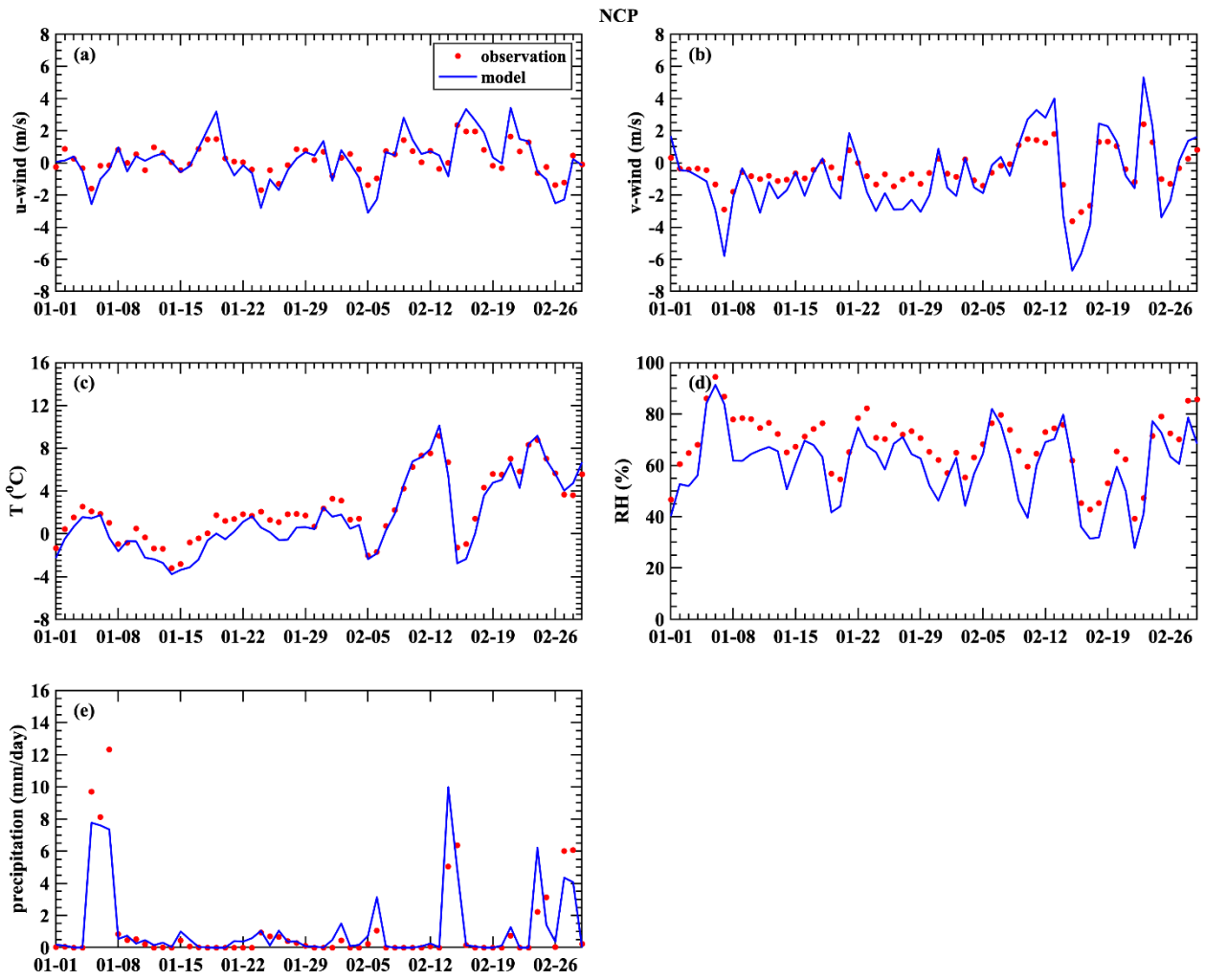
126
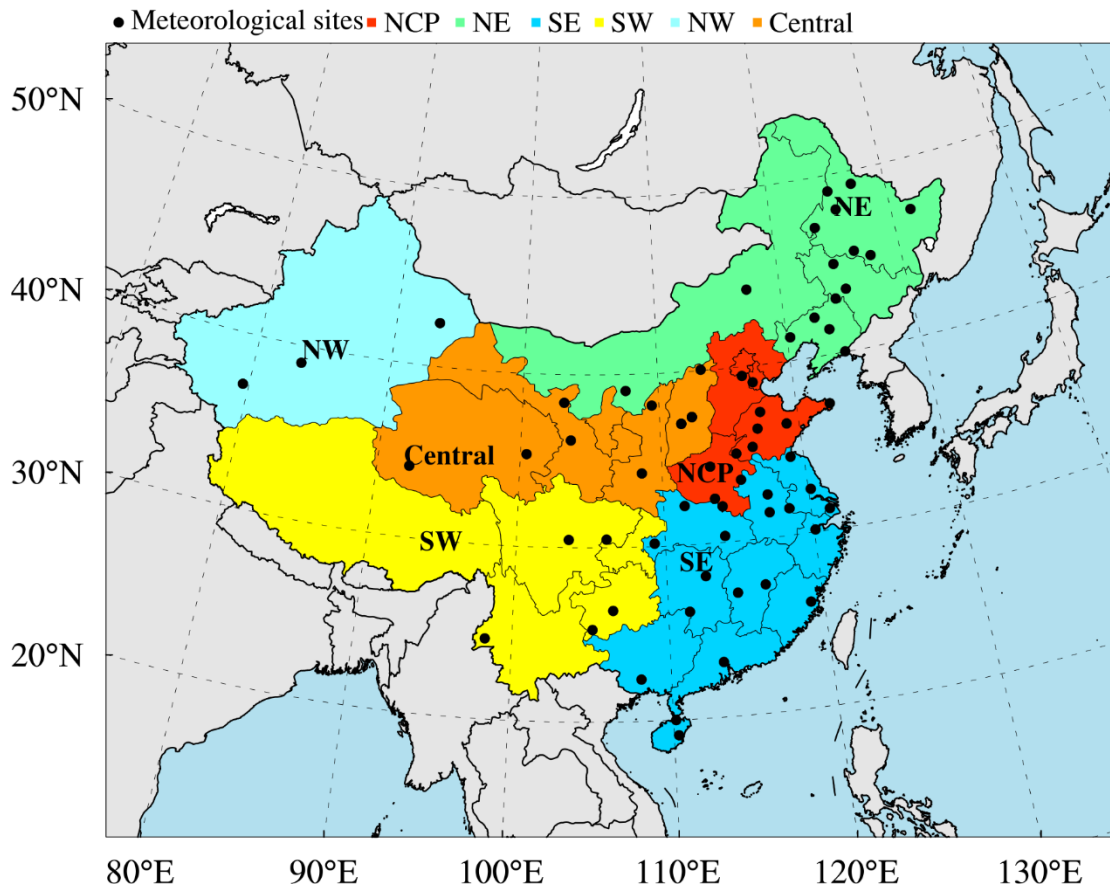
127 **Figure S25: Spatial distribution of meteorological observation sites used in the evaluation of meteorology simulations over different regions of**
128 **mainland China.**

129

NCP
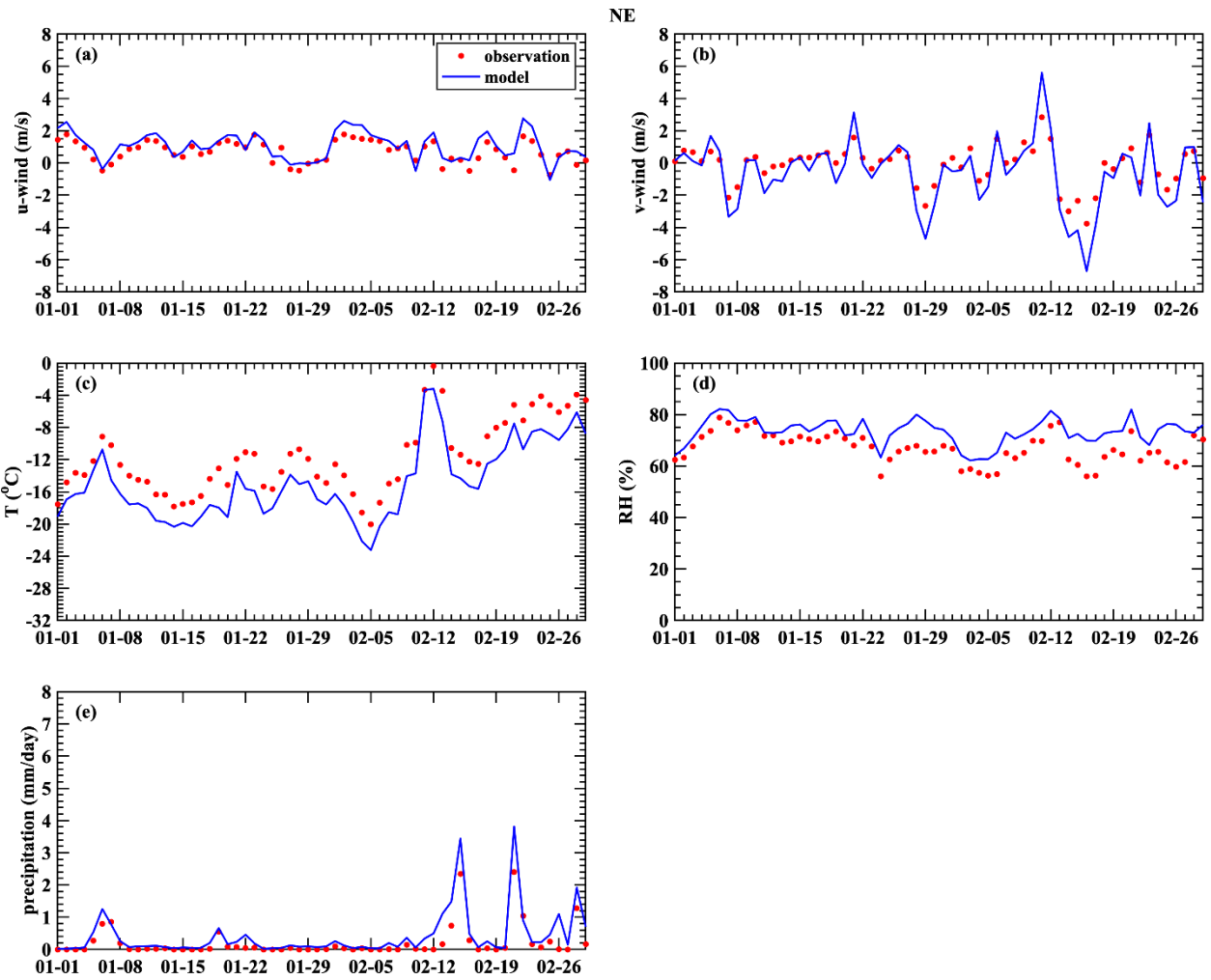

130

Figure S26: Timeseries of observed (red dots) and simulated (blue line) values of (a) u-wind, (b) v-wind, (c) temperature, (d) relative humidity
and (e) precipitation over NCP region from 1st Jan 2020 to 29th Feb 2020.

NE

133

134   **Figure S27: Same as in Figure S20 but over the NE region.**
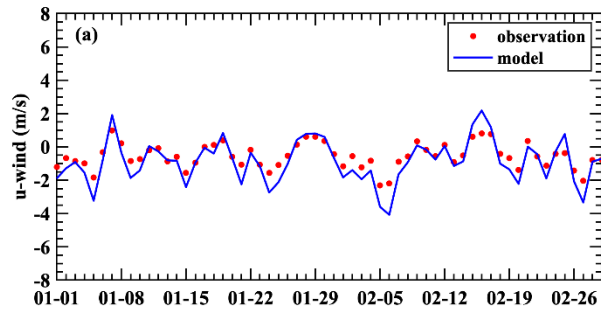
SE

135

136   **Figure S28: Same as in Figure S20 but over the SE region.**

SW

137

138   **Figure S29: Same as in Figure S20 but over the SW region.**

NW

139

Figure S30: Same as in Figure S20 but over the NW region.
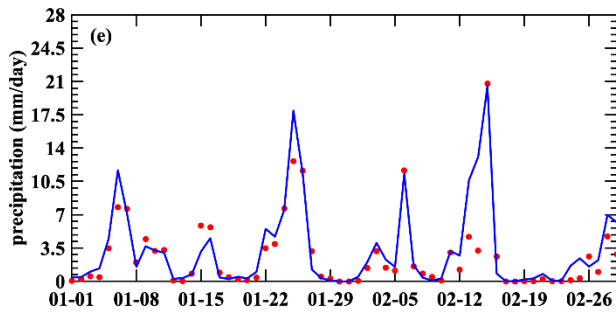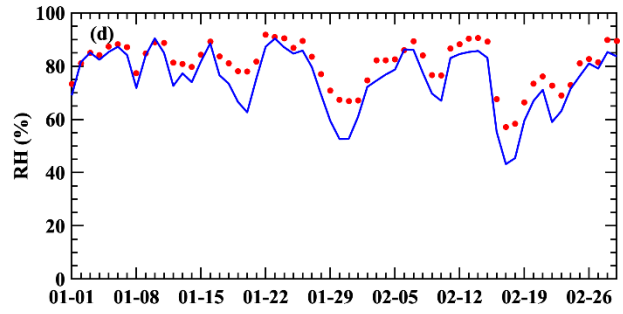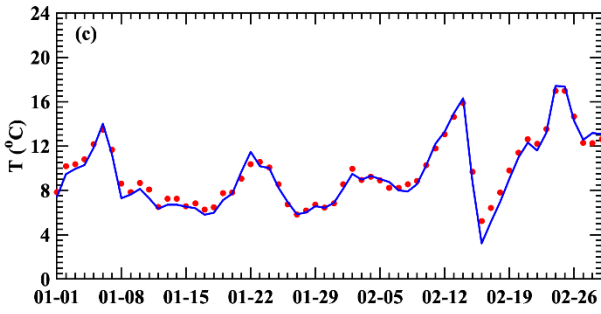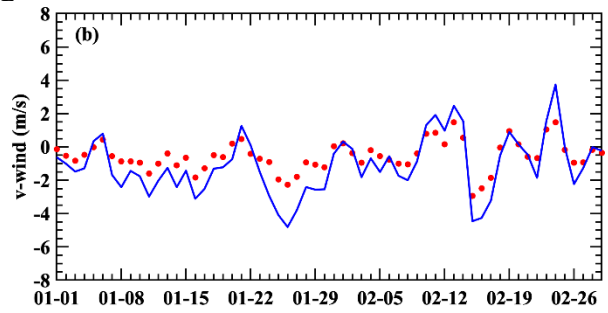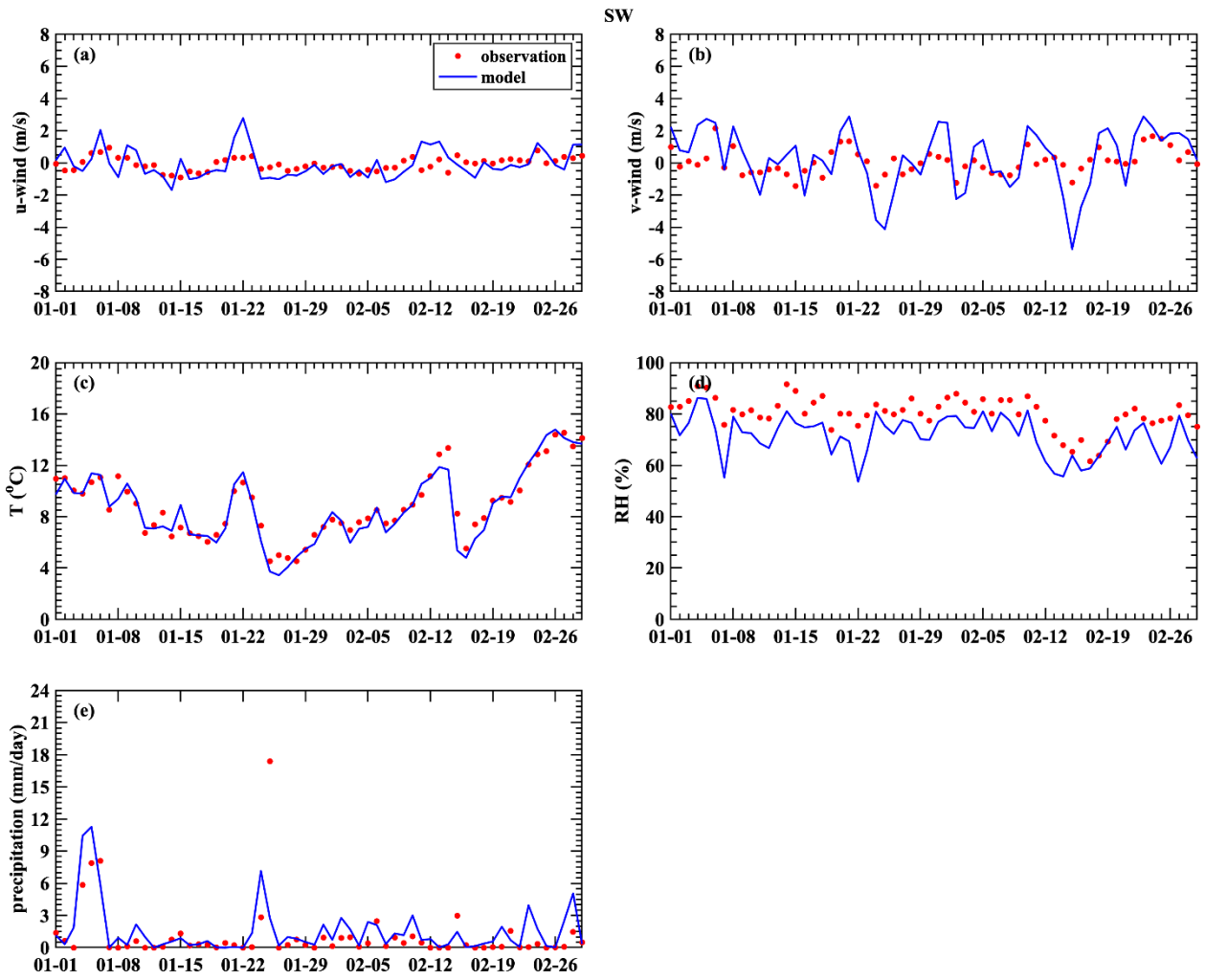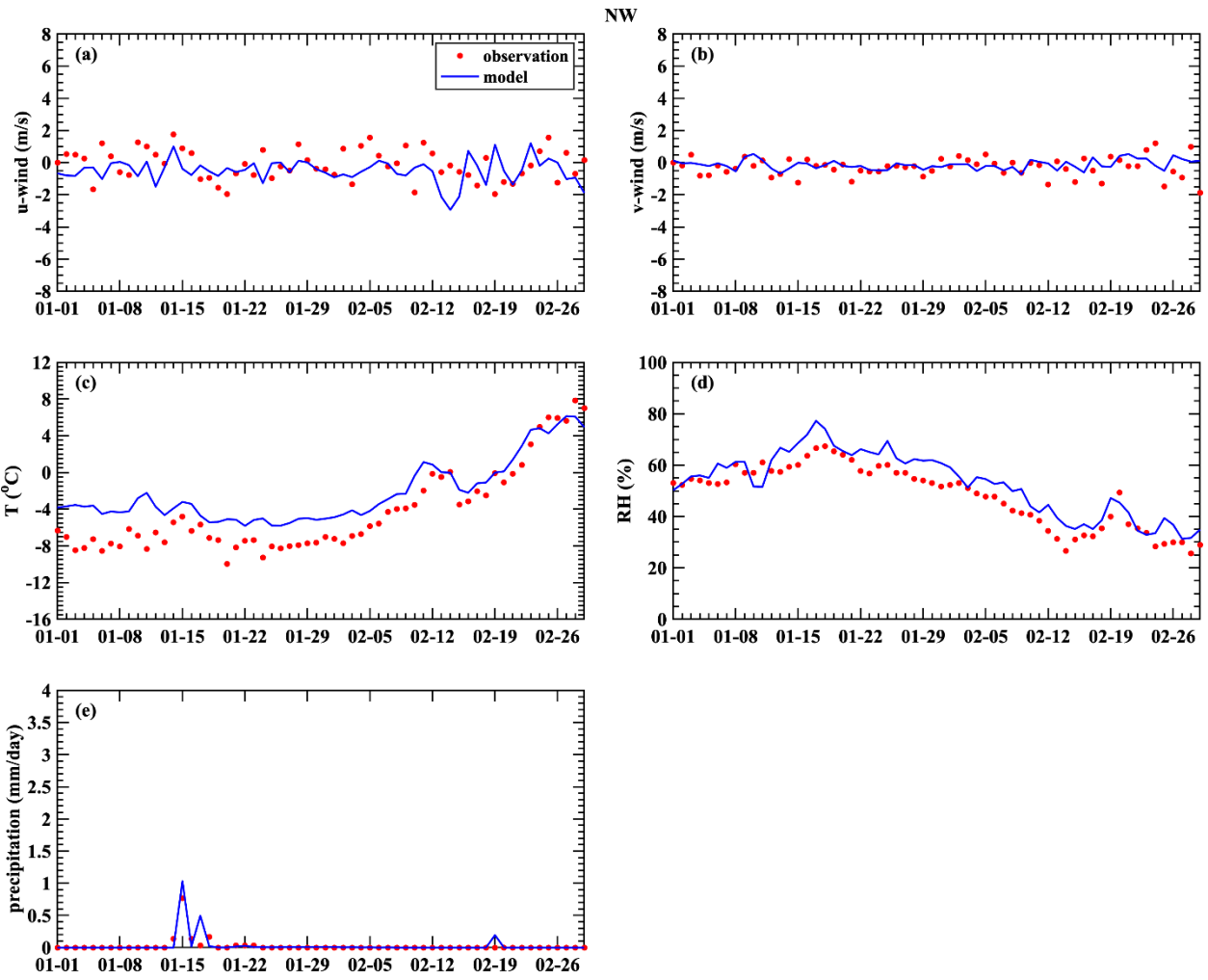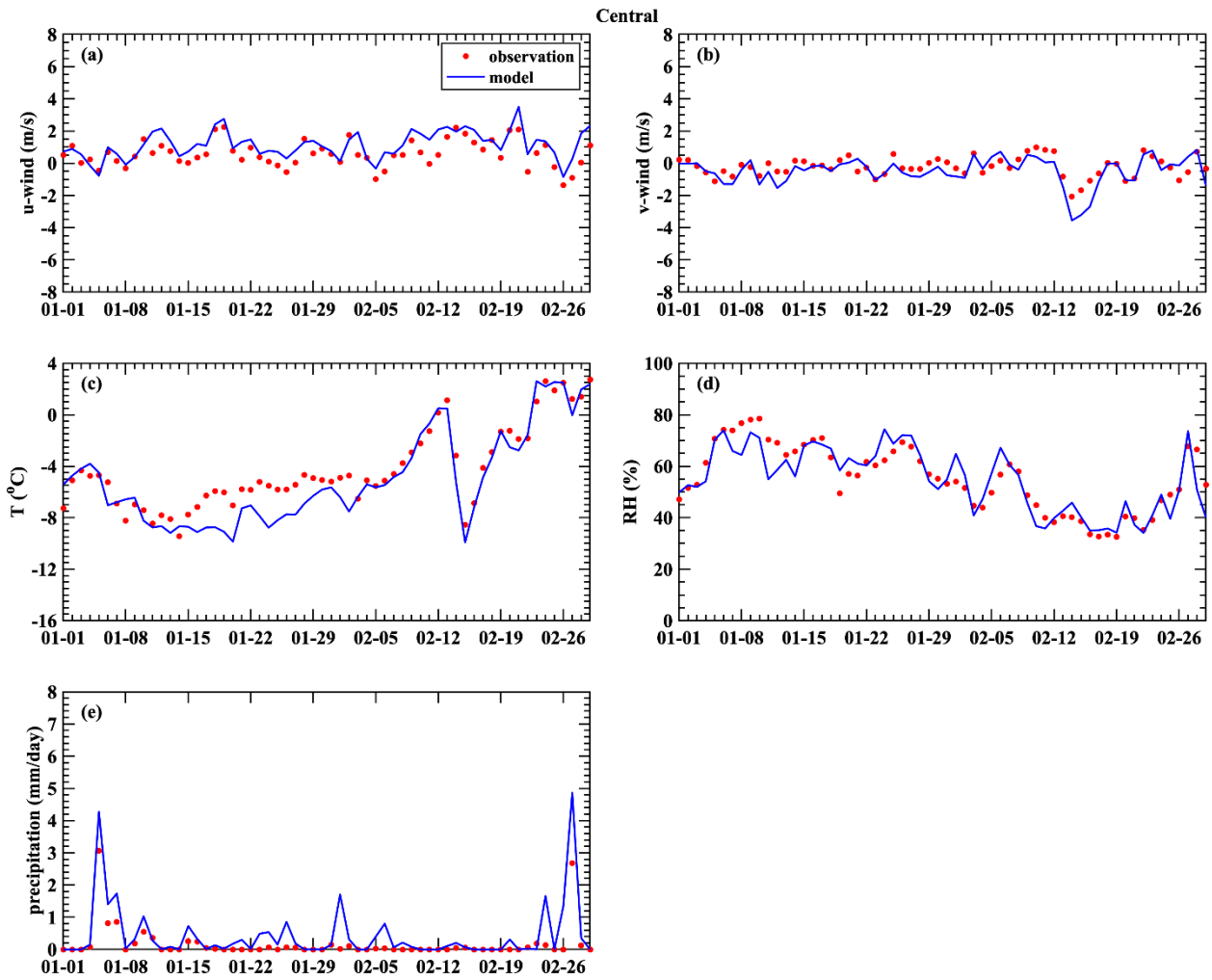
Central

141

Figure S31: Same as in Figure S20 but over the Central region.

143

144

145

146

147

148

149

150

151

152

153

154 **Tables**

155 **Table S1: Evaluation statistics of cross-validation run (outside of bracket) and a priori simulation (inside bracket)**

	$PM_{2.5}$ ($\mu g/m^3$)				PM_{10} ($\mu g/m^3$)			
	R	MBE	NMB(%)	RMSE	R	MBE	NMB (%)	RMSE
NCP	0.94 (0.81)	5.3 (66.5)	7.1 (90.0)	14.4 (77.4)	0.92 (0.77)	2.6 (65.1)	2.6 (66.6)	19.2 (79.8)
NE	0.91 (0.74)	4.1 (1.2)	7.1 (2.0)	13.2 (19.5)	0.87 (0.72)	4.3 (-6.9)	5.7 (-9.0)	17.8 (23.0)
SE	0.89 (0.64)	6.0 (68.5)	15.7 (179.0)	12.2 (73.8)	0.86 (0.54)	5.7 (74.6)	11.6 (153.6)	14.2 (81.6)
SW	0.75 (0.05)	1.2 (54.4)	3.1 (141.5)	9.1 (63.1)	0.70 (-0.08)	-1.6 (53.4)	-3.1 (102.6)	12.6 (65.9)
NW	0.74 (0.32)	4.9 (-62.3)	5.3 (-67.7)	32.2 (71.1)	0.63 (0.32)	3.9 (-84.3)	3.3 (-70.8)	42.4 (94.6)
Central	0.90 (0.70)	-2.7 (12.6)	-3.9 (18.3)	13.2 (27.9)	0.83 (0.41)	-7.3 (-4.6)	-7.5 (-4.7)	20.6 (39.2)

	NO_2 ($\mu g/m^3$)				SO_2 ($\mu g/m^3$)			
	R	MBE	NMB(%)	RMSE	R	MBE	NMB (%)	RMSE
NCP	0.94 (0.62)	1.7 (7.6)	5.3 (24.2)	5.9 (14.6)	0.79 (0.60)	0.0 (57.1)	0.4 (455.4)	2.8 (63.3)
NE	0.91 (0.55)	1.4 (-0.2)	5.1 (-0.7)	5.7 (10.6)	0.71 (0.54)	1.1 (32.8)	6.2 (187.8)	4.6 (36.1)
SE	0.91 (0.49)	0.6 (9.5)	2.7 (45.5)	5.1 (13.3)	0.61 (0.35)	-0.6 (42.5)	-9.5 (680.1)	1.2 (44.7)
SW	0.76 (0.23)	0.0 (-2.0)	0.0 (-10.6)	6.1 (8.8)	0.51 (0.16)	-0.5 (42.4)	-6.7 (565.8)	1.7 (45.5)
NW	0.78 (0.27)	-4.9 (-22.3)	-12.6 (-57.3)	12.3 (28.3)	0.23 (-0.02)	-1.2 (13.5)	-8.2 (88.7)	5.6 (17.9)
Central	0.90 (0.57)	-2.0 (-6.1)	-6.5 (-20.0)	6.5 (13.1)	0.73 (0.54)	-1.3 (53.0)	-6.5 (270.9)	4.9 (58.6)

	CO (mg/m^3)				O_3 ($\mu g/m^3$)			
	R	MBE	NMB(%)	RMSE	R	MBE	NMB (%)	RMSE
NCP	0.92 (0.85)	-0.03 (0.08)	-2.2 (7.5)	0.16 (0.23)	0.78 (0.61)	-14.5 (-28.8)	-28.6 (-56.9)	20.7 (33.1)
NE	0.92 (0.78)	0.05 (-0.33)	5.4 (-34.5)	0.15 (0.43)	0.64 (0.58)	-17.7 (-25.3)	-32.7 (-46.7)	22.7 (28.5)
SE	0.83 (0.74)	-0.05 (0.11)	-6.0 (13.9)	0.10 (0.19)	0.79 (0.74)	-7.2 (-18.2)	-14.0 (-35.6)	15.8 (22.3)
SW	0.63 (0.62)	-0.08 (-0.02)	-10.0 (-1.9)	0.17 (0.18)	0.83 (0.82)	-5.7 (3.0)	-11.8 (6.2)	11.7 (10.5)
NW	0.70 (0.08)	0.11 (-1.13)	7.6 (-76.3)	0.46 (1.26)	0.66 (0.38)	-18.9 (-4.7)	-37.6 (-9.3)	25.4 (21.4)
Central	0.91 (0.76)	-0.08 (-0.37)	-7.5 (-33.5)	0.18 (0.43)	0.74 (0.70)	-17.9 (-14.8)	-35.3 (-29.3)	23.7 (22.2)

156

157

158

159

160

161

162 **Table S2. The time of degrading responses level to COVID-19 virus in each province of mainland China.**

Province	Region	date	Measurement
Beijing	NCP	30th Apr 2020	Degrade first level of response to second level
Tianjin	NCP	30th Apr 2020	Degrade first level of response to second level
Hebei	NCP	30th Apr 2020	Degrade first level of response to second level
Henan	NCP	19th Mar 2020	Degrade first level of response to second level
Shandong	NCP	7th Mar 2020	Degrade first level of response to second level
Inner Mongolia	NE	25th Feb 2020	Degrade first level of response to third level
Jilin	NE	26th Feb 2020	Degrade first level of response to second level
Liaoning	NE	4th Mar 2020	Degrade first level of response to second level
Shanghai	SE	24th Mar 2020	Degrade first level of response to second level
Anhui	SE	25th Feb 2020	Degrade first level of response to second level
Guangdong	SE	24th Feb 2020	Degrade first level of response to second level
Guangxi	SE	24th Feb 2020	Degrade first level of response to third level
Jiangsu	SE	25th Feb 2020	Degrade first level of response to second level
Jiangxi	SE	12th Mar 2020	Degrade first level of response to second level
Zhejiang	SE	2nd Mar 2020	Degrade first level of response to second level
Hainan	SE	26th Feb 2020	Degrade first level of response to third level
Hubei	SE	2nd May 2020	Degrade first level of response to second level
Hunan	SE	10th Mar 2020	Degrade first level of response to second level
Fujian	SE	27th Feb 2020	Degrade first level of response to second level
Yunnan	SW	24th Feb 2020	Degrade first level of response to third level
Sichuan	SW	26th Feb 2020	Degrade first level of response to second level
Guizhou	SW	24th Feb 2020	Degrade first level of response to third level
Chongqing	SW	10th Mar 2020	Degrade first level of response to second level
Xizang	SW	7th Mar 2020	Degrade first level of response to third level
Ningxia	Central	28th Feb 2020	Degrade first level of response to second level
Shanxi	Central	24th Feb 2020	Degrade first level of response to second level
Gansu	Central	21st Feb 2020	Degrade first level of response to third level
Shanaxi	Central	28th Feb 2020	Degrade first level of response to third level
Qinghai	Central	26th Feb 2020	Degrade first level of response to third level
Xinjiang	NW	26th Feb 2020	Degrade first level of response to second level

163

164

165

166

167

168 **Table S3. Inversion estimated emissions of different air pollutants in southeast China as well as their changes between different periods in**
169 **COVID-19 time**

	NO_x	$PM_{2.5}$	PM_{10}	SO_2	CO
P1 (Gg/day)	57.1	34.8	60.9	17.9	876.3
P2 (Gg/day)	32.9	31.8	52.1	16.0	774.7
P3 (Gg/day)	35.9	34.3	71.0	17.0	805.2
(P2-P1)/P1	-42.4%	-8.6%	-14.3%	-10.9%	-11.6%
(P3-P2)/P1	5.2%	7.2%	31.0%	5.7%	3.5%
(P3-P1)/P1	-37.2%	-1.4%	16.6%	-5.2%	-8.1%

170

171 **Table S4: Evaluation statistics for the meteorology simulation**

Region	U (m/s)			V (m/s)			T (℃)			RH (%)			Precipitation (mm/day)		
	R	MBE	RMSE	R	MBE	RMSE	R	MBE	RMSE	R	MBE	RMSE	R	MBE	RMSE
NCP	0.92	-0.04	0.72	0.96	-0.38	1.31	0.98	-0.71	1.07	0.91	-7.95	9.76	0.88	0.06	1.22
NE	0.90	0.35	0.51	0.97	-0.45	1.01	0.98	-3.13	3.25	0.79	6.53	7.47	0.95	0.20	0.36
SE	0.95	-0.32	0.69	0.96	-0.55	1.07	0.99	-0.21	0.58	0.96	-5.44	6.80	0.91	0.59	1.96
SW	0.46	0.00	0.78	0.65	0.24	1.48	0.96	-0.19	0.81	0.81	-8.53	9.66	0.56	0.42	2.38
NW	-0.01	-0.39	1.27	0.16	0.16	0.64	0.96	2.07	2.60	0.94	4.71	6.23	0.86	0.01	0.08
CENTRAL	0.92	-0.04	0.72	0.78	-0.26	0.60	0.94	-0.73	1.42	0.88	-0.40	6.14	0.91	0.26	0.53

172

173 **References:**

174 Dunlea, E. J., Herndon, S. C., Nelson, D. D., Volkamer, R. M., San Martini, F., Sheehy, P. M., Zahniser, M. S.,
175 Shorter, J. H., Wormhoudt, J. C., Lamb, B. K., Allwine, E. J., Gaffney, J. S., Marley, N. A., Grutter, M., Marquez,
176 C., Blanco, S., Cardenas, B., Retama, A., Villegas, C. R. R., Kolb, C. E., Molina, L. T., and Molina, M. J.:
177 Evaluation of nitrogen dioxide chemiluminescence monitors in a polluted urban environment, Atmos. Chem.
178 Phys., 7, 2691-2704, https://doi.org/10.5194/acp-7-2691-2007, 2007.
179 Lamsal, L. N., Martin, R. V., van Donkelaar, A., Steinbacher, M., Celarier, E. A., Bucsela, E., Dunlea, E. J., and
180 Pinto, J. P.: Ground-level nitrogen dioxide concentrations inferred from the satellite-borne Ozone Monitoring
181 Instrument, J. Geophys. Res.-Atmos., 113, https://doi.org/10.1029/2007JD009235, 2008.
182